TECHNISCHE UNIVERSITÄT MÜNCHEN
FAKULTÄT FÜR PHYSIK

Crystals of Topological Solitons: an Effective Field Theory Approach

Claudio Benzoni

Vollständiger Abdruck der von der Fakultät für Physik
der Technischen Universität München
zur Erlangung des akademischen Grades eines
Doktors der Naturwissenschaften (Dr. rer. nat.)
genehmigten Dissertation.

Vorsitzender: Prof. Dr. Christian Back

Prüfer der Dissertation: 1. TUM Junior Fellow Dr. Sergej Moroz
2. Prof. Dr. Martin Zacharias

Die Dissertation wurde am 05.10.2021 bei der Technischen Universität München
eingereicht und durch die Fakultät für Physik am 26.11.2021 angenommen.

Abstract

The number of constituents that compose macroscopic systems makes condensed matter a very diverse area of physics. Therefore, it is of extreme importance to discover common themes and properties that permit the description of distinct systems similarly. One of these themes is to identify and study gapless excitations at long wavelengths and small energies. Crystals are the most familiar systems that exhibit gapless degrees of freedom, called phonons. This thesis applies field theory methods to study long-wavelength excitations of topological solitons that arrange themselves into crystal structures and emerge as ground states of superfluids and chiral magnets. First, using boson-vortex duality, we formulate a low-energy effective theory of a two-dimensional vortex lattice in a bosonic Galilean-invariant compressible superfluid by describing vortices as two-dimensional point charges moving in a magnetic background. We extract the excitation spectrum, which contains a gapped Kohn mode and an elliptically polarized Tkachenko mode that has quadratic dispersion relation at low momenta. We couple the theory to an external U(1) gauge field and extract the particle number current transport. Second, we study edge waves travelling along the lattice's boundary in two-dimensional skyrmion lattices which appear in thin-film chiral magnets. In elastic systems, these excitations are known as Rayleigh waves. We find that the direction of propagation of the Rayleigh modes is determined not only by the thin film's chirality but also by the Poisson ratio of the crystal. Furthermore, we discover three qualitatively different regions distinguished by the low-frequency edge waves' chirality and inspect their properties.

Zusammenfassung

Die Anzahl der Bestandteile, aus denen sich makroskopische Systeme zusammensetzen, macht die kondensierte Materie zu einem sehr vielfältigen Bereich der Physik. Daher ist es von äußerster Wichtigkeit, gemeinsame Themen und Eigenschaften zu entdecken, die es erlauben, unterschiedliche Systeme auf ähnliche Weise zu beschreiben. Eines dieser Themen ist die Identifizierung und Untersuchung von lückenlosen Anregungen bei langen Wellenlängen und kleinen Energien. Kristalle sind die bekanntesten Systeme mit lückenlosen Freiheitsgraden, den sogenannten Phononen. In dieser Arbeit werden feldtheoretische Methoden angewandt, um langwellige Anregungen topologischer Solitonen zu untersuchen, die sich in Kristallstrukturen anordnen und als Grundzustände von Superfluiden und chiralen Magneten auftreten. Zunächst formulieren wir unter Verwendung der Boson-Vortex-Dualität eine niederenergetische effektive Theorie eines zweidimensionalen Wirbelgitters in einem bosonischen, Galilei-invarianten kompressiblen Suprafluid, indem wir die Wirbel als zweidimensionale Punktladungen beschreiben, die sich in einem magnetischen Hintergrund bewegen. Wir arbeiten das Anregungsspektrum aus, das eine lückenhafte Kohn-Mode und eine elliptisch polarisierte Tkachenko-Mode enthält, wobei letztere bei niedrigen Impulsen eine quadratische Dispersionsbeziehung aufweist. Wir koppeln die Theorie an ein externes U(1)-Eichfeld und extrahieren den Teilchenzahl-Stromtransport. Zweitens untersuchen wir Randwellen, die sich entlang der Gittergrenze in zweidimensionalen Skyrmionengittern bewegen, die in chiralen magnetischen Dünnschichten auftreten. In elastischen Systemen sind diese Erregungen als Rayleigh-Wellen bekannt. Wir stellen fest, dass die Ausbreitungsrichtung der Rayleigh-Moden nicht nur von der Chiralität des Dünnfilms, sondern auch von der Poissonzahl des Kristalls bestimmt wird. Außerdem entdecken wir drei qualitativ unterschiedliche Regionen, die sich durch die Chiralität der niederfrequenten Randwellen unterscheiden, und untersuchen ihre Eigenschaften.

Contents

Some results, text, figures in this thesis are taken from the following author's publications:

- Sergej Moroz and Carlos Hoyos and Claudio Benzoni and Dam Thanh Son, "Effective field theory of a vortex lattice in a bosonic superfluid", SciPost Phys., 5, 4, (2018).
- "Rayleigh edge waves in two-dimensional crystals with Lorentz forces: From skyrmion crystals to gyroscopic media", Benzoni, Claudio and Jeevanesan, Bhilahari and Moroz, Sergej, Phys. Rev. B, 104, 2,024435 (2021)

In order to provide a structure better suited to this thesis, certain sections have been merged, rearranged or renamed.

Introduction

Our currently accepted understanding of elementary particles is the Standard Model, which predicts that fermions and the Higgs boson compose matter, and four vector bosons mediate the three fundamental forces: electromagnetic, weak and strong. However, much more is going on when we investigate matter assembled in large ensembles. When we consider systems composed of a macroscopic number of particles, it seems as there is no remembrance of the underlying microscopic structure. In fact, condensed matter and many-body physics is the science of *emergence* [1]. As large crowds of people behave surprisingly differently from what we expect their individuals to act, also matter does similarly. This problem is not just an issue related to the microscopic theories' lack of predictivity due to our limited computational resources. At every scale of size and complexity, new *fundamental* laws might appear, making irrelevant or less relevant the old-scale's laws. Topological phases, crystals, Bose–Einstein condensates and superfluids, superconductors, supersolids, Fermi and non-Fermi liquids, and many more are all phenomena that arise from the same constitutive elements, but are indeed bewilderingly different. We urge a broad classification, to get some sense of this astonishing variety in which condensed matter unravel. To that end, it is useful to count how many ways a system has to be excited above its ground state at long wavelengths, and with small energies [2]. According to this approach, physical systems divide into those that possess a finite excitation gap, the ones with few soft modes, and those which enjoy many ways to realise gapless quasi-particle excitations.

In this thesis, we focus on systems that fall into the second category. *Symmetries* characterise this class. A system obeys a symmetry if, under a transformation, its properties do not change. Symmetries can also be approximate, when they arise at large distances. For instance, a football is not a perfect sphere, but we would assure its rotational invariance if we watch it from far enough. The appearance of few gapless modes is a consequence of *spontaneous symmetry breaking*. This far-reaching concept is a novel feature steming from having to deal with a macroscopic number of particles and infinite volumes. Taken a microscopic theory which has a continuous symmetry, thus a whole manifold of degenerate

ground states, the environment chooses one in particular, and the symmetry is lost. Something similar also happens in the biological world. Flat fishes live on the bottom of the sea, and have both eyes on one side. While the halibut put them on the left side, the flounder put them on the opposite side. To put in another way, evolution broke parity symmetry [3].

The consequence of the ground state's degeneracy and spontaneous symmetry breaking are the gapless excitations, namely the *Nambu–Goldstone bosons*. Pions in heavy-ion collisions manifest the spontaneous breaking of chiral symmetry, Bogoliubov phonons in superfluids, of U(1) phase symmetry, phonons in crystals, of translational symmetry. For all of these systems, effective actions can be written based only on symmetry considerations, keeping in mind that every term which is not prohibited should be included [4].

Crystals constitute the central theme of this thesis. Faithful to the long-wavelength viewpoint, we rely on the elasticity theory, a field of continuum mechanics that assigns a displacement from a preferred equilibrium configuration at every point in space. The original translational symmetry's remainder (a subset) imposes conditions on the elastic tensor structure. While, historically, elasticity was developed to describe crystals and solid bodies made of particles, our research concentrated on elastic solids composed of topological solitons. These are localised solutions of field theories that possess conservation laws that do not follow from continuous symmetries and from Noether's theorem. Due to their topological charge conservation, topological solitons can not be smoothly deformed into topological trivial field configurations. Consequently, we can divide a theory's solutions space into separated topological sectors.

The first crystal of topological solitons we considered emerges in superfluids. From standard arguments, a superfluid is necessarily irrotational. However, if it is put under external rotation, the ground state of a superfluid can carry angular momentum by nucleation of quantised vortices. The density of vortices scales with the angular velocity [5]. For moderate rotations, and until the vortex density reaches a critical value of the order of magnitude of the density of particles, vortices arrange themselves in a regular crystal which is known as the Abrikosov lattice, and that found its experimental incarnations both in superfluid Helium [6] and cold atomic Bose–Einstein condensates [7]. Using the boson-vortex duality [8, 9], we provided an effective field theory description of the vortex crystal phase [10].

The other crystal we considered emerges in magnetic systems. For a long time, a mysterious small pocket of the phase space presented anomalous magnetic properties, and was called 'A-phase'. Experiments in transition metal compounds with cubic symmetry [11] provided incontestable proof that this phase consists of a lattice of topological solitons called skyrmions. Such name comes from pioneering works of the nuclear physicist Tony Skyrme [12]. Exploring waves that remain

confined to the boundary of a semi-infinite domain, we found the skyrmion lattice exhibits quadratically dispersing surface Rayleigh waves whose direction of propagation can be tuned and classified by changing a dimensionless ratio between the elastic parameters [13] .

We organised this thesis as follows:

In Chapter 1, we review linear elasticity. This is the coarse-grained framework we used to describe crystals as homogenous systems. Displacement from equilibrium positions is the degree of freedom that describes elastic solids most properly. From displacement, two tensor quantities called strain and stress are constructed. We show how we can decompose them into elementary pieces, each understandable in simple physical terms, and provide some examples. The crystal symmetry puts constraints on the elastic energy. We then study how waves propagate in an infinite elastic system and how their nature change when we apply sensible boundary conditions.

In Chapter 2, we introduce topological solitons in a model-independent fashion. However, first, we start from a historic excursus into developments that eventually led to introducing topological conservation laws in physics. Then, we illustrate the concept of topological charge, homotopy class, topological soliton in increasing levels of complexity. For this reason, we start with topological solitons in one spatial dimension (kinks) and then discuss vortices and skyrmions in two dimensions.

In Chapter 3, we develop an effective field theory to describe vortex crystals in rotating compressible bosonic superfluids. We discuss how quantum field theory can be used for the non-relativistic limit of interacting bosons. We lay out the basics of effective actions for a superfluid in the absence of vortices and the modifications needed when there are topological defects. We derive boson-vortex duality, which incorporates the superfluid as a gauge degree of freedom and vortices as point charges moving in a uniform dual magnetic field. We use it to provide a low-energy description of the vortex lattice, and extract transport.

We finally devote Chapter 4 to investigate surface waves in skyrmion crystals in thin-film chiral magnets. We fully map their dispersion relation in terms of a ratio between the crystal parameters and find exciting consequences regarding the direction of propagation.

We summarise and foresee the possible outlook of our work in the conclusions.

Chapter 1

Elasticity theory

In this initial chapter, we introduce the foundations and the tools to describe elastic solids that we will use throughout this thesis. This approach goes under the name of elasticity theory. It is based on the assumption that we can describe solids as continuous distributions of their constituents, at least at a coarse-grained level. First, we illustrate the generic description of small displacements in deformable bodies and specialise it to elastic media, whose main characteristic is the ability to retain their shape after they have been deformed. Then, we illustrate elasticity's essential building blocks. These are strain and stress, tensor quantities that are built from displacements. Symmetry poses constraints on the tensor structure of observables. In the last part, we study how waves propagate in elastic bodies, both in the bulk of the system and -more interesting for us- at its boundaries. Everywhere, we assume Einstein's convention on summation over repeated indices.

1.1 Continuous description of elastic solids

Conventionally, the study of mechanical systems starts by introducing the concept of *point particle*, an idealisation of material bodies in which the latter are represented as zero-dimensional objects. By definition, such representation provides neither a shape nor a volume. The discussion usually proceeds with the study of particles' kinematics and dynamics in the three-dimensional Euclidean space, first by using Newton's laws and then developing the Lagrangian formalism ([14, 15]).
The point particle working hypothesis holds whenever the bodies' size is much smaller than the space where their motion occurs. In this case, the positions fully determine the state of bodies at rest. For example, the only relevant information about grains of sand that make up a sandcastle is to stay on top of each other appropriately.

If we want to describe an extended object, we also require the knowledge of its *orientation*, in other words, the angles that put in relation the body-fixed coordinate system with an external reference frame. Therefore, we need a more general working concept to replace the point particle. This new paradigm is the *solid body*, defined as a collection of point particles whose motion or forces do not alter their mutual distance.
Lastly, we might even relax the assumption concerning the rigidity of bodies. If the mutual distance between point particles can change, bodies alter both in their shape and in volume. The study of the configuration of a *deformable body* requires another ingredient, on top of its position and its orientation. This new degree of freedom that describes deformations is called *strain*, and it is crucial to investigate *elastic solids*. Elastic solids are continuous distributions of masses that oppose deformation and return to their original configuration when the forces that cause the deformation cease. A theory that can describe such a setting is necessarily a continuum theory, in which the number of degrees of freedom is infinite and, in general, no microscopic lengthscales are involved. It must be kept in mind that, as every *effective* description, *elasticity theory* is not fundamental, and it may only be valid within a regime of length scales and energies.

1.1.1 Helmholtz's theorem and partial motions

We present a very illustrative decomposition of the most general motion that happens for a generic deformable body in three dimensions, which might be a fluid or a solid. This result is one of the many contributions by Helmholtz ([16], as cited in [17]). It separates the displacement of a continuous deformable body into the sum of three independent *partial motions*. One of these is constructed using *strain*, which is the key element to describe elastic bodies.
We start this discussion by considering two points belonging to a body, P and O, whose coordinates are (x, y, z) and $(0, 0, 0)$, respectively. If some rearrangement of the body takes place, the point P gets infinitesimally displaced to $P = (\xi, \upsilon, \zeta)$ with

$$\begin{aligned} \xi &= \xi_0 + x\,(\partial_x \xi) + y\left(\partial_y \xi\right) + z\,(\partial_z \xi) + \cdots \\ \upsilon &= \upsilon_0 + x\,(\partial_x \upsilon) + y\left(\partial_y \upsilon\right) + z\,(\partial_z \upsilon) + \cdots \\ \zeta &= \zeta_0 + x\,(\partial_x \zeta) + y\left(\partial_y \zeta\right) + z\,(\partial_z \zeta) + \cdots\ , \end{aligned} \tag{1.1}$$

where dotted terms are of higher order in derivatives.
The three partial derivatives of the three components of the displacement field can be labelled as $a_{11} = \partial_x \xi$, $a_{12} = \partial_y \xi$ and so on. Namely, they compose an object a_{ij} with nine components and two indices. If we introduce its antisymmetric $a_{[i,j]} \equiv \frac{1}{2}\left(a_{ij} - a_{ji}\right)$ and symmetric $a_{(i,j)} \equiv \frac{1}{2}\left(a_{ij} + a_{ji}\right)$ parts, equation (1.1)

automatically splits into three peculiar components

$$\begin{aligned}\xi &= \xi_0 + y\ a_{[1,2]} + z\ a_{[1,3]} + x\ a_{11} + y\ a_{(1,2)} + z\ a_{(1,3)}\\ \upsilon &= \upsilon_0 + x\ a_{[2,1]} + z\ a_{[2,3]} + x\ a_{(2,1)} + y\ a_{22} + z\ a_{(2,3)}\\ \zeta &= \zeta_0 + x\ a_{[3,1]} + y\ a_{[3,2]} + x\ a_{(3,1)} + y\ a_{(3,2)} + z\ a_{33}.\end{aligned}$$

With no surprise, we identify in the above expression two families of terms that are present also for the rigid body, giving rise to motion of all the body's constituents as a whole.
While the first *partial motion* $\mathbf{s}_0 \equiv (\xi_0, \upsilon_0, \zeta_0)$ represents a uniform translation, the second type of terms, which stem from antisymmetrisation, constitute a rotation. We arrange the latter as the second partial motion $\mathbf{s}_1$, that is a cross product between the position $\mathbf{r}$ and the rotation $\mathbf{\Phi} \equiv (a_{[2,3]}, a_{[3,1]}, a_{[1,2]})$,

$$\mathbf{s}_1 \equiv \mathbf{r} \wedge \mathbf{\Phi}. \tag{1.2}$$

Rotations, by definition, do not change the mutual distance between points. Indeed, after the displacement, the distance between the two points $|\mathbf{r} + \mathbf{s}_1|^2 = |\mathbf{r}|^2 + 2\mathbf{r} \cdot \mathbf{s}_1 + \dots$ coincides with their original distance $|\mathbf{r}|^2$, because the original position and $\mathbf{s}_1$ are orthogonal to each other by construction.
The last partial motion $\mathbf{s}_2 \equiv (\xi_2, \upsilon_2, \zeta_2)$ originates from the symmetrised parts, and it takes into account the local change of the mutual distance between the constituents of the body

$$\begin{aligned}\xi_2 &= x\ a_{(1,1)} + y\ a_{(1,2)} + z\ a_{(1,3)}\\ \upsilon_2 &= x\ a_{(2,1)} + y\ a_{(2,2)} + z\ a_{(2,3)}\\ \zeta_2 &= x\ a_{(3,1)} + y\ a_{(3,2)} + z\ a_{(3,3)}.\end{aligned}$$

It is natural to introduce a second-rank tensor $u_{ij} \equiv a_{(i,j)}$ to incorporate the partial derivatives of the displacement components, such that $\mathbf{s}_2 = \underline{\mathbf{u}}\ \mathbf{r}$.
Elastic solids are insensitive to where they are in space or how they are oriented. Therefore, they do not react to the first $\mathbf{s}_0$ and the second $\mathbf{s}_1$ partial motions, but they react to $\mathbf{s}_2$. The tensor u_{ij} is the peculiar feature of elastic bodies, it is the *strain* we were looking for, and it deserves a discussion on its own, without bothering about the translations and rotations. The following part concerns the description of strain for elastic bodies in dimension $d \geq 2$.

1.2 Displacement and strain

We characterise every point of an elastic solid [18] by a vector $\mathbf{x}$ that describes its position before the deformation, and by one vector after, $\mathbf{x}'$. The main degree

of freedom in elasticity is thus the difference between the two previous quantities, the so-called **displacement field**

$$\mathbf{u}(\mathbf{x}) \equiv \mathbf{x}' - \mathbf{x}. \tag{1.3}$$

Transformations in which the displacement vector is a constant correspond to translations of the body as a whole. Therefore they do not produce deformations. In light of this, we consider only displacements that change locally in space. The appropriate quantity we examine is the gradient of the displacement field $\partial_i u_j$. The knowledge of the dependence of the displacement regarding the original positions completely determines and solves the problem.

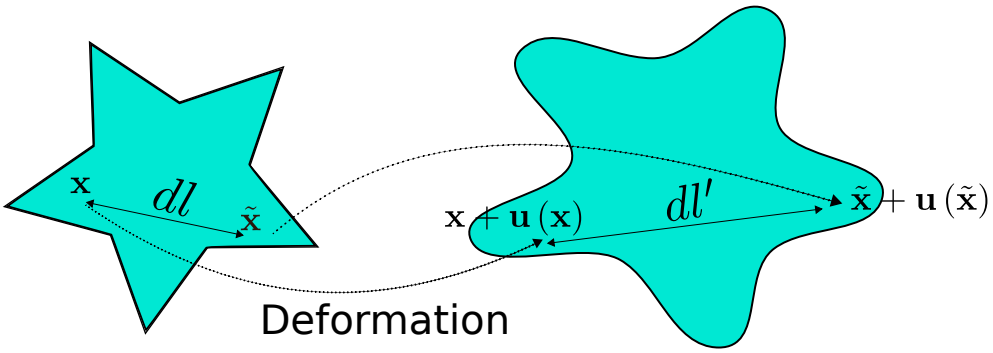

Figure 1.1: Two points $\mathbf{x}$ and $\tilde{\mathbf{x}}$, that originally are at a distance dl, get displaced non-homogeneously by a field $\mathbf{u}$, ending up having distance dl'.

If we take two points $\mathbf{x}$, $\tilde{\mathbf{x}}$ (see figure (1.1)) that are initially infinitesimally close $\tilde{\mathbf{x}} - \mathbf{x} \equiv d\mathbf{x}$ at a distance $dl = \sqrt{d\mathbf{x}^2}$, when the deformation of the body happens, their mutual distance changes according to

$$(dl')^2 = dl^2 + 2dx_j dx_i \left[\frac{1}{2}(\partial_j u_i + \partial_i u_j) + \frac{1}{2}(\partial_i u_l)(\partial_j u_l)\right]. \tag{1.4}$$

We encode the information about the changes of the displacement vector in space by introducing a symmetric second-rank tensor called the **strain tensor**

$$u_{ij} \equiv \frac{1}{2}\left[(\partial_j u_i + \partial_i u_j) + (\partial_i u_l)(\partial_j u_l)\right]. \tag{1.5}$$

As with every real symmetric tensor, we can reduce it to a diagonal form after finding its eigenvalues and eigenvectors. In the context of continuum mechanics, eigenvalues $\{u^{(i)}\}$ are referred to as *principal values*, and eigenvectors as

principal axis because they are the local basis in which the tensor is diagonal. Assuming we diagonalised the tensor, we decompose a generic length element along the principal axis (1, 2, 3) into the sum of three independent contributions

$$(dl)^2 \to (dl')^2 = dx_1^2[1 + 2u^{(1)}] + dx_2^2[1 + 2u^{(2)}] + dx_3^2[1 + 2u^{(3)}]. \tag{1.6}$$

The above equation shows that deformation affects the mutual distance between points dl' by modifying the length elements along the three principal axis dx_1, dx_2, dx_3. Depending if the principal values are positive or negative, local dilations dx_i' of the original length elements dx_i are either expansions or compressions

$$dx_i \to dx_i' = dx_i\sqrt{1 + 2u^{(i)}}. \tag{1.7}$$

If we consider stable bodies, the distance between two points is always larger than its relative variation $(dx' - dx)/dx = \sqrt{1 + 2u^{(i)}} - 1 \approx u^{(i)}$, and the deformation is small. However, small deformation does not imply small displacement. As a matter of fact, objects in which one dimension is tiny with respect to the others can undergo small deformations, but they are still described by a large displacement[1]. Nonetheless, for extended objects, the displacement vector is always very small, and we approximate the equation (1.5) for the strain tensor by keeping only the linear terms

$$u_{ij} \approx \frac{1}{2}\left(\partial_j u_i + \partial_i u_j\right) \equiv \partial_{(i}\, u_{j)}. \tag{1.8}$$

To conclude this discussion, let us see how the deformation of an elastic body reflects on a physical quantity that can be easily measured, for example, an infinitesimal volume element dV. In general, the determination of the principal values $\{u^{(i)}\}$ and the principal axis of a generic tensor is a pretty demanding approach. However, we want to convey that the eigensystem analysis is unnecessary because we can express sensible physical quantities using tensor invariants instead. According to (1.7), a deformation transforms a volume element $dV = dx_1 dx_2 dx_3$ into

$$dV' = dV(1 + u^{(1)} + u^{(2)} + u^{(3)}). \tag{1.9}$$

The trace of a Cartesian tensor is an invariant. Hence, we can use the expression for the trace of the strain tensor in the original coordinate systems instead of going through diagonalisation procedures. The new volume element is

$$dV' = dV(1 + u_{ii}). \tag{1.10}$$

The relative volume change in a deformed body associated with a given displacement field **u** is the sum of the diagonal components of the strain tensor, hence

[1] As an example, think about lifting a heavy boot with a fishing rod: the rod will be drastically bent.

$(dV' - dV)/dV = u_{ii}$.
In the following sections, we will come back to a general decomposition of strain into two parts, *dilations* and *shears*.

1.3 Stress

A spring is the most straightforward system that shares with elastic solids the fundamental property of reacting to deformation. Thus, we can understand *elasticity theory* as an infinite collection of springs at every point in space, that oppose forces to stretches. We have already clarified that in elastic systems strain plays the role of stretch. Now, we will see how the role of forces is embedded into a quantity known as *stress*.
As in the case of a spring, all the parts of an undeformed elastic body are in mechanical equilibrium. Thus, we assume that the net force which acts on them from the surrounding environment vanishes. Under strain, the elementary constituents (atoms, molecules, grains) try to get the body back to its equilibrium position, giving rise to internal forces.
One of the assumptions of elasticity theory is that the scale at which the constituents' interactions happen is microscopic, while the scales of phenomena that it describes are macroscopic. There is a clear separation of scales: the effect of short-range forces on a given element of the body can be considered at large scales as contact interactions through its enclosing surfaces.
We examine the sum of all force densities f_i that act on an infinitesimal volume element dV. We want to rewrite $\int dV\ f_i$ only in terms of forces that act through the surface of dV. We employ *Stokes theorem*[2], at the price of introducing a second-rank tensor T_{ij} whose divergence is the force

$$\partial_j T_{ij} = f_i. \tag{1.11}$$

The sum of forces acting on a volume element of an elastic body can thus be expressed using T_{ij}, as

$$\int dV\ f_i = \int dV\ \partial_k T_{ij} \to \oint_{\partial V} dS_k\ T_{ik}. \tag{1.12}$$

We arrived at the second local quantity that describes elastic solids, the *stress tensor*[3] T_{ij}. If the surrounding medium exerts a force along the outer surface

[2]Stokes theorem is usually presented in basic electromagnetism and permits to transform volume integrals of the divergence of the electric field (a scalar) into integrals of the vector field through the enclosing surface, $\int\ dV\ (\partial_k E_k) = \oint_{\partial V}\ dS_k\ E_k$.

[3]Some authors use a different sign convention, where they define the stress tensor as the net force per unit area that the body exerts on its surroundings, rather than the opposite.

normal, T_{ij} is positive. If the surrounding medium exerts a force inward, T_{ij} is negative [19].

Force balance conditions

For a body at equilibrium, internal stresses should not give rise to any forces, so $\partial_j T_{ij} = 0$ holds. However, in the case of a body of density ρ immersed in a force field, as the gravitational field, the equilibrium condition that must be fulfilled is $\partial_j T_{ij} + \rho g_i = 0$.
If the body is subject to forces $(f_{\text{ext}})_i$ applied to its external surface with normal n_j, we must solve the equilibrium condition by also including the boundary condition $T_{ij} n_j = (f_{\text{ext}})_i$.

1.3.1 Considerations around the stress tensor

For elastic systems in d spatial dimensions, the number of components of the stress tensor T_{ij} is d^2. However, on general grounds, we argue that the number of independent components is reduced to $d\,(d+1)\,/2$ because T_{ij} is symmetric. In three dimensions, we infer this property by imposing that torque $m_i = \epsilon_{ijk} f_j r_k$ which acts on the infinitesimal volume element should act only through its boundaries, analogously to what we did for $\int dV\, f_i$. By using (1.11), we obtain as total torque $\int dV\ \epsilon_{ijk}(\partial_p T_{jp}) r_k = \int dV \epsilon_{ijk} \partial_p [T_{jp} r_k] - \int dV \epsilon_{ijk} T_{jk}$. While we can work out the first integral using the divergence theorem, the second term in

$$\oint dS_p \epsilon_{ijk} T_{jp} r_k - \int dV \epsilon_{ijk} T_{jk} \tag{1.13}$$

must vanish. Otherwise, we face the inconsistency of having volume forces. Because the integral that has to vanish contains the contraction of T_{jk} with the antisymmetric symbol, the stress tensor has to be symmetric, $T_{ik} = T_{ki}$.
Despite being irrelevant for our work, it is still interesting to point out that nonsymmetric stress tensors arise in Cosserat or micropolar theories [20, 21]. In these theories, the constituents of the system have internal orientational properties [22].

1.3.2 Examples of stress

Apart from the symmetric condition, stress can be arbitrarily complicated. As a result of this, we want to illustrate and explicitly compute three simple examples. Then we provide a general understanding, by using the properties of Cartesian tensors in three dimensions.

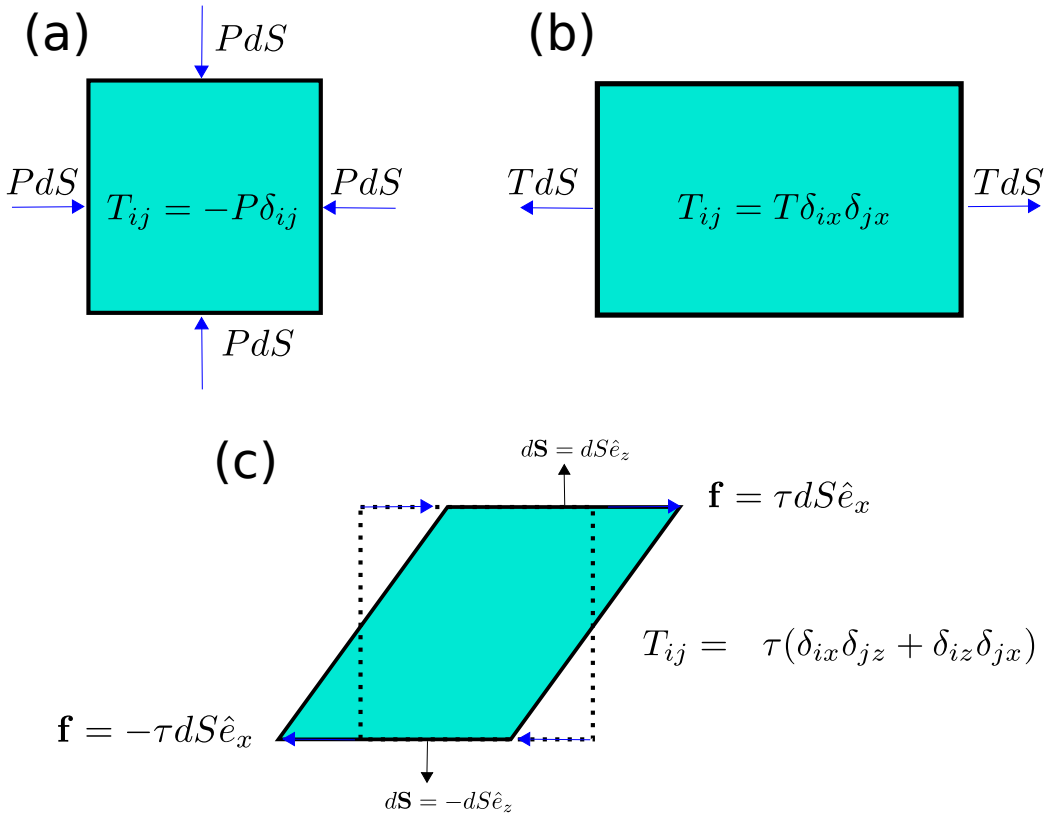

Figure 1.2: Three types of stress: uniform compression (a), tension (b) and shear (c). For simplicity, the images depict two-dimensional objects.

- The simplest example of stress that we can imagine is *uniform compression*, analogous to *hydrostatic pressure*. We can think of the effect a fluid exerts on a solid body immersed in it: pressure will isotropically push every body's surface inwards. In such a situation, the force is $f_i = -PdS_i$ or, in terms of the stress tensor,

$$T_{ik} = -P\delta_{ik}, \tag{1.14}$$

  i.e. all the elements of T_{ik} are equal and belong to the diagonal. Pressure is the only stress force that normal fluids at rest can sustain.

- *Tension* is a type of uniaxial stress in which forces are oriented along only one direction of the solid, outwards with respect to its enclosing surfaces. In this respect, they act in the opposite sense compared to pressure. For instance, tension applied in the horizontal direction, is described by the stress

$$T_{ij} = T\delta_{ix}\delta_{jx}. \tag{1.15}$$

  In the *isotropic body*, tension leads to the concepts of *Young modulus* and *Poisson ratio*, whose role will be fundamental, later on, in this dissertation.

- Shear forces are tangential forces that act perpendicularly with respect to the surface they are applied to. In Fig. 1.2 we introduce a shear deformation that makes parts of the body at equal height glide with respect to each others. Since the volume is preserved, the trace of the corresponding stress tensor vanishes.

1.3.3 Intermezzo: irreducible representations of a tensor in Euclidean space

The number of components N of a tensor can become unbearable, increasing the rank and the dimension of the space. It is usually very convenient to decompose a tensor into the sum of parts that are "as small as possible" [23], so that they realise *irreducible representations* of the rotation group, built by acting linearly with the metric $g_{ij} = \delta_{ij}$ on the original tensor. For example, a second-rank tensor C_{ij} in d dimensions has $N = d^2$ independent components, which can be arranged in smaller tensors as:

1. The simplest object we can realise is a contraction with the metric, the trace $C_{ii} \equiv \delta_{ij}C_{ij}$. The trace is a scalar, so the number of independent components is $N_t = 1$.

2. The antisymmetric part $R_{ij} \equiv C_{[i,j]}$. In three dimensions, the number of independent components is $N_a = 3$.

3. The symmetric, traceless, *deviatoric* part $\tilde{C}_{ij} \equiv C_{(i,j)} - \frac{1}{d} C_{ii}\delta_{ij}$ [24]. In three dimensions, the fact that the deviatoric part comes from a symmetrisation procedure reduces the number of independent components to 6, and the vanishing of the trace reduces it furthermore, down to $N_d = 5$.

There are no smaller parts that we can obtain by combining linearly C_{ij}, δ_{ij} and the Levi–Civita symbol ϵ_{ij}.
We rewrite the original tensor as the combination of its irreducible representations

$$C_{ij} = \frac{C_{ii}}{d}\delta_{ij} + \tilde{C}_{ij} + R_{ij} \tag{1.16}$$

where, naturally, $N = N_t + N_a + N_d$.
The dimension of the irreducible representations of SO(3) is always odd, and it is labeled by $N_{\text{irr}} = 2l + 1$. Therefore, the three irreducible tensorial parts of a second rank tensor in three dimensions are $l = 0$ (the trace part, a spherical tensor), $l = 1$ (the antisymmetric part), $l = 2$ (the deviatoric part).

Irreducible parts of strain

At the beginning of this chapter, we have conveyed that the gradient of the displacement field $\partial_i u_j$ is the main actor of elastic systems. In this case, its irreducible parts have a straightforward physical interpretation:

1. The trace u_{ii} expresses changes in volume of the body, expansions and compressions. It already appeared in (1.10).

2. The antisymmetric part R_{ij} expresses rotations that do not deform the original body but only change its global orientation. Elastic materials do not change shape under rotations, so there is no point in considering this part of $\partial_i u_j$. Instead, it is more thoughtful to remove the antisymmetric part by working directly with symmetrised *strain tensor*, which we introduced in (1.5).

3. The deviatoric part expresses deformations that transform an object's shape but preserve its volume. For example, the pure shear deformation represented in Fig. 1.3 is given by the displacement $\mathbf{u} = \varepsilon\,(y, x)$ and corresponds to the traceless strain tensor $u_{ij} = \left(\begin{smallmatrix} 0 & \varepsilon \\ \varepsilon & 0 \end{smallmatrix}\right)$

The decomposition of the symmetrised strain tensor into a sum of its irreducible parts, which are compressions and shears, is

$$u_{ij} = \frac{1}{d}u_{kk}^2\delta_{ij} + \left(u_{ij} - \frac{1}{d}u_{kk}^2\delta_{ij}\right) \equiv \frac{1}{d}u_{kk}^2\delta_{ij} + \tilde{u}_{ij}. \tag{1.17}$$

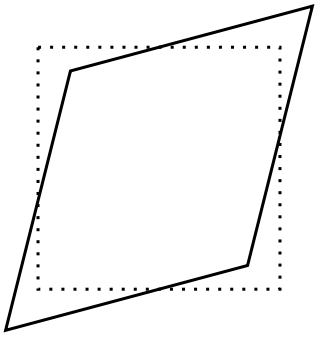

Figure 1.3: A pure shear deformation applied to the dotted square transforms it into a parallelogram with the same area.

1.4 Elastic energies

We have understood that we can think of elastic materials as continuous, higher dimensional versions of the simple spring. Hence, it is also natural to assume a linear relationship between stress and strain analogous to Hooke's law[4]. Therefore, we encode the cost of deforming a body that otherwise is at equilibrium into an elastic energy quadratic in strain

$$\mathcal{E}_{\text{el}} = \frac{1}{2} K_{ijkl} u_{ij} u_{kl}. \tag{1.18}$$

Instead of a single spring constant k, we have introduced a fourth rank tensor K_{ijkl}, called *elastic modulus tensor*. The number of components of a fourth rank tensor scales rapidly with the dimension d of space, as d^4. Fortunately, many of the elements of K_{ijkl} are equal to each others by construction. Given that the strain tensor u_{ij} is constructed as a symmetric object, also K_{ijkl} is invariant under permutations $i \leftrightarrow j$ and $k \leftrightarrow l$. Furthermore, since the elastic energy (1.18) is quadratic in strains, also K_{ijkl} should be invariant under swaps $ij \leftrightarrow kl$. Already

[4]Although we only consider situations where the proportionality between stress and strain is linear (Hookean), we can easily imagine that materials exhibit upper bounds where this relationship is no longer valid. If this were not the case, springs in cars' shock absorbers would fulfil their purpose forever. Unfortunately, this is not the case. After having passed the direct proportionality between stress and strain, there is a regime in which the material is still elastic (when unstressed, it goes back to its original shape), but the behaviour is not anymore just linear. After having passed the elastic limit, the material gets permanently bend. Increasing further the stress, arrived at the *yield* limit, the material begins to show *plasticity*: very little stress causes enormous strains to the system. At last, at the *rupture point*, the material cracks. To give some numbers: for most solids, the elastic and yield points are small numbers, with the notable exception of rubber, that is elastic until stretches that are approximately eight times its original size, and that it is seldom in the Hookean regime.

these symmetries

$$K_{ijkl} = K_{jikl} = K_{ijlk} = K_{jilk} = K_{klij} \tag{1.19}$$

considerably reduce the number of independent components. In three dimensions the reduction is from $3^4 = 81$ to 21, and in two dimensions from $2^4 = 16$ to 6. Apart from the above trivial symmetries, the solid under investigation's point symmetries decrease even more the number of independent components of K_{ijkl}. The more symmetric the solid, the less the number of independent *elastic moduli*.

1.4.1 Two-dimensional elastic energies

For research's purposes which we reported in this thesis, we limit ourselves to the two-dimensional case. There is one element per direction with four equal indices (K_{xxxx}, and K_{yyyy}), two elements with two equal indices ($K_{xxyy} = K_{yyxx}$), four elements with two couples of mixed indices ($K_{xyxy} = K_{yxxy} = K_{xyyx} = K_{yxyx}$), and twice four with three same indices ($K_{xxxy} = K_{xxyx} = K_{xyxx} = K_{yxxx}$ and $K_{yyyx} = K_{yyxy} = K_{xyyy} = K_{yxyy}$). Putting all the pieces of information together, the density of the free energy (1.18) in two dimensions is proportional to

$$K_{ijkl}u_{ij}u_{kl} = K_{xxxx}u_{xx}^2 + K_{yyyy}u_{yy}^2 + 2K_{xxyy}u_{xx}u_{yy} + \tag{1.20}$$

$$+ 4K_{xxxy}u_{xx}u_{xy} + 4K_{yyxy}u_{yy}u_{xy} + 4K_{xyxy}u_{xy}^2. \tag{1.21}$$

1.4.2 Isotropic body

In elastic media, the concept that realises the highest possible symmetry is called the *isotropic body*. In such a medium, all physical properties do not on a specific direction: none is special. Thus, the isotropic body sounds like a very tempting but irrealistic concept to describe real systems. Still, surprisingly, most of the materials fall into this description if we use the concept of scale separation.

- It is usually the situation that real materials, such as polycrystalline metals, have a microscopic structure that is ordered and periodic, but is arranged in randomly oriented grains. On scales that are much larger than the microscopic ordered one, the orientation of individual grains is averaged out by all the others [25], and the material behaves isotropically [26]. Glasses lack long-range order, so we can consider them isotropic as well. Furthermore, for crystalline solids, the continuum approximation holds on scales that are larger than 10^{-8} m [27].

- Even our current comprehension of the Universe relies on the assumption that the Universe, seen on sufficiently large scales, is isotropic and homogeneous: these are the essential ingredients of the *cosmological principle*.

Figure 1.4: Kepler in [29] depicted the position of Earth ('M', for Latin "Mundus") as just one of many other celestial bodies. Interestingly enough, Kepler represented the isotropic Sky as a triangular lattice.

> The principle fulfils the Copernican requirement that neither the Sun nor the Earth should be privileged points of observation of our Universe (see Fig. 1.4). We notice stellar systems, galaxies and clusters in preferred directions only because we do not look distant enough. It took until the end of the twentieth-century [28] to experimentally prove -through redshift surveys- that the Universe, coarse-grained over distances of $100\ \mathrm{Mpc}$, is isotropic until the largest distance observable, $3000\ \mathrm{Mpc}$.

To describe the isotropic body, we have to construct a sensible elastic moduli tensor K_{ijkl} composed of smaller tensors that are themselves isotropic. If the aim is to realise fourth rank tensors, there is no other possible choice than to combine two Kronecker deltas

$$K_{ijkl} = \lambda\ \delta_{ij}\delta_{kl} + a\ \delta_{ik}\delta_{jl} + b\ \delta_{il}\delta_{jk}. \tag{1.22}$$

The requirement that the permutation symmetries (1.19) should be satisfied imposes the condition $a = b \equiv \mu$,

$$K_{ijkl} = \lambda\ \delta_{ij}\delta_{kl} + \mu(\delta_{ik}\delta_{jl} + \delta_{il}\delta_{jk}). \tag{1.23}$$

The coefficients λ, μ are characteristic of the system under investigation, and they are called *Lamé coefficients*.

The elastic energy density (1.18) for the isotropic body is

$$\mathcal{E}_{\rm el} = \frac{1}{2}\left[\lambda u_{ii}^2 + 2\mu (u_{il})^2\right]. \tag{1.24}$$

Following the spirit of previous discussions, it often is more convenient to split strain into its irreducible parts, that have a neat physical interpretation. Using the decomposition of the strain tensor (1.17) we arrive[5] at the elastic energy of the isotropic body being

$$\mathcal{E}_{\rm el} = \frac{1}{2}\left[\left(\lambda + \frac{2\mu}{d}\right) u_{ii}^2 + 2\mu\left(\tilde{u}_{il}\right)^2\right] \tag{1.25}$$

$$= \frac{1}{2}\left[B u_{ii}^2 + 2\mu(\tilde{u}_{il})^2\right]. \tag{1.26}$$

The coefficient in front of the trace part is called the *bulk modulus* $B \equiv \lambda + 2\mu/d$. It depends on dimensionality and expresses the body's resistance to altering its volume. The parameter μ is called the *shear modulus* and measures the solid's resistance to shearing. Since every strain introduced in a system at equilibrium should increase the internal energy, $\mathcal{E}_{\rm el}$ is minimum for zero strain $u_{ij} = 0$. Hence, in the isotropic body, both B and μ are positive.

Order of magnitude of elastic constants for various materials To evaluate the value of the elastic constants that compose the elastic moduli tensor K_{ijkl} requires a microscopic understanding of the given substance that, in general, is difficult to obtain. However, we can understand the order of magnitude using a fly by night approach [30]. Strain is a dimensionless quantity. Therefore, elastic constants should have the dimension of energy densities. In ordinary solids, a reasonable choice is

$$[K] = \frac{[\text{binding energy}]}{[\text{interparticle spacing}]^3}. \tag{1.27}$$

In an ionic solid (NaCl, for example), the binding energy is of the order of a few eV, while the separation between particles is of the order of a couple of Ångstroms. Thus we can estimate the values of the elastic moduli to be about $20\ \mathrm{GPa}$[6]. In the following table, we report a comparison of the measured values of elastic moduli for cubic[7] and isotropic solids that elucidates why certain materials appear more rigid than others.

[5] The deviatoric tensor $\tilde{u}_{ij}$ is traceless, $(u_{ij})^2 = u_{ii}^2/d + (\tilde{u}_{ij})^2$.

[6] 1 GPa $= 10^{10}$ Dyn/cm^2, 1 Dyn = 10^{-5}N, 1 eV $= 1.6 \times 10^{-19}$J.

[7] In a cubic crystal, the bulk modulus is given by $B = (K_{11} + 2K_{12})/3$.

	Elastic Moduli (GPa)
Air	$B = 10^{-4}$, $\mu = 0$
Water	$B = 2$, $\mu = 0$
NaCl [31]	$K_{11} = 48.70$, $K_{12} = 13.11$, $K_{44} = 12.66$ ($B = 24.97$)
Copper	$B = 130$, $\mu = 45$
4340 Steel [32]	$B = 210$, $\mu = 83$
Diamond [27]	$K_{11} = 1760$, $K_{12} = 125$, $K_{44} = 576$ ($B = 670$)

Table 1.1: Bulk modulus B for various ordinary materials.

1.4.3 Relation between stress, strain and free energy

We derive the relation between strain, stress and free energy by considering the work done W by a force in displacing a volume element by the infinitesimal amount δu_i. Assuming that the stress tensor T_{ik} is symmetric and integrating by parts, we get $W = -\int dx\ T_{ik}\delta u_{ik}$. At a constant temperature, the change in free energy given by internal forces is minus the work done, consequently we obtain

$$T_{ij} = \frac{\delta \mathcal{E}_{\text{el}}}{\delta u_{ij}}. \tag{1.28}$$

For the isotropic body in d dimensions, then it must hold that the relation between stress and strain is

$$T_{ij} = \left(\lambda + \frac{2\mu}{d}\right) u_{ll}\delta_{ij} + 2\mu\tilde{u}_{ij} = Bu_{ll}\delta_{ij} + 2\mu\tilde{u}_{ij}, \tag{1.29}$$

or the dimension-independent equivalent form in terms of Lamé parameters,

$$T_{ij} = \lambda u_{ll}\delta_{ij} + 2\mu u_{ij}. \tag{1.30}$$

If, instead, we want the inverse form, namely strain in terms of stress, its expression is

$$u_{ij} = \left(\frac{1}{Bd^2}\right) T_{ll}\delta_{ij} + \frac{1}{2\mu}\tilde{T}_{ij} = \left(\frac{1}{Bd^2} - \frac{1}{2\mu d}\right) T_{ll}\delta_{ij} + \frac{1}{2\mu}T_{ij}. \tag{1.31}$$

As we already encountered various types of stresses earlier on (see (1.14) and (1.15)), now we want to understand how the isotropic body deforms -how it produces strains- as a reaction to those particular kinds of stress.

Uniform compression

The isotropic body reacts to compression by producing strains that are $u_{ij} = -[P/(Bd)]\delta_{ij}$. According to (1.10), the relative volume change is the strain tensor's trace, $\Delta V = u_{ll} = -P/B$. For positive pressure, the isotropic body reacts by reducing its volume with proportionality that is inverse to the compressional modulus B. The bulk modulus is related to the *isothermal compressibility* as $B = 1/\kappa = VdP/dV$.

Uniaxial stress

A couple of forces that pulls only one set of opposite faces of a solid is an example of uniaxial stress (see again Fig. 1.2). If we orient both forces along the surfaces' normals (outwards), the corresponding stress is called *tension*, and we denote its magnitude as T. If pulling happens in the horizontal direction, the produced stress is $T_{ij} = T\delta_{ix}\delta_{jx}$, and, by using (1.31), we obtain the corresponding strain

$$u_{ij} = \delta_{ij}\left[T\left(\frac{1}{Bd^2} - \frac{1}{2\mu d}\right)\right] + \delta_{ix}\delta_{jx}\left(\frac{T}{2\mu}\right). \tag{1.32}$$

There are two inequivalent classes of strain, the one that arises in the direction of elongation ($u_{\rm e} \equiv u_{xx}$)

$$u_{\rm e} = \frac{T}{d}\left[\frac{d-1}{2\mu} + \frac{1}{Bd}\right], \tag{1.33}$$

and the strain produced in the orthogonal directions, $u_{\rm o} \equiv u_{yy}$ (in two dimensions) or $u_{\rm o} \equiv u_{yy} = u_{zz}$ (in three dimensions)

$$u_{\rm o} = \frac{T}{d}\left[-\frac{1}{2\mu} + \frac{1}{Bd}\right]. \tag{1.34}$$

Quite intuitively, $u_{\rm e}$ possesses the same sign of tension: pulling ($T > 0$) implies elongation, while pushing ($T < 0$) implies contraction.
The sign's dependence of $u_{\rm o}$ on the combination $[-(2\mu)^{-1} + (Bd)^{-1}]$ is less trivial and suggests there might be situations in which normal intuition fails (that an object will necessarily contract in the directions orthogonal to stretching). Tension produces a volume variation (1.10) which is $\Delta V = TB/d$.
The ratio between the applied tension T and strain in the stressed direction defines the *tensile* or *Young's modulus*

$$Y \equiv \frac{T}{u_{\rm e}} = \frac{2\mu Bd^2}{Bd(d-1) + 2\mu} = \begin{cases} \dfrac{9B\mu}{3B+\mu}\,, & \text{(3D)} \\ \\ \dfrac{4B\mu}{B+\mu}\,, & \text{(2D)} \end{cases}. \tag{1.35}$$

A material with large Young's modulus is stiff and tries to oppose to elongation when subject to tension.
The ratio between the two different strains in the isotropic body defines (minus) a dimensionless constant known as the *Poisson ratio*

$$\sigma \equiv -\frac{u_{\rm o}}{u_e} = \frac{Bd - 2\mu}{Bd\,(d-1) + 2\mu} = \begin{cases} \dfrac{1}{2}\left(\dfrac{3B - 2\mu}{3B + \mu}\right) , & (3\text{D}) \\ \\ \left(\dfrac{B - \mu}{B + \mu}\right) , & (2\text{D}). \end{cases} \tag{1.36}$$

In contrast to elastic moduli, which are necessarily positive to ensure the system's stability, the Poisson ratio can have a negative sign. However, while bulk B and shear μ moduli can have arbitrary magnitude, the Poisson ratio can take values only within the numerical intervals

$$-1 \leq \sigma \leq 1/2\,, \qquad (3\text{D}) \tag{1.37}$$

$$-1 \leq \sigma \leq 1\,, \qquad (2\text{D}). \tag{1.38}$$

Very incompressible 3D materials, such as rubbers and liquids, discourage volume changes while favouring shape changes ($B \gg \mu$). Hence, they saturate the Poisson ratio's upper bound, $\sigma \to 1/2$. Most engineering materials, both the very stiff (metals), but also the very complaint (polymers) lie in the range $0.25 < \sigma < 0.42$. Despite their elastic moduli have several orders of magnitude of difference, the ratio B/μ is roughly the same. Gases exhibit $\sigma \to 0$. Materials that possess very rigid links and struts in the directional orthogonal to load oppose transverse deformations when stretched [33]. A notable example is cork, used to seal wine bottles, among other historical and biological reasons, because it exhibits $\sigma = 0$ thanks to its microscopic honeycomb structure.
Until the late eighties, it was believed that stable isotropic materials with negative Poisson ratio $\sigma \in (-1, 0)$ would not exist[8]. These materials would have enjoyed the counter-intuitive property to expand in the orthogonal direction when stretched and to contract when compressed. These materials, now known as *auxetic*, were first proven to exist in re-entrant foams [35] and in mechanical models of hinged polygons that are free to rotate [36]. Applications of this peculiar quality were envisaged already in [37] and, in the last years, have found practical applications even in day-to-day objects. For instance, auxetic metamaterials are used to construct soles for running shoes [38].

[8]However, certain brilliant people were not excluding the existence of auxetic materials already during the sixties [34].

1.5 Elastodynamics

Up to this point, we have considered how non-homogeneous displacements $\mathbf{u}(\mathbf{x})$ give rise to *strain* and how an elastic system responds to it by producing *stress*, and therefore, internal forces f_i^{stress}. So far, we have not considered situations in which displacements $u(\mathbf{x}, t)$ depend on time as well. For this reason, here we investigate disturbances that propagate through a solid in the form of *elastic waves*. Newton's second law prescribes that the evolution of momentum under the effects of both internal and external forces follows $\partial_t (\rho \dot{u}_i) = f_i^{\text{stress}} + f_i^{\text{ext}}$. In principle, this is a complicated equation, where the whole triplet ρ, $\mathbf{u}$, $\dot{\mathbf{u}}$ should be determined. We can linearise it by remembering that we always consider small displacements in the case of extended bodies and linear elasticity. If we also assume that density variations around a static equilibrium distribution are minor or that density is constant throughout the system, we arrive at the linearised equation

$$\rho \ddot{u}^i = \partial_j T_{ij}. \tag{1.39}$$

The expression of the stress tensor T_{ij} that we use depends on the physical system we investigate.
As our prime example, we consider the isotropic body and its expression of T_{ij} (1.30). Apart from the apparent structural engineering case, the propagation of elastic waves in isotropic bodies is also fundamental in geophysical sciences. In fact, Earth can be considered an isotropic body, to a first approximation. We will see less traditional systems that behave as isotropic bodies in Chapter 3 and Chapter 4.
In the previous sections, we constructed T_{ij} using symmetry arguments and found that it contains two material Lamé parameters, λ and μ (1.30). We also noticed that the irreducible parts of T_{ij} are directly related to the bulk B and shear μ moduli, see (1.29). We further remark that only B inherits the dependence of the solid's dimensionality from λ.
If the typical scale of variations of the material parameters (λ, μ or B, μ) is much larger than the scale of variations introduced by disturbances, the elastic moduli can be considered constant, and the dynamical equation (1.39) leads to

$$\rho \ddot{u}^i = (\lambda + \mu)\partial_i(\partial_j u_j) + \mu \partial^2 u_i. \tag{1.40}$$

We consider the bulk of the system, where the system is translationally invariant. Assuming plane waves as solutions $\mathbf{u}(\mathbf{x}, t) \sim \exp[i(\mathbf{k} \cdot \mathbf{x} - \omega(\mathbf{k})t)]$, and $k \equiv |\mathbf{k}|$, the above equation becomes algebraic

$$\rho\, \omega^2 u_i = (\lambda + \mu)k_i(k_j u_j) + \mu k^2 u_i, \tag{1.41}$$

where the solution of frequency $\omega(\mathbf{k})$ with respect to wavevector determines the *dispersion relation*. We decouple the previous equations into orthogonal subspaces, by using the transverse $P^{\mathrm{t}}_{im} \equiv \delta_{im} - (k_i k_m)/k^2$ and longitudinal $P^{\mathrm{l}}_{im} \equiv (k_i k_m)/k^2$ projectors. The displacement field splits into the sum $u_i = u^{\mathrm{t}}_i + u^{\mathrm{l}}_i$ of its transverse $u^{\mathrm{t}}_i \equiv P^{\mathrm{t}}_{im} u_m$ and longitudinal $u^{\mathrm{l}}_i \equiv P^{\mathrm{l}}_{im} u_m$ components

$$\rho\omega^2 u_i = (\lambda + 2\mu) k^2 u^{\mathrm{l}}_i + \mu k^2 u^{\mathrm{t}}_i. \tag{1.42}$$

By taking in one case the curl of (1.42), and in the other case the divergence, we obtain two set of equations that depend exclusively on either u^{t}_i or u^{l}_i. Solutions for ω in term of $k = |\mathbf{k}|$ results in two modes that disperse linearly with wavenumber. The respective group velocity $v_{\mathrm{g}} \equiv d\omega/dk$ and phase velocity $v_{\mathrm{ph}} = \omega/k$ of the two modes coincide: if we construct a wavepacket, all its components will progress at the same speed. Therefore, the wave equation (1.42) is non-dispersive.

1.5.1 Transverse mode

The transverse mode u^{t}_i is an excitation in which the displacement field vibrates in the direction orthogonal to the advance of the wave, as it happens for vibrations of musical instruments' strings. In other words, the vector field is incompressible $k_i u^{\mathrm{t}}_i = 0$ and does not produce any volume variations in the sample[9]. In three dimensions u^{t}_i has two polarization, while, in two dimensions, it has only one. The transverse's mode dispersion relation is linear $\omega_t = c_t |\mathbf{k}|$ with speed

$$c_t \equiv \sqrt{\frac{\mu}{\rho}} \tag{1.43}$$

which depends only by the shear modulus in any dimension.

1.5.2 Longitudinal mode

The longitudinal mode u^{l}_i is an excitation in which the displacement field oscillates in the direction parallel to the direction of propagation of the wave. The vector field is irrotational $\epsilon_{mi} k_m u^{\mathrm{l}}_i = 0$ and produces volume variations $u^{\mathrm{l}}_{ii} \neq 0$. The longitudinal mode's dispersion is linear $\omega_l = c_l |\mathbf{k}|$ hence it is analogous to pressure waves and sound modes in fluids. However, the solid's ability to sustain

[9] Volume variations are given by the trace of the correspondent strain tensor, see the discussion around (1.10).

shear enhances the longitudinal speed

$$c_l \equiv \sqrt{\frac{\lambda + 2\mu}{\rho}} = \left(\frac{B + 2\mu\left(d-1\right)/d}{\rho}\right)^{1/2} = \begin{cases} \left(\dfrac{B + 4\mu/3}{\rho}\right)^{1/2}, & \text{(3D)} \\ \left(\dfrac{B + \mu}{\rho}\right)^{1/2}, & \text{(2D)} \end{cases} \tag{1.44}$$

due to the term $2\mu\left(d-1\right)/d$.
In any isotropic material that has non-zero compressibility modulus B, the longitudinal mode always travels faster than the transverse ones. In the case of two-dimensions and for $B = 0$, the two sound speeds coincide $c_s = c_t$.

1.6 Surface waves in elastic media

When an elastic medium has boundaries, we must supplement equations of motion with the boundary conditions regarding how the system behaves at its free surfaces.
Fascinating surface excitations already emerge if we consider a system that is bounded along one direction by vacuum. The investigation of waves that propagate along the free surface of an elastic solid and whose disturbance remains confined to the vicinity of the boundary is an old topic that goes back to the remarkable classic paper by Lord Rayleigh. In [39], Rayleigh numerically obtained a solution for the dispersion relation of such waves, known today as Rayleigh waves. He even suggested that those surface waves might play a crucial role in seismology [40].
Therefore, we restrict our discussion to an infinite solid in x and z directions, whereas it extends semi-indefinitely for $y < 0$, and possesses a free surface at $y = 0$. In three dimensions, we are not interested in the dependence in the z-direction.
There should be no force or transfer of momentum between the medium and vacuum, so we impose zero stress in the direction defined by the normal to the bounding surface, in this case, $\hat{n} \equiv (0, 1, 0)$ and

$$T_{ij} n_j \stackrel{!}{=} 0. \tag{1.45}$$

The above condition requires three strain tensor components to vanish, $T_{xy} = T_{yy} = T_{zy} \stackrel{!}{=} 0$.
In elastodynamics contexts, we usually have access to displacements **u** and want

to evaluate stress. Therefore, we express T_{ij} in terms of the Lamé parameters (1.30)

$$T_{xy} = 2\mu u_{xy} \tag{1.46}$$
$$T_{yy} = \lambda u_{xx} + (\lambda + 2\mu)\, u_{yy} + \lambda u_{zz} \tag{1.47}$$
$$T_{zy} = 2\mu u_{zy}. \tag{1.48}$$

While, in the previous section, we studied plane waves in the bulk of a translationally invariant system, here we want to focus on solutions that travel along the horizontal direction, but that remain close to the free surface, i.e. solutions that are exponentially suppressed in the negative y direction. This motivates the ansatz $\mathbf{u}\,(x, y, t) \sim \mathbf{u}\, \exp\left[i\,(kx - \omega t)\right] \exp\left[\kappa\,(k, \omega)\, y\right]$. We obtain the dependence of κ on k and ω by replacing $k_x \to k$ and $k_z \to -i\kappa$ in the solutions obtained for the bulk of the system

$$\kappa_t(k, \omega) = \sqrt{k^2 - \omega/c_l^2} \quad , \quad \kappa_t(k, \omega) = \sqrt{k^2 - \omega/c_l^2}. \tag{1.49}$$

We are interested only in stable surface excitations. Hence, we restrict our attention to the case in which κ, the inverse of penetration length, is real and positive. To achieve this requirement, we impose the square root's argument in the expression for (1.49) to be positive or, equivalently, that the frequency of surface excitations ω must live outside of the light-cones defined by the transverse and longitudinal speeds, $\omega < \omega_t \leq \omega_l$.
The third boundary condition (1.48) on T_{zy} and the above ansatz implies that the z component of $\mathbf{u}$ identically vanishes

$$T_{zy} = 2\mu u_{zy} = \partial_z u_y + \partial_y u_z = \partial_y u_z \stackrel{!}{=} 0 \longrightarrow u_z = 0. \tag{1.50}$$

For the reason that speeds of sound can be directly measured in a material, it is common [18] to substitute the Lamé parameters in favour of c_t and c_s and to rewrite the other two boundary conditions (1.46) and (1.47) as

$$\begin{aligned} (c_l^2 - 2c_t^2) u_{xx} + c_l^2 u_{yy} &= 0 \\ u_{xy} &= 0. \end{aligned} \tag{1.51}$$

Within the exponential ansatz, polarizations of the transverse and longitudinal modes are $u_{t,x}/u_{t,y} = i\kappa_t/k$ and $u_{l,x}/u_{l,y} = ik/\kappa_l$. As displacement $\mathbf{u}$ we use a linear combination of the transverse and longitudinal modes

$$\mathbf{u} = e^{ikx} \left[a\,(\kappa_t, -ik)^{\mathrm{T}}\, e^{\kappa_t y} + b\,(k, -i\kappa_l)^{\mathrm{T}}\, e^{\kappa_l y} \right]. \tag{1.52}$$

Inserting (1.52) into (1.51) and after manipulation, we obtain a matrix equation for the unknowns a and b

$$\begin{pmatrix} 2k\sqrt{k^2-\omega^2/c_t^2} & 2k^2-\omega^2/c_t^2 \\ 2k^2-\omega^2/c_t^2 & 2k\sqrt{k^2-\omega^2/c_l^2} \end{pmatrix} \begin{pmatrix} a \\ b \end{pmatrix} = 0. \tag{1.53}$$

We get the dispersion relation of surface waves $\omega(k)$ by setting the determinant of the above matrix to be zero. Since we expect to find a linear mode, we use the ansatz $\omega(k) = \chi c_t k$ in the determinant equation, which becomes

$$\chi^6 - 8\chi^4 - 8\chi^2\left[2\left(\frac{c_t^2}{c_l^2}\right) - 3\right] + 16\left[\left(\frac{c_t^2}{c_l^2} - 1\right)\right] = 0. \tag{1.54}$$

Solutions for χ express the speed of propagation of the surface wave $c_R \equiv \chi c_t$ and, for this reason, acceptable solutions for χ must be real, positive, and smaller than one. Until this point, we have considered the three-dimensional case. However, the identical considerations and procedures also hold for two dimensions, apart from those regarding u_z (1.50), that are not necessary. The only dimensionality dependence hides in the longitudinal sound speed (1.44).
Instead of looking for solutions for χ in terms of the ratio c_t/c_s, it is more practical to express χ in terms of the Poisson ratio σ (1.36). In fact, assuming the thermodynamic stability of the system, σ has narrow bounds, see (1.37) and (1.38). In addition, σ is a static property of the system, so that it is easier to measure than sound speeds. Notice that

$$\frac{c_t^2}{c_l^2} = \frac{1+\sigma-d\sigma}{2+4\sigma-2d\sigma} = \begin{cases} \dfrac{1-2\sigma}{2-2\sigma}\,, & \text{(3D)} \\ \\ \dfrac{1-\sigma}{2}\,, & \text{(2D)} \end{cases}. \tag{1.55}$$

In general, we resign to solve equation (1.54) numerically. Solutions in three and two dimensions are plotted in Fig. 1.5. In both cases, extremely stiff materials with $B \to +\infty$ ($\lambda \to +\infty$) realise the upper bound for the Poisson ratio, the ratio c_t/c_l vanishes because c_l is much larger than c_t and $\chi \approx 0.955312$. Cork-like materials which neither contract nor expand ($\sigma = 0$) under uniaxial tension possess in both dimensions the same solution $\chi \approx 0.874$. In extremely loose materials with vanishing bulk modulus $B = 0$, $\chi_{3\mathrm{D}}$ remains finite, whereas in two dimensions $\chi_{2\mathrm{d}} = 0$: the system exhibits time-independent surface waves, named in this context *floppy modes*.

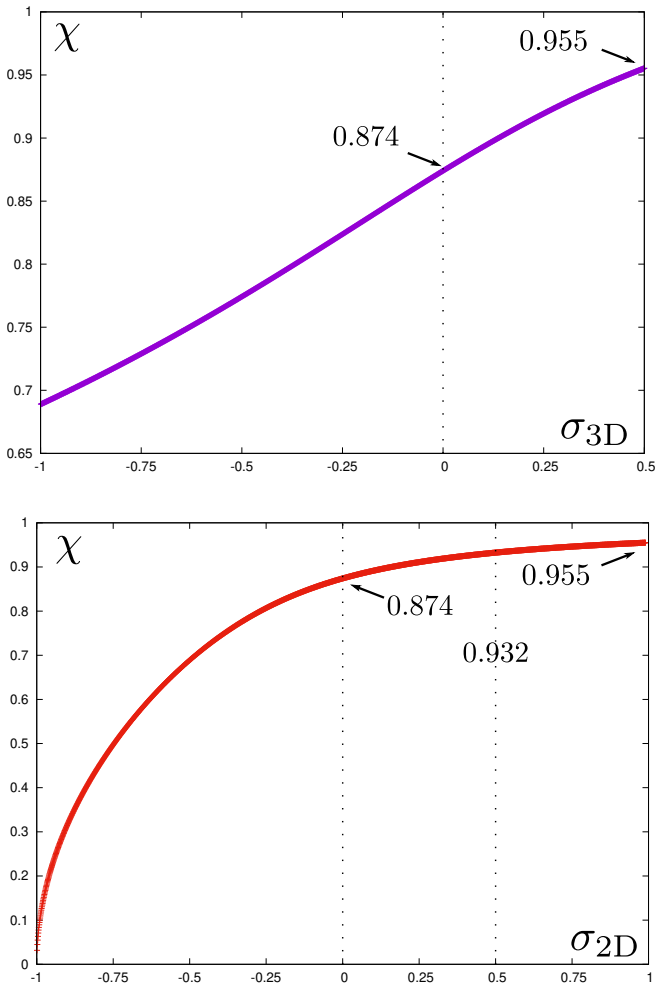

Figure 1.5: Rayleigh surface waves in isotropic elastic media are linear modes with dispersion $\omega = \chi c_t k$. To ensure the stability of excitations, χ must be less than one. The figure shows how χ evolves depending on the Poisson ratio σ, on the top in three dimensions, while on the bottom for two-dimensions. Asymptotic values for extremely-stiff materials $B \to +\infty$ ($\sigma \to 1$) are the same for both dimensionalities. For $\sigma_{\mathrm{2D}} = -1$, the system exhibits floppy surface modes with $\omega = 0$. Usual materials lie between $0 < \sigma_{\mathrm{3D}} < 1/2$.

Chapter 2

Topological solitons

In this chapter, we introduce the notion of topological solitons and some specific examples that are particularly relevant for the rest of the thesis. Loosely speaking, solitons are solutions of non-linear partial differential equations, in our case, that stem from field theories. Field configurations are topological if they can be smoothly deformed while retaining specific properties invariant. Such robust properties allow classifying the solutions of the theories of our interest into different topological sectors. First, we provide a short historical presentation of the seminal works that initiated investigating topological solitons in physics. Then, we focus on examples in one dimension, named kinks, and in two dimensions, called vortices and skyrmions. We will see that topological solitons can be distinguished not only by their dimensionality but also by their homotopy class. We made an effort to keep this chapter as independent as possible from the particularities of the physical systems in which such interesting configurations appear.

2.1 Historical interlude: an ambitious idea about constructing fermions out of bosons

The concepts of topological solitons and topological conservation laws that will appear in this dissertation trace their origins back to a visionary project undertaken by the British physicist Tony Skyrme during 1958-1962. At that time, the development of *Quantum Chromodynamics* still had a long way to go, and the community was trying to describe strong interactions in terms of long-distances degrees of freedom. Skyrme's aim was extremely ambitious: to describe *baryons* (fermions) as emergent features of *mesons* (bosons) [41–46].
Skyrme's influences and personal beliefs [12, 47] lead the following themes to form the basis of his approach:

1. Although the elementary constituents of matter in (3+1) dimensions appear to be either fermions or bosons, it would be desirable to arrive at a description in which only interacting bosonic fields are present. Within this description, baryons might arise as singularities of the underlying mesonic field rather than being independent degrees of freedom.

2. Both at a classical, but also at a quantum level, the concept of point particle leads to diverging quantities and *renormalization* is necessary to get rid of these infinities.
   Skyrme was very impressed by an earlier opinion of Lord Kelvin, who thought that the concept of indestructible particles was introduced by Newton only for convenience[1]. This strong belief found its incarnation in the *vortex atom* theory. Mesmerised by the smoke rings' ability to collide each others without distortions, Kelvin developed an approach in which the elementary constituents of matter were extended and stable objects moving in the aether.

3. Fermions do not possess a classical limit, and they are represented by *Grassmann variables*, both concepts that Skyrme thought to be too counterintuitive and unnatural.

4. The conservation of baryon number should be a property tied to the field configurations' structure, rather than originating from a Noether current, derived from the invariance of a theory's action under symmetry transformations (and its quantum extension known as *Ward identities*).
   The archetype of such a mechanism related to field configurations is the conservation of *circulation* in perfect fluids. Helmholtz gave the first proof of this invariance. Indeed, in [16] (as cited in [49]), he demonstrated that the product of vorticity into a vortex's cross-section is an invariant along the fluid motion.

Even though Skyrme never concluded the project, particular insights still live on today, and topological objects found their incarnations in systems that Skyrme probably never imagined. We begin by introducing the concepts of winding number, topological current and smooth non-trivial maps, in the most straightforward setting.

[1] In his 1869 work, Kelvin even got to the point where he defined Newton's point particle as a "monstrous assumption" [48].

2.2 Constrained O(N) models

We start by considering the paradigmatic class of O(N) models: at each point in spacetime x^μ, we define N real scalar fields. We can conveniently accommodate these fields in an array $n_\mathrm{i} \equiv (n_1, n_2, \ldots, n_N)$. By definition, the action does not change its values under internal orthogonal rotations of the fields, $n_\mathrm{i} \to R_\mathrm{ij} n_\mathrm{j}$. Consequently, it should be constructed only by using the invariant terms $(\partial_\mu n_\mathrm{i})(\partial_\mu n_\mathrm{i})$, $(n_\mathrm{i} n_\mathrm{i})$, and their higher powers:

$$S = \frac{1}{2} \int dt\, dx [(\partial_t n_\mathrm{i})^2 - (\partial_j n_\mathrm{i})^2 - m^2 (n_\mathrm{i} n_\mathrm{i})] + \cdots \tag{2.1}$$

To lowest order, each component of the field satisfies a Klein–Gordon equation $(-\partial_t^2 + \partial_j^2 - m^2) n_\mathrm{i} = 0$, a linear partial differential equation whose solutions are well-known. We could increase the complexity of the problem and the richness of its solutions by including higher-order non-linear terms in the action (2.1). If we do so, equations of motion become non-linear partial differential equations, and there might be the chance that some of their solutions are interesting topological solitons.
However, instead of writing more terms in the action, an alternative and equivalent possibility is introducing *constraints* on the fields. A simple, yet non-linear, constraint is to impose that the admittable field configurations must satisfy the relation

$$n_\mathrm{i} n_\mathrm{i} = n_1^2 + n_2^2 + \cdots + n_N^2 \stackrel{!}{=} 1. \tag{2.2}$$

This constrained route allows us to think of fields as geometrical vectors that live on the unit hypersphere S^N. Throughout this chapter, we will elucidate this undemanding mental picture's extreme elegance and utility. Constrained O(N) models are also called *non-linear sigma* models [50].

2.3 O(2) models

For the sake of simplicity, we first restrict the discussion to the case with only two real fields. We will comment on the importance of O(2) at the end of the section. For $N = 2$, the condition (2.2) simplifies to having only field configurations that live on a unit circle S^1

$$n_1^2 + n_2^2 \stackrel{!}{=} 1. \tag{2.3}$$

It is evident that we fulfill the above constraint by introducing an angle variable $\theta(x^\mu)$. Therefore, we solve the constraint with the parametrization

$$(n_1, n_2) = (\cos\theta, \sin\theta). \tag{2.4}$$

2.3.1 One spatial dimension: kinks

In general, field theories in lower dimensions are easier to solve. Therefore, we start our discussion with a field theory in one spatial and one temporal dimension. In this case, spacetime coordinates are $x^\mu = \{t, x\}$. The Lagrangian that corresponds to the action (2.1), and that obeys the constraint (2.3) acquires an uncomplicated form in terms of the angular parametrization (2.4), namely $\mathcal{L} = \frac{1}{2}[(\partial_t\theta)^2 - (\partial_x\theta)^2]$.

First in [41] and, later on in [43], systematically, Skyrme guessed that actions that satisfy a constraint like (2.3) possess a current density whose conservation depends neither on equations of motion, symmetries and Noether theorem, nor on local properties. Consequently, such current must be *topological*,

$$j^\alpha_{\rm top} \equiv \frac{1}{2\pi}\epsilon^{\alpha\beta}\epsilon_{\mathfrak{ij}}n_{\mathfrak{i}}\partial_\beta n_{\mathfrak{j}}, \tag{2.5}$$

where Greek letters label spacetime coordinate, and Gothic letters label the internal indices of the field[2]. Specifically for the O(2) model, Gothic letters run from 1 to 2.

We can prove the conservation law $\partial_\mu j^\mu_{\rm top} = 0$ in at least two complementary ways [51]. One 'geometrical' approach is noticing that the divergence of the current (2.5) is the Jacobian determinant [43] of the map from spacetime coordinates x^μ to the fields $n_{\mathfrak{m}}$

$$\partial_\alpha j^\alpha_{\rm top} \propto \epsilon^{\alpha\beta}\epsilon_{\mathfrak{ij}}\partial_\alpha n_{\mathfrak{i}}\partial_\beta n_{\mathfrak{j}} = \det(\partial_\gamma n_{\mathfrak{m}}). \tag{2.6}$$

A map's Jacobian determinant expresses the ratio between the area spanned in the target space (n_1, n_2), as an arbitrary area in the base space is covered, $\Delta t\ \Delta x$. However, due to the constraint (2.3), any area gets mapped into a circumference, that by definition has zero area. Hence, the above expression vanishes.

The other route is using the explicit parametrization (2.4) and computing the current in terms of the angular variable,

$$j^\alpha_{\rm top} = \frac{1}{2\pi}\epsilon^{\alpha\beta}[n_1\partial_\beta n_2 - n_2\partial_\beta n_1] = \frac{1}{2\pi}\epsilon^{\alpha\beta}\partial_\beta\theta. \tag{2.7}$$

On account of the presence of the antisymmetric symbol and by assuming the smoothness of θ, if we contract the current with a gradient, we automatically prove the conservation law $\partial_\alpha j^\alpha_{\rm top} = 0$.

The first entry of the topological current density (2.5) is a density of the topological charge. The total topological charge is obtained by integration over space

$$Q^{\rm top} \equiv \frac{1}{2\pi}\int_{\mathcal{R}} dx\ \partial_x\theta = \frac{1}{2\pi}[\theta(+\infty) - \theta(-\infty)]. \tag{2.8}$$

[2]We have introduced the factor $1/2\pi$ for later convenience.

Evidently, only field configurations that take on different values at infinity can have non-zero topological charge. Usual particle solutions do not enjoy this property, because they are well-localised in space.
We impose periodic boundary conditions, both on the original fields n_{i} and on the one-dimensional space. These conditions allow us to relate Q^{top} with the *winding number*, which is the number of times the target space is covered while sweeping once the base space circuit. Since the angular variable is a parameterization of the unit circle, the asymptotic identification $n_{\mathrm{i}}(+\infty) \stackrel{!}{=} n_{\mathrm{i}}(-\infty)$ results in a condition $\theta(+\infty) - \theta(-\infty) = 2\pi N$, where N is an integer. Moreover, because we glued together the one-dimensional strip's endpoints, the topological charge (2.8) is computed as $Q^{\mathrm{top}} = (2\pi)^{-1} \oint dx\ \partial_x \theta = N$. Which is, precisely, the *winding number*.
Having wrapped both the base space (the physical coordinate) and the target space (the field configurations), the angle variable θ is now a map from a ring to a ring $\theta : S^1 \to S^1$. It enjoys the so-called *topological protection*[3], and it can not be smoothly deformed into a map with a different winding number. For this reason, we can arrange the solutions of such constrained models into different topological sectors, each characterised by the value of Q^{top}. This property's robustness inspired Skyrme's idea to classify particles as emergent properties of field configurations with a well-defined topological charge, rather than their symmetry properties. In mathematical jargon, the homotopy class characterising the mapping is the *first homotopy* or *fundamental group* $\pi_1(S^1) = \mathbb{Z}$.
Let us investigate topologically a specific constrained model, where we also allow higher-order terms in (2.1). Following the footsteps of [41], a possible choice is to include terms that respect square rotational ($R : \theta \to \theta + \pi/2$, $R : (n_1, n_2) \to (n_2, -n_1)$) and time-reversal ($T : n_{\mathrm{i}} \to -n_{\mathrm{i}}$) invariance. The simplest non-linear term in powers of n_{i} which satisfy the symmetry requirements is $n_1^4 + n_2^4$, analogous to the cubic-symmetry term in three-dimensions [53]. If we plug in the parametric representation (2.4), use the trigonometric identities $\frac{\sin^4}{\cos^4}(\theta) = \frac{1}{8}\big(3 \mp 4\cos(2\theta) + \cos(4\theta)\big)$, and drop unnecessary constants, we obtain the following:

$$\begin{aligned} \mathcal{L} &= \frac{1}{2}[(\partial_t n_{\mathrm{i}})^2 - (\partial_x n_{\mathrm{i}})^2] + \frac{\kappa^2}{4}(n_1^4 + n_2^4) \\ &= \frac{1}{2}[(\partial_t \theta)^2 - (\partial_x \theta)^2] + \frac{\kappa^2}{16}\cos(4\theta). \end{aligned} \tag{2.9}$$

Variations with respect to θ lead to the sine–Gordon–Skyrme equation $(\partial_t^2 - \partial_x^2)\theta + \frac{\kappa^2}{4}\sin(4\theta) = 0$. It is a non-linear partial differential equation and its solutions can be constructed using the Inverse Scattering Method [54], which was later

[3]Tony Zee in [52] provides a very vivid analogy of topological protection: "Think of wrapping a loop of string around a ring".

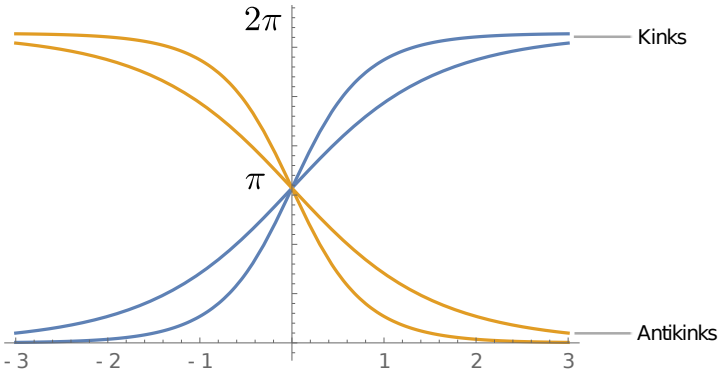

Figure 2.1: One-soliton solutions $\theta_\kappa\,(x - x_0)$ of the sine–Gordon–Skyrme equation are represented. Solutions divide into kinks (blue, $\kappa > 0$) and antikinks (orange, $\kappa < 0$). These solutions can be thought as smoothed step functions at $x_0 = 0$, with the smoothing's rate that increases with $|\kappa|$.

developed. It is conventional to rescale the variable as $4\theta \to \theta$, obtaining

$$(\partial_t^2 - \partial_x^2)\theta + \kappa^2 \sin(\theta) = 0. \tag{2.10}$$

Skyrme found few non-trivial solutions of the above equation, and it is not an understatement to say he was one of the first investigators of the branch of mathematical physics dubbed nowadays as integrable models [55]. In particular, an interesting class of static solutions is

$$\theta_\kappa(x - x_0) \equiv 4\arctan(\exp(\kappa(x - x_0))). \tag{2.11}$$

As we can see in Fig. 2.1, solutions (2.11) represent field's disturbances that are concentrated around a specific point in space x_0 and, in a small region of space centred around it, they rapidly change from 0 to 2π. As a consequence, their associated energy is finite.
Furthermore, they naturally come in two 'flavours', depending on the sign of κ. As Skyrme did [41], we might as well be tempted to identify them as 'particle' and 'antiparticles' pairs. Due to this analogy, solutions with positive κ are called *kinks* while, those with negative κ, are called *antikinks*[4].
Solutions (2.11) possess topological charge (2.8) which depends on the sign of κ. Because the difference between the solution at infinite distances is $\pm 2\pi$, they either have charge $Q^{\text{top}} = 1$ (for positive κ) or $Q^{\text{top}} = -1$ (for negative κ). Accordingly, kinks and antikinks furnish our first examples of topologically non-trivial field configurations. Without the angle variable's rescaling, (2.11) would

[4]In early literature on the subject [56, 57], the names 'kinks' and 'antikinks' were reserved for solitary wave solutions of φ^4 theory in two dimensions.

still be topologically non-trivial, but quarterly charged.
The theory we started with (2.9) was Lorentz invariant, so we find time-dependent solutions that travel uniformly with speed $\pm v$ by doing boosts. The transformation consists in replacing the solution's argument as $x-x_0 \to (x-x_0 \pm vt)/(1-v^2)^{1/2}$.

2.3.2 Two spatial dimensions: vortices

The Skyrme toy model in two-dimensional spacetime was rich enough to introduce the concepts of topological current, topological number, and the $\pi_1(S^1)$ homotopy. On that account, it is natural to wonder if we can extend these ideas for studying topological solitons of the constrained O(2) model in higher dimensions. The question then arises: how can we characterise solutions in two spatial dimensions with the ring-to-ring homotopy?
While the unit field constraint (2.3) guarantees the *target space* to be S^1, the plane can not be compactified to be S^1. We avoid this problem, and use the topological characterisation we employed for kinks, with the following device. We consider as *base space* the plane's boundary, the asymptotic circle S^1_∞, namely every point at infinite distance. In a plane, topological solitons are called *vortices*. Their winding number is defined as the number of times N they cover the target space by running once along S^1_∞. Maps with a negative winding number are called *antivortices*.
We hereby work out an explicit example. A single-charged vortex located at the origin, is given by the configuration $\mathbf{n}_v(x,y) = (x/\rho, y/\rho) = (\cos\theta, \sin\theta) = \hat{e}_\rho$, where $\theta \equiv \mathrm{atan}(y/x)$ and $\rho \equiv (x^2+y^2)^{1/2}$. We obtain configurations with winding number N by taking the parametrization $\mathbf{n}_v = (\cos(N\theta), \sin(N\theta))$. The associated topological current [51] can be found using (2.5) or (2.7) with Greek indices running over the spatial dimensions, i.e.

$$j^i_{\mathrm{top}} = \frac{N}{2\pi}\left(\frac{x}{\rho^2}, \frac{y}{\rho^2}\right). \tag{2.12}$$

At the origin, something fishy is going on, and the vector field possesses a singularity. This is a novel feature the solitons of sine–Gordon–Skyrme model (2.11) did not posses, and bring forth interesting properties.
The divergence of (2.12) reflects the vector field's singular nature: it vanishes almost everywhere, except at the origin, where it contains a two-dimensional Delta distribution $\partial_i j^i_{\mathrm{top}} = N\ \delta^{(2)}(\mathbf{x})$. We perform its integration over a closed two-dimensional surface which encloses the position of the vortex by using the polar form $j^i_{\mathrm{top}} = [N/(2\pi)]\epsilon^{ip}\partial_p\theta$ and Stokes' theorem,

$$\oiint_{\mathcal{S}} \partial_i j^i_{\mathrm{top}} = N = \oint_{\mathcal{C}} d\theta. \tag{2.13}$$

The result is topological: as long as we choose a closed path $\mathcal{C}$ which encloses the vortex, the integral's value does not change.
There are two features of (2.13) that are remarkable. Fist, we can interpret the above equation in hydrodynamic terms, as the quantisation of a vortex velocity field's circulation. Introducing the velocity field as $v_{\mathrm{v}}^{i} \equiv \partial_i \theta$ [58], its circulation is an integer multiple of 2π, $\epsilon^{ij}\partial_i v_j = 2\pi N \delta(\mathbf{x})$. Furthermore, (2.13) is very reminiscent of Gauss law in two dimensions, in the presence of a point particle with charge N. We might and, in Chapter 3, we will, make good use of this intuition. In the case of vortices, we will consider the topological current density as a two-dimensional electric field generated by point charges with charge q_v given by their winding number N. There, the compressibility of superfluids will also give rise to a dual magnetic field.
The energy of a vortex is a logarithmic-divergent extensive quantity

$$E = \int_{\mathcal{R}^2} d^2x \; j^2_{\mathrm{top}} \propto N^2 \log\left(L/\xi\right) \tag{2.14}$$

which scales with the system size L. Alas, vortices are the first solitons whose energy fall victim to Hobart–Derrick's theorem [59, 60]. When dealing with scale-invariant theories of scalar fields (for example $\mathcal{L} = \partial_\mu\psi\partial^\mu\psi - U(\psi)$), or multi-component scalar fields, and in spatial dimensions $D \geq 2$, there are no localised, time-independent solitonic solutions with finite energy [61]. The issue appears because there is no term in the action which is able to fix the solitons' size. A possible solution is to add more derivatives or to add mixed terms. Another way to circumvent the theorem is to introduce an additional degree of freedom, for example spinors or gauge fields. In the latter case, it is sufficient to couple the theory to an external field through a minimal coupling procedure $\partial_i \to D_i = \partial_i + iA_i$, and to require that the two terms in the covariant derivative $D_i\theta$ make the integrand die faster than $1/\rho$, at spatial infinity. Also, in (2.14), we had to introduce an ultraviolet cutoff ξ, which is the lengthscale where the model's validity breaks down. In weakly interacting Bose gases, ξ is denoted as *healing length* and is the typical lengthscale of density variations [62].
If we stress the *dual gauge* analogy we mentioned earlier, the associated electrostatic energy is $\propto \int_{\mathcal{R}^2} d^2x \; \mathbf{e}^2$.
We now introduce a complex representation for O(2) models which is less cumbersome than dealing with a doublet (n_1, n_2). We combine the two components of n_{i} into a complex field $\varphi \equiv n_1 + in_2$. The original rotations are realised as $U(1)$ phase transformations $\varphi \to e^{i\alpha}\varphi$, and the Lagrangian (2.1) becomes $\mathcal{L} = \frac{1}{2}(|\partial_t\varphi|^2 - |\partial_j\varphi|^2 - m^2|\varphi|^2) - g|\varphi|^4 + \cdots$. This representation is a more standard approach [63] to illustrate some topological statements that we have made and used, that even hold for more generic scalar theories. As a matter of fact, we can weakly relax the assumption of φ having fixed amplitude (alternatively,

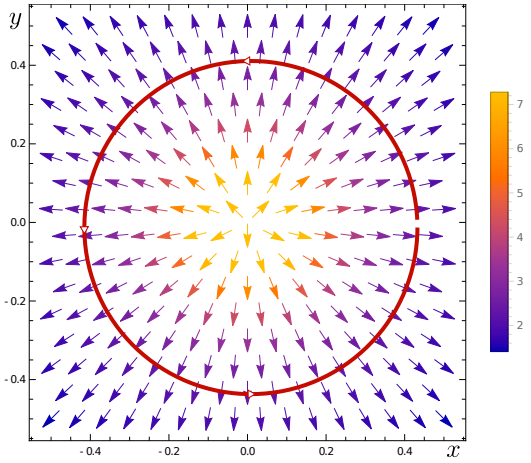

Figure 2.2: Topological current j^i_{top} associated with a single vortex configuration placed in the origin. The red oriented path (forming the base space S^1) can not be shrunk to a point without encountering the singularity at the centre of the vortex core.

fixed $n_{\text{i}} n_{\text{i}}$). The non-linear sigma model is the limit of the above theory in its symmetry-broken phase, provided density fluctations are infinitely-massive [64].
In two dimensions and in the complex φ language, the smooth maps U_N that map a ring into a ring, while covering the target space N times, are complex exponentials $U_N \equiv \exp(iN\theta)$, where θ is, as usual, the polar angle.
In the first place, we prove the winding number's invariance under smooth deformations of the map. Given a map U_N, we compute its winding number N as the integral $(i/2\pi) \int d\theta \; U_N(\partial_\theta U_N^\dagger)$. The requirement of deformations to be smooth is crucial because we can realise them as sums of infinitesimal ones, $U_N \to U_N + \delta U_N$. We demonstrate that the consequent variation δN does vanish. We start from the unitarity condition $U_N^\dagger U_N = 1$, and notice that $\delta[U_N \partial_\theta U_N^\dagger] = -\partial_\theta [U_N^\dagger \delta U_N]$. Therefore

$$\delta N = \frac{i}{2\pi} \int_0^{2\pi} -d\theta \; \partial_\theta [U_N^\dagger \delta U_N] = \frac{-i}{2\pi} \; U_N^\dagger \delta U_N \Big]_0^{2\pi} = 0, \tag{2.15}$$

because the map U_N is a continuous function of θ, and the points 2π and 0 are identified.
Next, we prove Derrick's theorem in the specific case of vortices: without additional degrees of freedom, non-trivial maps always end up creating a $1/\rho$ singularity, thus giving rise to a divergent energy $E = \int d^2x \; |\partial_i \varphi|^2$. Earlier on, we had to impose boundary conditions on the field at infinity which, indeed for vortices, was pointing radially. In complex representation, the asymptotic condition takes the shape $\varphi(\rho \to +\infty, \theta) = U(\theta)$. Hereby we guess some aspects of the solution by

extending it to the whole plane. We make the ansatz $\varphi\left(\rho,\theta\right)=f\left(\rho\right)U\left(\theta\right)$, where $f\left(\rho\right)$ is a regular function that is well behaved at the origin and approaches unity at infinity, $f(0)=0$ and $f(+\infty)\to 1$. By computing its gradient square in polar coordinates, and keeping track of the Jacobian determinant for polar coordinates in the integral, the energy associated to the ansatz is

$$E=2\pi\int^{+\infty}d\rho\,[\,\left|f'(\rho)\right|^2+\frac{N^2}{\rho}\left|f(\rho)\right|^2]. \tag{2.16}$$

Due to the assumptions on the function $f(\rho)$, the first term in the above expression can be neglected at infinity, whereas the second one gives rise to a logarithmic divergence. We ended up with the desired result: no finite-energy topological solitons solutions can be obtained in simple scalar theories, and an additional mechanism must be added to require the stability of finite-energy topological solitons.

Vortices as topological defects

Even though we never mentioned it, O(N) models are good descriptions of systems with continuous phase transitions. In two spatial dimensions, the O(N=2) model describes both planar magnets and superfluids [65].
According to the Landau paradigm of phase transitions, we can classify the *disordered* and *ordered* phases of a system by their symmetries. In the former case, the ground state enjoys all the symmetries of the original action. In the latter one, the symmetry group is reduced. In this *broken symmetry phase*, field configurations that encode small fluctuations of the order parameter are *Nambu–Goldstone bosons*.
When they represent an order parameter, vortex configurations are peculiar objects. At their core, the original symmetry group is restored [66]. Therefore, in this context, vortices are usually referred to as *topological defects*.

2.4 O(3) models, two dimensions: skyrmions

Despite possessing topological properties, we have seen that vortices are not quite the direct two-dimensional equivalent of kinks. Rather than being smooth configurations, vortices possess a singularity in their origin and a diverging extensive energy. In contrast, *topological textures* are finite-energy field configurations that continuously vary over space, with interesting topological features. Structures that fullfill the above properties in (2+1) dimensional spacetime are called *skyrmions* or *baby skyrmions*[5], but they also go by the name of *continuous Anderson–Toulouse–*

[5]The terminology is introduced to distinguish them from the ones Skyrme introduced in (3+1) dimensions.

Chechetkin vortices in the He-3 literature [67].
The extension of finite-energy topological solitons into the plane demands an enlargement of the target space. Instead of living on the ring S^1 (2.3) like the kinks, the degrees of freedom are a triplet of fields $n_{\mathfrak{p}}$ ($\mathfrak{p} = 1, 2, 3$) that obey the unit constraint $n_{\mathfrak{p}} n_{\mathfrak{p}} \stackrel{!}{=} 1$, consequently living on a two-sphere S^2. The requirement for static solutions to have finite energy $E = \int_{\mathcal{R}^2} d^2x \ (\partial_\gamma n_{\mathfrak{m}})^2$ imposes that the field in polar coordinates satisfies $\rho |\nabla \mathbf{n}| \to 0$ as $\rho \to +\infty$. Equivalently, $\mathbf{n}$ must point in the same direction at infinite distance, however it is reached in the base space,

$$\mathbf{n}(\rho \to +\infty) = \mathbf{n}_\infty = \textbf{const}. \tag{2.17}$$

The above condition allows for a *compactification* of the base space: the Cartesian plane $\mathbb{R}^2$ is mapped into the two-sphere S^2. Pictorially, the procedure can be imagined by merging together the margins of an infinite paper sheet, ending up with a paper ball. Since, now, both the base space and the target space are compact, we can classify field configurations into different topological sectors.
The required topological invariant is the amount of times (by definition, an integer) the target sphere is covered by traversing once the base sphere. In this case, the homotopy class is $\pi_2(S^2) = \mathbb{Z}$. Consequently, we extend the line of reasoning that we introduced in two spacetime dimensions and two real fields, to the case of three spacetime dimensions and three fields. The topological conserved current density associated to the O(3) non-linear model is the natural generalisation of (2.5), i.e.

$$J^{\text{top}}_\alpha = \frac{1}{8\pi} \epsilon_{\alpha\beta\gamma} \epsilon_{\mathfrak{ijm}} n_{\mathfrak{i}} \partial_\beta n_{\mathfrak{j}} \partial_\gamma n_{\mathfrak{m}}, \tag{2.18}$$

with Greek letters that run over t, x, y and Gothic letters that run over 1, 2 and 3. The first entry ($\alpha = t$) of J^{top}_α represents the density of topological charge. In this case, it goes by the name of *Pontryagin density* [58]

$$\rho^{\text{top}} = \frac{1}{8\pi} \epsilon_{\beta\gamma} n_i \epsilon_{\mathfrak{ijm}} \partial_\beta n_{\mathfrak{j}} \partial_\gamma n_{\mathfrak{m}} = \frac{1}{4\pi} n_{\mathfrak{i}} \epsilon_{\mathfrak{ijm}} \partial_x n_{\mathfrak{j}} \partial_y n_{\mathfrak{m}} = \frac{1}{4\pi} \mathbf{n} \left[\partial_x \mathbf{n} \wedge \partial_y \mathbf{n} \right]. \tag{2.19}$$

Its integration over the (base) space permits to identify non-trivial topological configurations as the ones having

$$Q^{\text{top}} = \frac{1}{4\pi} \int dx \ dy \ \left[n_{\mathfrak{i}} \epsilon_{\mathfrak{ijm}} \partial_x n_{\mathfrak{j}} \partial_y n_{\mathfrak{m}} \right] \neq 0. \tag{2.20}$$

Driven by the conformal properties of the non-linear O(3) model, Belavin and Polyakov [68] had a brilliant idea to check whether the *stereographical mapping*, in which a unit sphere is projected into a plane[6] (while angles are preserved) would

[6] We use here the equatorial convention.

represent a one-skyrmion configuration:

$$\mathbf{n}\,(x,y) = \left(\frac{2x}{x^2+y^2+1}, \frac{2y}{x^2+y^2+1}, \frac{x^2+y^2-1}{x^2+y^2+1}\right) \tag{2.21}$$

On the one hand, at infinity the vector field points from the South to the North Pole $\mathbf{n}\,(\rho \to \infty) = (0,0,1)$, hence satisfying (2.17). On the other hand, at the origin of the plane, $\mathbf{n}$ points in the opposite direction, from the North to the South pole, $\mathbf{n}\,(\mathbf{0}) = (0,0,-1)$. In between those two extrema, the behaviour is smooth: it is indeed a *texture*.

Moreover, by sweeping the whole plane, the above solution covers the sphere once, therefore it must possess a non-zero winding number. The associated topological charge density is rotationally invariant in the plane $\rho^{\text{top}}(x,y) = -(\pi(1+x^2+y^2)^2)^{-1}$ and its integration in the base space[7] yields indeed non-zero topological charge. However, for (2.21) one finds $Q^{\text{top}} = -1$ so (2.21) should be classified as an *antiskyrmion*, not as a *skyrmion*.

In contrast to vortices (2.14), the energy associated to the above solution is finite, and does not contain any lengthscale, $E = 4\pi$. While not being extensive is sort of a relief, the fact that it does not depend on the size of the topological texture might be highly puzzling and disappointing. If this was the case, skyrmions that are solutions would be energetically favourable regardless of their size. This might have been a glitch, hidden in the fact that the projection used (2.21) was that of a sphere with unit radius $R = 1$; but, it is not. It is, again, a manifestation of the theory's scale-invariance. The size of the soliton can be fixed only by including higher-order terms in the action. The choice of the terms to include depends on the physical system under consideration. For example, in chiral magnets, the term that does the trick is the Dzyaloshinskii–Moriya interaction [69].

[7] $\int_0^{+\infty} d\rho \frac{-\rho}{\pi(1+\rho^2)^2} = -1/(2\pi)$

Chapter 3

Effective field theory of a vortex lattice in a bosonic superfluid

In this chapter, we provide an effective field theory description of the vortex lattice phase of rotating bosonic superfluids. We start with a relativistic description of interacting bosons and elucidate how its non-relativistic limit emerges. Assuming that, below a critical temperature, bosons occupy the lowest state, we provide a semi-classical description of the Bose–Einstein condensate in terms of a scalar field. In the symmetry-broken phase, the bosonic field describes a superfluid. If the system is put under rotation, it nucleates quantised vortices that arrange themselves in a regular triangular crystal, which we describe using the methods we presented in Chapter 1. We illustrate an effective theory of this regime, which also includes the emergent vortices. Then we show how we incorporated the superfluid part in terms of a more convenient dual electromagnetic gauge field. We also extract transport of the system in the dual language, where the coupling to an external source is natural.

3.1 φ^4 theory

At the beginning of the XX century, quantum mechanics and special relativity shook the grounds of physics with their novel concepts and predictions. While the first introduced the concept of *state*, the second required that space and time had to be treated on the same footing [63]. It took the genius of P.A.M. Dirac to construct one of the first successful marriages between quantum mechanics and relativity, despite certain drawbacks (see more in [70]). Quantum field theory (QFT) was born. Dirac paid a high price to make his theory consistent: he had to deal with an infinite number of degrees of freedom.
Later on, this peculiarity of QFTs turned out to be helpful also in non-relativistic

contexts, where the creation (emission) or annihilation (absorption) of photons comes as no surprise. Also, the formalism comes in handy when the number of particles is conserved. For example, the many-body problem often involves solving the multiparticle Schrödinger equation, and states should undergo either anti-symmetrisation (fermions) or symmetrisation (bosons). By using the tools developed in QFT, the tedious procedures related to particles' statistics are already taken care of.

3.1.1 Lorentz-invariant φ^4 theory

Everything we discuss in this thesis concerns non-relativistic phenomena, i.e. phenomena happening at velocity scales that are much smaller than the speed of light. We expect that a theory that enjoys a larger symmetry group should also contain its counterpart which enjoys a smaller subgroup. Therefore, we start the discussion with a Lorentz-invariant theory and work out its non-relativistic limit [52].
Self-interacting massive bosons are described by a complex φ^4 theory, which, upon quantisation, gives rise to bosonic particles. The theory is described by the action

$$S = \int dx \, \left[-\partial^\mu \Phi^\dagger \partial_\mu \Phi - m^2 c^2 \Phi^\dagger \Phi - \lambda (\Phi^\dagger \Phi)^2 \right]. \tag{3.1}$$

We restrict to a positive interaction term with $\lambda > 0$ because only one-species systems of repulsive bosons can undergo a stable Bose–Einstein condensation. One of the first steps to analyse a field theory is to find which transformation laws leave the action invariant. These *symmetries* are connected to currents that are conserved at a classical level, named Noether currents[1]. In the above case, the theory (3.1) enjoys the $U(1)$ global phase symmetry

$$\Phi \to \, e^{i\alpha}\Phi \approx \Phi + i\alpha\Phi \quad , \quad \Phi^\dagger \to \, e^{-i\alpha}\Phi \approx \Phi^\dagger - i\alpha\Phi^\dagger. \tag{3.2}$$

We obtain the conserved 4-current J^μ by promoting the infinitesimal transformation parameter to be local $\alpha \to \alpha\,(x)$, and by arranging the consequent action's variation in the form $\delta S = \int dx J^\mu \partial_\mu \alpha$. In this instance, the Noether current of (3.1) is[2]

$$J^\mu = i\Phi^\dagger \overset{\leftrightarrow}{\partial^\mu} \Phi. \tag{3.3}$$

[1] Usually, authors do not agree on how to evaluate conserved currents connected to symmetry transformations. A comprehensive way to find and classify all equivalent conserved currents can be found in [71].

[2] We introduce here the notation $\overset{\leftrightarrow}{\partial} \equiv \overset{\rightarrow}{\partial} - \overset{\leftarrow}{\partial}$.

3.1.2 Non-relativistic limit of the free theory

The theory defined by (3.1) is an interacting theory. To unfold some understanding, for the moment, we turn off the interaction and develop the non-relativistic limit of the free theory. In this case, the equation of motion for (3.1) is the Klein–Gordon equation

$$\left(\Box + m^2c^2\right)\Phi = 0, \tag{3.4}$$

where $\Box \equiv -\eta^{\mu\nu}\partial_\mu\partial_\nu = (1/c^2)\partial_t^2 - \partial_i^2$ [3]. Upon canonical quantisation, solutions of (3.4) for the field Φ are expressed in terms of bosonic particles (a) and antiparticles (b)

$$\Phi(x,t) = \int \frac{d^Dp}{(2\pi)^{D/2}\left(2E_{\mathbf{p}}\right)^{1/2}}\left[a_{\mathbf{p}}e^{-i\left(E_{\mathbf{p}}t-\mathbf{p}\cdot\mathbf{x}\right)} + b_{\mathbf{p}}^\dagger e^{i\left(E_{\mathbf{p}}t-\mathbf{p}\cdot\mathbf{x}\right)}\right] \tag{3.5}$$

with particle and antiparticle excitations[4] that oscillate as a function of the energy $\pm iE_{\mathbf{p}}t$. In the non-relativistic limit $c \to +\infty$, we expand the modes' energy in inverse powers of the speed of light $E_{\mathbf{p}} = \sqrt{m^2c^4 + p^2c^2} \approx mc^2 + p^2/(2m) + \ldots$, where we notice the rest energy as the dominant contribution. Hence, it gives rise to a fast oscillatory phase which makes it natural to factorise the field Φ as

$$\Phi(x,t) = \underbrace{\left[e^{-imc^2t}\right]}_{\text{fast}}\overset{\text{non-relat.}}{\varphi(x,t)}. \tag{3.6}$$

Introducing this expression in (3.5), we obtain a modal decomposition for the non-relativistic part φ,

$$\begin{aligned}\varphi(x,t) &= \int \frac{d^Dp}{(2\pi)^{D/2}\left(2E_{\mathbf{p}}\right)^{1/2}}\left[a_{\mathbf{p}}e^{-i\left(\frac{p^2t}{2m}-\mathbf{p}\cdot\mathbf{x}\right)} + e^{2imc^2t}b_{\mathbf{p}}^\dagger e^{i\left(\frac{p^2t}{2m}-\mathbf{p}\cdot\mathbf{x}\right)}\right] \\ &\approx \int \frac{d^Dp}{(2\pi)^{D/2}}\left[a_{\mathbf{p}}e^{-i\left(\frac{p^2t}{2m}-\mathbf{p}\cdot\mathbf{x}\right)}\right].\end{aligned}$$

In analogy with the rotating wave approximation, we safely dropped the antiparticle ($b_{\mathbf{p}}^\dagger$) contribution because it wildly oscillates in time, twice as much as the already "fast" phase mc^2t. Therefore, its contribution to any slow process is negligible.

[3] We use the "East-Coast" convention $\eta^{ij} = \mathrm{diag}(-1,1,1,1)$, where the signature of the spatial part of the metric is +1. Four-gradients are $\partial_\mu \equiv \partial/\partial x^\mu = \left(\partial_t/c, \partial_i\right)$ and $\partial^\mu \equiv \partial/\partial x_\mu = \left(-\partial_t/c, \partial_i\right)$. With this metric, there is no distinction between the covariant and contravariant spatial components. Other reasons to prefer this convention can be found at [72].

[4] Particles and antiparticles satisfy their own canonical commutation relations.

Instead of (3.4), the remaining slow field φ obeys the linear equation

$$\underset{\text{subleading}}{-\frac{1}{2mc^2}\partial_t^2\varphi} + i\left(\partial_t\varphi\right) = -\frac{1}{2m}\partial^2\varphi \tag{3.7}$$

which, in the limit $(2mc^2)^{-1} \to 0$, is formally equivalent to a Schrödinger equation for particles of mass m. The dynamics of φ is linear in time. Accordingly, it is easy to guess that it comes from a Lagrangian which has first order time-derivatives

$$\mathcal{L} = \frac{i}{2}\varphi^\dagger \overset{\leftrightarrow}{\partial_t}\varphi - \frac{1}{2m}(\partial^i\varphi^\dagger)(\partial_i\varphi). \tag{3.8}$$

The conserved current (3.3) for the above theory expresses the particle-number conservation, and it formally matches the probability current in quantum mechanics, with

$$J_0 = \varphi^\dagger\varphi \equiv n \quad , \quad J^i = -\frac{i}{2m}(\varphi^\dagger \overset{\leftrightarrow}{\partial_i}\varphi). \tag{3.9}$$

3.1.3 Non-relativistic limit of the interacting theory

By using the wisdom that we developed in the previous subsection, now we aim to obtain the non-relativistic version of the action for interacting repulsive bosons (3.1). We decouple the two terms into the fast and slow components $\Phi = e^{-imc^2t}\varphi/\sqrt{2mc}$, and we obtain the low-energy action

$$S = \int dt\, d^Dx \left[\frac{i}{2}\varphi^\dagger \overset{\leftrightarrow}{\partial_t}\varphi - \frac{1}{2m}(\partial^i\varphi^\dagger)\left(\partial_i\varphi\right) - \frac{g}{2}(\varphi^\dagger\varphi)^2 + \mu\varphi^\dagger\varphi\right], \tag{3.10}$$

with the new coupling constant defined as $g/2 \equiv \lambda/(4m^2)$. In contrast to relativistic theories, that usually describe zero-density states, condensed matter describes physics with a finite number of particles. We achieved the latter by having introduced the chemical potential μ. It is worth to recognise the chemical potential's appearance as a negative mass squared term. Also the interacting theory obeys the conservation of $U\left(1\right)$ particle number $N \equiv \int d^Dx\, n$.

We started this chapter by introducing an action (3.1) which was invariant under Lorentz transformations. After we found its low-velocity limit (3.10), we might ask ourselves what is left over of that symmetry. What remains is Galilean invariance, an often underappreciated symmetry [30]. The Italian scientist taught us two things: time is absolute and physics should be the same either we stay still or in uniform motion with velocity β^i. Therefore, transformations $t \to t' = t$ and $x^i \to (x')^i = x^i + \beta^i t$ should not modify physical predictions. This is indeed the case, as one can verify that the action (3.10) is invariant in the boosted reference

frame, where derivatives act as $\partial_i \to \partial_{i'} = \partial_i$, $\partial_t \to \partial_{t'} = \partial_t - \beta^i \partial_i$ while fields pick up a phase

$$\varphi(x) \to \varphi'\left(x'\right) = \varphi(x) \exp(im\Lambda) \quad , \quad \Lambda \equiv \beta^i x^i + \beta^2 t/2. \tag{3.11}$$

The Noether current associated with Galilean invariance implies that the system's centre of mass X carries conserved momentum $p_i = mN\frac{dX^i}{dt}$ [66].
At the level of (3.10), the theory is still classical, and its quantisation requires the functional integral's evaluation along all the possible field configurations $Z = \int \mathcal{D}\varphi \ \exp(iS)$. If we wanted to obtain observables for finite-temperature states, we should evaluate the partition sum of the Euclidean action S_{E} by switching to imaginary time (the Gian Carlo Wick's rotation). Since it is out of the scope of this thesis, we will focus only on the case with $T = 0$.
As Richard Feynman showed in his PhD thesis [73] for path integrals in quantum mechanics, the most important trajectory in the limit $\hbar \to 0$ is the one that solves the classical equations of motion, obtained by minimizing the action $\delta S = 0$ with respect to variations $\delta\varphi$. In the context of functional integrals, this is known as semi-classical or saddle-point solution[5], and assumes that the largest contribution to an oscillatory integral (due to the presence of the imaginary i) is the one that oscillates the slowest.

3.2 Bosonic superfluids

3.2.1 Classical theory

The saddle-point equation for the action (3.10) is the Gross–Pitaevskii equation (which was derived indipendently in [75] and [62]), i.e.

$$\left[i\partial_t + \frac{1}{2m}\partial_i^2 - g|\varphi|^2 + \mu\right]\varphi = 0. \tag{3.12}$$

In the absence of an external trapping potential, the classical ground state is time-independent and uniform, $\varphi = \mathrm{const}$. We distinguish two very different families of solutions, depending on the sign of the chemical potential [76]. Above a certain critical temperature, the chemical potential is negative, and the solution is the trivial $\varphi = 0$. For a positive chemical potential, equation (3.12) specifies only the boson density $\varphi^\dagger\varphi \equiv n_0 = \mu/g$, while leaving the field to pick an arbitrary phase, hence $\varphi = e^{i\theta}\sqrt{\mu/g}$. The sudden development of an order parameter φ by crossing a critical temperature is a characteristic of continuous phase transitions à

[5] In Hamiltonian approaches to superfluids, the procedure equivalent to the saddle-point is commonly called 'mean-field' [74].

la Landau, here of the Bose–Einstein/superfluid transition. Therefore, for positive chemical potential, the systems possess long-range order. At saddle-point level, knowing φ in a specific point of space, enables us to know it everywhere.

Trapped BECs Since the first experimental realisation of Bose–Einstein condensation in 1995 ([77] and [78]), ultracold atomic gases provided a formidably tunable platform to study quantum matter and collective dynamics.
In typical settings, these systems exhibit a critical temperature of order 10^2 to 10^3 nanokelvins [79]. To prevent touching the chamber's walls (which are at room temperatures), the atoms have to be confined by external potentials. Hence, in the description of the order parameter (3.12), we have to add $V_{\text{ext}}(x)$. Neglecting gradient terms, the solution assumes the Thomas–Fermi profile $\varphi^\dagger\varphi\,(x) = \left(\mu - V_{\text{ext}}(x)\right)/g$. If we approximate the trapping potential as harmonic, the condensate density takes the form of an inverted parabola.

3.2.2 Effective theory

Having elucidated the ground state for the system, here we show an effective action for its elementary excitations, which will turn out to be linearly-dispersing and gapless. This does not happen by chance: the excitations are the Nambu–Goldstone bosons associated with the particle number symmetry breaking due to the system spontaneously choosing a phase.
First, for convenience, we introduce a polar representation of the complex field $\varphi = \sqrt{n}e^{i\theta}$ in terms of a density n and a phase θ. We assume that both are smooth and differentiable functions. In these variables, the action (3.10) is

$$\mathcal{L} = \frac{i}{2}\left(\partial_t n\right) - \frac{\left(\partial_i n\right)^2}{8mn} + n\left[\mu - \left(\partial_t\theta\right) - \frac{1}{2m}\left(\partial_i\theta\right)^2\right] - g\frac{n^2}{2}. \tag{3.13}$$

Then, we look at small fluctuations h around its saddle point[6] configuration $n_0 = \mu/g$,

$$n = n_0 + h. \tag{3.14}$$

The obtained Lagrangian contains two terms that we drop: one because it is a total derivative, and $\sim \left(\partial_i h\right)^2/n_0$ because it is subleading to h^2 in the long-wavelength

[6]This saddle-point approximation is nothing else than the minimization of the infamous 'wine bottle potential' [80]. While going around the rim of the bottom of the bottle (phase fluctuations) does not cost anything, density fluctuations cost a lot. In the wine bottle potential analogy, they correspond to climb the concave bottom up to where the person who pours the wine put the thumb. Therefore, h are necessarily small, if the perturbative approach is justified.

limit[7]. We obtain a particularly simple action for h and θ,

$$\mathcal{L} = h\left[\mathsf{X} - gn_0\right] + n_0\mathsf{X} - \frac{g}{2}h^2, \tag{3.15}$$

where we used the notation $\mathsf{X} \equiv gn_0 - \partial_t\theta - \frac{1}{2m}\left(\partial_i\theta\right)^2$ introduced in [81].
Since the density fluctuations enter only quadratically, they can be integrated out exactly. If we introduce the speed of sound $c_s^2 = gn/m$, we obtain the following effective Lagrangian

$$\mathcal{L}_{\text{eff}} = -n_0\left[(\partial_t\theta) + \frac{1}{2m}(\partial_i\theta)^2\right] + \frac{n_0}{2mc_s^2}\left[(\partial_t\theta) + \frac{1}{2m}(\partial_i\theta)^2\right]^2. \tag{3.16}$$

The Lagrangian contains only derivative terms $\partial_\mu\theta$ because it should be invariant under $U\left(1\right)$ particle number symmetry, for which the phase variable transforms inhomogeneously as $\theta \to \theta + \alpha$. As a consequence, non-uniform configurations are penalised, and the system manifests rigidity.
Apart from the compactness[8] of θ, (3.16) is exactly the same Lagrangian as the one for a hydrodynamic, ideal classical fluid with homentropic flow[9] [66]. Therefore, (3.16) suggests to identify the superfluid velocity as $v_s^i \equiv (\partial_i\theta)/m$.
The appearance of the combination

$$(\partial_t\theta) - 1/2m(\partial_i\theta)^2 \tag{3.17}$$

is not a mere coincidence. It is consistent with general considerations regarding Galilean symmetry in single-species systems of condensed bosons [82]. As a matter of fact, it is easy to check that the combination is invariant under Galilean boosts (3.11), that act on the phase variable as $\theta \to \theta + m\Lambda$.
We obtain the conserved charge and current associated to particle number symmetry with the method reviewed in [71]. The variation of the action with respect to local transformations $\theta \to \theta + \alpha(x^\mu)$ is arranged in the form $\delta S = \int(\rho\partial_t\alpha + J^i\partial_i\alpha)$, with

$$\rho \equiv n_0 - \frac{n_0}{mc_s^2}\left[\partial_t\theta + \frac{1}{2m}\left(\partial_i\theta\right)^2\right] \quad , \quad J_i \equiv \rho\left(\frac{\partial_i\theta}{m}\right). \tag{3.18}$$

Derivative expansion Since we assumed only slowly-varying θ, we can perform a derivative expansion neglecting cubic terms. The nonlinear Lagrangian

[7] There might be situations in which this devil-may-care attitude is not tolerable, because large density fluctuations happen on a short lengthscale.

[8] However, in Chapter 2 we have seen that a variable being compact allows for deep implications.

[9] In homentropic flows, the entropy per unit mass is constant, so pressure is a function only of the density.

(3.16) expanded to quadratic order in fluctuations is

$$\mathcal{L}^{(2)}_{\text{eff}} = -n_0\partial_t\theta + \frac{n_0}{2mc_s^2}[(\partial_t\theta)^2 - c_s^2(\partial_i\theta)^2], \tag{3.19}$$

and physically describes propagating density waves on top of a constant background. These excitations are gapless, linearly dispersing as $\omega(k) = c_s k$, and are called Bogoliubov phonons[10].

3.2.3 Vortices

In the previous subsection, we derived an effective action assuming that both the scalar field's density n and the phase θ were smooth, differentiable functions. We relax the latter assumption, because the superfluid phase might contain a singular part, on top of the regular one, $\theta = \theta_{\text{reg}} + \theta_{\text{sing}}$. Vortices in two-dimensional superfluids precisely belong to this class of field configurations. The phase $\theta_{\text{sing}} \equiv \theta_{\text{v}}$ of a vortex located at the position $x^i = X^i$ winds up a number q_v of times, i.e.

$$\epsilon^{ij}\partial_i\partial_j\theta_{\text{v}} = 2\pi q_{\text{v}}\delta^{(2)}(x^i - X^i), \tag{3.20}$$

where q_v is the *vortex charge* and it is an integer number[11].

3.2.4 Two-dimensional boson-vortex duality

Boson-vortex duality [8, 9] opened an interesting perspective on the physics of two-dimensional superfluids and quantum vortices. In the dual formulation, a $U(1)$ superfluid is identified with the Coulomb phase of a two-dimensional compact $u(1)$ gauge theory without instantons [83, 84]. The dual photon has only one polarization and corresponds to the Goldstone boson of the spontaneously broken particle number symmetry. In this language, vortices are point-like charges coupled minimally to the dual $u(1)$ gauge field a_μ. The latter has a finite background magnetic field fixed by the superfluid density that gives rise to the transverse Magnus force acting on vortices.

To derive the duality between two-dimensional vortices and point charges, we have to keep track of potential dangerous terms coming from the derivatives acting on the singular part. Following the notation of [51, 85] we represent the field φ in a polar form which involves three ingredients $\varphi = \sqrt{n}\, e^{i\theta_{\text{reg}}} e^{i\theta_{\text{v}}} \equiv \sqrt{n}\, e^{i\theta_{\text{reg}}}\chi$.

[10] Sometimes, people refer to 'relativistic' dispersion, considering the phonon as a 'slow' photon. In two dimensions, this statement is far from trivial, as we will realise in the next section.

[11] Take a look at our discussion of vortices in O(2) models, which we developed in Chapter 2.

We obtain the hydrodynamic form of φ^4 in the presence of vortices by the substitution $\partial_\mu\theta \to \partial_\mu\theta - i\chi^\dagger\partial_\mu\chi$ in (3.13)

$$\mathcal{L} = -n\left(\partial_t\theta - i\chi^\dagger\partial_t\chi\right) - \frac{\left(\partial_i n\right)^2}{8mn} - \frac{n}{2m}\left(\partial_i\theta - i\chi^\dagger\partial_i\chi\right)^2 + n\mu - \frac{g}{2}n^2. \quad (3.21)$$

We remove the quartic term in χ by using a Hubbard–Stranovich transformation[12], at the expense of introducing an additional *auxiliary* three-current $j^\mu \equiv \left(n, \sigma^i\right)$

$$\mathcal{L} = \frac{m}{2n}\sigma^2 - \frac{\left(\partial_i n\right)^2}{8mn} - j^\mu\left(\partial_\mu\theta - i\chi^\dagger\partial_\mu\chi\right) + n\mu - \frac{g}{2}n^2. \quad (3.22)$$

In the third term of the above Lagrangian, the regular part of the superfluid appears only once, hence its integration in the functional integral generates an effective action

$$\int \mathcal{D}j^\mu\mathcal{D}\chi\; e^{iS[\chi,j^\mu]} \int \mathcal{D}\theta\; e^{iS[\theta]} \to \int \mathcal{D}j^\mu\mathcal{D}\chi\; e^{iS_{\text{eff}}[\chi,j^\mu]}, \quad (3.23)$$

where j^μ obeys the constraint $\partial_\mu j^\mu = 0$. In other words, we chose the notation j^μ because we are dealing with a conserved three-current.
The constraint is automatically satisfied by expressing the current j^μ in terms of a gauge field a_μ which lives in three-dimensional space-time,

$$j^\mu = \epsilon^{\mu\alpha\beta}\partial_\alpha a_\beta. \quad (3.24)$$

In two spatial dimensions, the dual gauge field defines a magnetic field $b = \epsilon^{ij}\partial_i a_j$, and an electric field $e_i = \partial_t a_i - \partial_i a_t$ which possess only one polarization. Therefore, the components of the current in terms of physical degrees of freedom are

$$\begin{aligned} n &= b \\ \sigma^i &= -\epsilon^{ij}e_j. \end{aligned} \quad (3.25)$$

The next step is to express S_{eff} in terms of the gauge field. By massaging the third term in (3.22) and using the regular part smoothness $\epsilon^{\mu\nu\rho}\partial_\nu\partial_\rho\theta_{\text{reg}} = 0$, we recognise a coupling between the gauge field and a vortex current $-a_\mu j^{\text{vort}}_\mu$, where we define

$$j^\mu_{\text{vort}} \equiv \epsilon^{\mu\nu\rho}\partial_\nu\partial_\rho\theta_{\text{v}}. \quad (3.26)$$

Furthermore, the above coupling is the standard coupling of matter and three-dimensional electromagnetism. The full dual action is

$$\mathcal{L} = \frac{m\mathbf{e}^2}{2b} - \frac{\left(\partial_i b\right)^2}{8mb} + b\mu - \frac{g}{2}b^2 - a_\mu j^\mu_{\text{vort}}. \quad (3.27)$$

[12] $-U/2\,[\hat{o}(\theta,\chi)]^2 \to \sigma^2/(2U) - \sigma\,[\hat{o}(\theta,\chi)]$ using the conventions of [52, 86].

As we mentioned above, within this description, vortices are charged point particles that move in an emergent electromagnetic field. Hence, they feel an orthogonal Lorentz force from a magnetic field related to the original superfluid density (3.25). In the superfluid variables, the idea that the superfluid density acts on quantised vortices as a magnetic field acts on point charges was first intuited in [87] and the first derivation of the transverse force was obtained in [88].

3.3 Vortex lattices in bosonic superfluids

Since the discovery of superfluidity in ^{4}He, superfluids provide a never-ending source of inspiration for experimental and theoretical research in low-temperature physics. Although a regular superfluid flow is necessarily irrotational, superfluids can carry finite angular momentum in the form of topological defects known as quantum vortices, which nucleate naturally in response to external rotation. Under slow rotation, the density of bosons is much larger than that of the topological defects and the quantum vortices form a regular vortex lattice, which has been observed in superfluid He [6] and more recently also in cold atomic BECs [7]. At larger rotation frequencies, the vortex cores start to overlap, and at a certain point the vortex lattice is expected to undergo a melting transition into an incompressible bosonic quantum Hall regime [89].

The physics of a quantum vortex lattice in bosonic superfluids attracted considerable interest in the past (for reviews see [90–93]). In a series of beautiful papers, Tkachenko laid the theoretical foundations of this field. In the incompressible limit, he analytically demonstrated that the triangular arrangement of vortices has the lowest energy [94] and determined low-energy linearly-dispersing collective excitations [95, 96], known today as Tkachenko waves. In later years, the hydrodynamics of Tkachenko waves in incompressible superfluids was developed in [97–99]. With the advent of cold atom experiments, the main interest in this field shifted towards vortex lattices in compressible superfluids. These support a soft Tkachenko mode with a low-energy quadratic dispersion [100, 101], whose signatures were experimentally observed in [102]. The discrete time-reversal T and parity P symmetries of a two-dimensional bosonic superfluid are broken by external rotation (while its product PT is preserved).

In this section, using the boson-vortex duality [8, 9, 103], we write down a low-energy effective theory of an infinite vortex lattice in a bosonic superfluid. It will be argued below that this dual formulation, where the superfluid degrees of freedom are parametrized by a gauge field, has certain advantages compared to an effective theory previously introduced in [104]. After discussing the symmetries of the theory, we compute the $U(1)$ particle number and stress tensor linear responses to external sources. In addition to P and T-invariant responses, we

extract the Hall conductivity.

We concentrate on the bulk properties of two-dimensional vortex lattices, and thus consider infinite uniform systems, where momentum is a good quantum number. We expect that our results should be relevant to cold atom experiments with large vortex lattices (where the angular frequency of rotation Ω approaches the transverse trapping frequency $\omega_\perp$) and numerical simulations, where periodic boundary conditions are used. The effective field theory developed is not applicable in the quantum Hall regime.

3.3.1 Effective field theory of a vortex lattice

In [104] Watanabe and Murayama started from the microscopic Lagrangian of a two-dimensional weakly-coupled repulsive Bose gas that rotates with the angular frequency Ω and is trapped in a harmonic potential of frequency $\omega_\perp$ which is larger but very close to Ω. In a series of steps they arrived to a low-energy non-linear effective theory of an (essentially) infinite vortex lattice

$$\mathcal{L}_{\rm WM} = \mathsf{X}^2/g - \mathcal{E}_{\rm el}(u^{ij}), \tag{3.28}$$

where

$$\mathsf{X} \equiv \mu - \dot{\varphi} - m\Omega\epsilon_{ij}u^i\dot{u}^j - \frac{1}{2m}\big[\partial_i\varphi + 2m\Omega\epsilon_{ij}u^j + \, m\Omega\epsilon_{kl}u^k\partial_i u^l\big]^2, \tag{3.29}$$

μ is the chemical potential, φ is the regular part of the superfluid phase, and u^i is the vortex lattice's displacement from its equilibrium position. The Lagrangian also contains the elastic energy density $\mathcal{E}_{\rm el}(u^{ij})$ of the vortex lattice which depends on the strain tensor[13] $u^{ij} = (\partial^i u^j + \partial^j u^i - \partial_k u^i \partial^k u^j)/2$. Its functional form is fixed only by the geometry of the lattice, whatever its constituents are.
For a triangular vortex lattice, the elastic energy density, up to quadratic order in deformations, is [98, 101, 105]

$$\mathcal{E}^{(2)}_{\rm el}(\partial u) = 2C_1(\partial_i u^i)^2 + C_2\big[(\partial_x u^x - \partial_y u^y)^2 + (\partial_y u^x + \partial_x u^y)^2\big], \tag{3.30}$$

where C_1 and C_2 denote the compressional and shear modulus, respectively. The elastic properties of a two-dimensional triangular lattice are characterised by only two elastic moduli C_1 and C_2 and thus, in this respect, the lattice is indistinguishable from an isotropic medium [105]. As a result, although continuous rotation symmetry is broken spontaneously to a discrete subgroup, the theory and all observables respect continuous rotation symmetry[14]. In contrast to ordinary solids

[13] The sign discrepancy with (1.5) originates from a convention introduced in [109]. In the limit of small displacements and Cartesian coordinates, this difference is negligible.

[14] The violation of this symmetry is expected to arise from higher-derivative terms not included here.

we considered in Chapter 1, the vortex lattice's bulk modulus C_1 does not have to be non-negative to insure the system's stability [98, 101].
We obtain the superfluid density n_s and current j_s^i by coupling (3.28) to an external $U(1)$ source via the minimal coupling $\partial_\mu \to \partial_\mu + \mathcal{A}_\mu$ and computing

$$n_s = -\frac{\delta S_{\text{WM}}}{\delta \mathcal{A}_t} = \frac{2}{g}\Big(\mu - \dot{\varphi} - \mathcal{A}_t - m\Omega\epsilon_{ij}u^i\dot{u}^j - \frac{1}{2m}\big[\partial_i\varphi + \mathcal{A}_i + \\ + 2m\Omega\epsilon_{ij}u^j + m\Omega\epsilon_{kl}u^k\partial_i u^l\big]^2\Big), \tag{3.31}$$

$$j_s^i = -\frac{\delta S_{\text{WM}}}{\delta \mathcal{A}_i} = \frac{n_s}{m}\delta^{ij}\Big(\partial_j\varphi + \mathcal{A}_j + 2m\Omega\epsilon_{jk}u^k + m\Omega\epsilon_{kl}u^k\partial_j u^l\Big). \tag{3.32}$$

3.3.2 Dual effective field theory of a vortex crystal

We now use the vortex-boson duality we introduced in Subsection 3.2.4 and formulate the low-energy effective theory of an infinite two-dimensional vortex lattice in a bosonic superfluid rotating with an angular frequency Ω. In this formulation, the vortex lattice is a two-dimensional triangular lattice of point charges embedded into a static $u(1)$-charged background that neutralises the system, see Fig. 3.1. The theory is defined by the following Lagrangian

$$\mathcal{L}(e_i, b, u^i; \mathcal{A}_\mu) = \frac{m\mathbf{e}^2}{2b} - \varepsilon(b) - m\Omega b\epsilon_{ij}u^i D_t u^j + 2m\Omega e_i u^i + \\ - \mathcal{E}_{\text{el}}(u^{ij}) - \epsilon^{\mu\nu\rho}\mathcal{A}_\mu\partial_\nu a_\rho. \tag{3.33}$$

Here m denotes the mass of the elementary Bose particle, $D_t = \partial_t + v_s^k\partial_k$ is the convective derivative, and we have introduced the dual electric and magnetic fields (3.25) that are related to the coarse-grained superfluid number density n_s and coarse-grained superfluid velocity v_s^i,

$$n_s = b, \qquad v_s^i = -\frac{\epsilon^{ij}e_j}{b}. \tag{3.34}$$

The first two terms in the Lagrangian (3.33) represent the Galilean-invariant coarse-grained superfluid characterised by the internal energy density $\varepsilon(n_s)$ (see, for example, [106]). The fields u^i represent the Cartesian components of the coarse-grained displacements of the vortices from their equilibrium lattice positions. As will become explicit later, these fields are the Goldstone bosons of the translations which are spontaneously broken by the vortex lattice ground state. The third term in the Lagrangian (3.33) is the Magnus term that produces a force

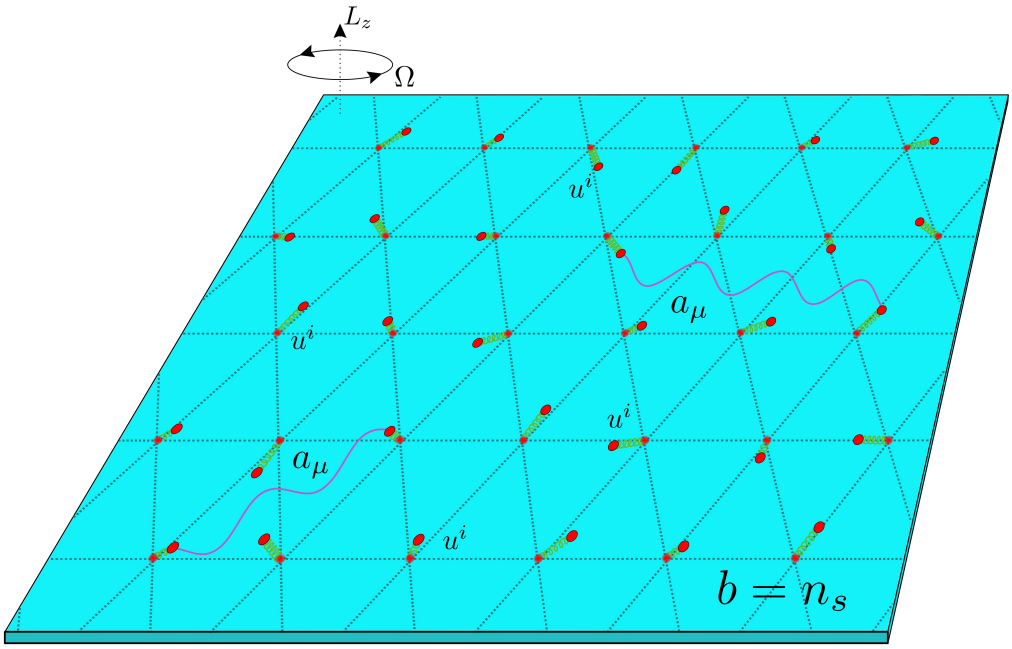

Figure 3.1: Dual crystal: point charges (red dots) form a triangular lattice in a homogenous neutralising background (cyan). Microscopic displacements and photons of the dual gauge field are represented by green springs and violet wavy lines, respectively. The degrees of freedom u^i and a_μ of the effective theory (3.33) are coarse-grained averages over large number of unit cells.

acting in the direction perpendicular to the velocity of vortices relative to the superfluid. Since the vortices are charged with respect to the dual field a_μ, the term $\sim e_i u^i$ in (3.33) represents the dipole energy density of displaced lattice charges in the presence of a static neutralising background. Finally, the last term in the Lagrangian (3.33) takes into account the coupling of the global $U(1)$ coarse-grained current

$$j^\mu_s = -\frac{\delta S}{\delta \mathcal{A}_\mu} = \epsilon^{\mu\nu\rho}\partial_\nu a_\rho = (n_s, n_s v^i_s) \tag{3.35}$$

to an external $U(1)$ source field $\mathcal{A}_\mu$. Here the source is defined to vanish (up to a gauge transformation) in the ground state and thus is associated with the deviation of the external rotation frequency from its ground state value Ω. For an infinite vortex lattice, the ground state is a state with $u^i = 0$, $b = n_0 = \text{const}$, $e^i = 0$, where the ground state particle density n_0 is fixed by the condition $d\varepsilon/db = 0$.

3.3.3 Theory (3.28) is equivalent to the dual theory (3.33)

We emphasize that the form of the effective theory (3.33) is not merely a guess, but is closely related to the Lagrangian (3.28). As we demonstrate here, for a special choice of the energy density $\varepsilon(b)$, the Lagrangian (3.33) is dual to the Lagrangian $\mathcal{L}_{\rm WM}$. Moreover, the dual electric and magnetic fields are related to the regular part of the superfluid phase and displacement vectors via Eqs. (3.34) and (3.31), (3.32). The two theories are related by a Legendre transformation [107] between the gauge variables and the superfluid ones

$$\mathcal{L}(b, e_i) = \mathcal{L}_{\rm WM}(\dot\varphi, \partial_i\varphi) + \dot\varphi b - (\partial_i\varphi)\,\epsilon^{ij} e_j. \tag{3.36}$$

Using now $n_s = b$ and $j_s^i = -\epsilon^{ij} e_j$ in Eq. (3.31), (3.32) we find

$$\begin{aligned} \partial_i\varphi &= -m\frac{\epsilon_{ij}e^j}{b} - \mathcal{A}_i - 2m\Omega\epsilon_{ij}u^j - m\Omega\epsilon_{kl}u^k\partial_i u^l, \\ \dot\varphi &= \mu - \frac{gb}{2} - \mathcal{A}_t - m\Omega\epsilon_{ij}u^i\dot u^j - \frac{me^2}{2b^2}. \end{aligned} \tag{3.37}$$

With the help of these expressions we can eliminate the derivatives of the phase φ from the right-hand-side of Eq. (3.36). As a result, we arrive at the Lagrangian (3.33) with the energy density $\varepsilon(b) = gb^2/2 - \mu b$.

Despite being equivalent to the original theory of [104], the dual formulation (3.33) has an important conceptual advantage. In contrast to the effective theory of [104], the linearised form of the dual theory naturally fits into a derivative expansion. This allows us to order different terms in the dual Lagrangian according to their relevance at low energies and long wavelengths and systematically construct corrections to the leading-order theory. Later in this chapter, we will also construct the diffeomorphism-invariant version of the theory (3.33).

Symmetries

Now we turn to the discussion of symmetries of the theory (3.33). Generically, the action of a low-energy effective theory should inherit all symmetries (irrespective of whether they are spontaneously broken and not) of the microscopic model.

First, under discrete parity and time reversal, the fields and sources transform as follows:

$$\begin{aligned} &P \quad x \leftrightarrow y, \quad a_t \to -a_t, \quad a_x \leftrightarrow -a_y \quad u^x \leftrightarrow u^y, \quad \mathcal{A}_x \leftrightarrow \mathcal{A}_y\,, \\ &T: \quad t \to -t, \quad a_t \to -a_t, \quad \mathcal{A}_i \to -\mathcal{A}_i\,. \end{aligned} \tag{3.38}$$

We find that the Lagrangian (3.33) is not invariant separately under P and T since the terms proportional to Ω change sign under these transformations. However,

the Lagrangian is invariant under the combined PT symmetry. Note that if one flips the sign of the rotation frequency $\Omega \to -\Omega$ under parity and time-reversal, then the theory is separately invariant under P and T.

Second, we consider spatial translations. In a microscopic theory of a rotating Bose superfluid, the angular frequency Ω is equivalent to an effective constant magnetic field $B_{\text{eff}} = -2m\Omega$, and thus the action should be invariant under magnetic translations [104]. In an infinite vortex lattice, the ground state breaks this symmetry spontaneously. Since in the dual formulation, the fields b, e_i and u^i transform trivially under particle number $U(1)$ global symmetry, magnetic translations of the vortex lattice are implemented as usual translations on these fields. Under an infinitesimal constant spatial translation $x^i \to x^i + l^i$, the fields transform as $\delta_l \Phi = -l^k \partial_k \Phi$, where $\Phi = (e_i, b, \mathcal{A}_\mu)$, but $\delta_l u^i = -l^k \partial_k u^i + 2l^i$. As expected for a Goldstone boson of broken translations, the field u^i transforms inhomogeneously. Using the Bianchi identity $\epsilon^{\mu\nu\rho}\partial_\mu \partial_\nu a_\rho = 0$, it is straightforward to check that the action $S = \int dt\, d^2x\, \mathcal{L}$ is invariant under spatial translations.

Finally, we investigate Galilean boosts. Once again, we use the fact that b, e_i and u^i are neutral under the particle number $U(1)$ symmetry, and thus an infinitesimal Galilean boost with the velocity β^i is realised on these fields as a time-dependent spatial diffeomorphism $x^i \to x^i + \beta^i t$:

$$\begin{aligned} \delta_\beta b &= -\beta^k t \partial_k b, \\ \delta_\beta e_i &= -\beta^k t \partial_k e_i + b\epsilon_{ik}\beta^k, \\ \delta_\beta u^i &= -\beta^k t \partial_k u^i + 2\beta^i t. \end{aligned} \tag{3.39}$$

On the other hand, the electric and magnetic fields constructed from the $U(1)$ source should transform as

$$\begin{aligned} \delta_\beta \mathcal{E}_i &= -\beta^k t \partial_k \mathcal{E}_i + \epsilon_{ij}\beta^i(\mathcal{B} - 2m\Omega), \\ \delta_\beta \mathcal{B} &= -\beta^k t \partial_k \mathcal{B}, \end{aligned} \tag{3.40}$$

where we have defined $\mathcal{E}_i = \partial_t \mathcal{A}_i - \partial_i \mathcal{A}_t$ and $\mathcal{B} = \epsilon^{ij}\partial_i \mathcal{A}_j$. The action built from the Lagrangian (3.33) is invariant under Galilean transformations. As we will see in the following, Galilean invariance has important consequences for the spectrum of excitations and transport properties.

Excitations and particle number transport

In this section, we work out some physical properties of the effective theory (3.33). In particular, we analyse its excitations and extract the $U(1)$ particle number transport coefficients such as longitudinal and Hall conductivities. To this end, it is

sufficient to expand the Lagrangian (3.33) around the ground state $b = n_0 + \delta b$ and keep only terms quadratic in fields and sources,

$$\mathcal{L}^{(2)} = \underbrace{\frac{m}{2n_0}\mathbf{e}^2}_{\text{NLO}} \underbrace{-\frac{mc_s^2}{2n_0}\delta b^2 - n_0 m\Omega\epsilon_{ij}u^i\dot{u}^j + 2m\Omega e_i u^i - \mathcal{E}^{(2)}_{\text{el}}(\partial u) - \epsilon^{\mu\nu\rho}\mathcal{A}_\mu\partial_\nu a_\rho}_{\text{LO}}\,, \tag{3.41}$$

where overdot denotes the time derivative and $c_s = \sqrt{n_0\varepsilon''/m}$ is the speed of sound. This Lagrangian naturally fits into a derivative expansion within the following power-counting scheme

$$a_i,\, u^i,\, \mathcal{A}_i \sim O(\epsilon^0), \qquad a_t,\, \partial_i,\, \mathcal{A}_t \sim O(\epsilon^1), \qquad \partial_t \sim O(\epsilon^2), \tag{3.42}$$

where $\epsilon \ll 1$. In particular, one finds that all terms in Eq. (3.41), except the first one, scale as $O(\epsilon^2)$; these terms will be referred to as leading-order (LO) terms in the following. On the other hand, the electric term $\sim \mathbf{e}^2$ scales as $O(\epsilon^4)$ and thus contributes to the next-to-leading order (NLO) in this power-counting scheme. In the following, we will first work with the leading order Lagrangian and subsequently analyse the next-to-leading order corrections produced by the electric term.

Leading order

We first extract the excitations above the ground state from the LO part of the Lagrangian (3.41) in the absence of the source $\mathcal{A}_\mu$. In the LO theory, the Galilean symmetry is broken and the dual gauge field is not dynamical. The Gauss law $\delta S_{\text{LO}}/\delta a_t = 0$ implies $\partial_i u^i = 0$ and thus displacements are transverse. In other words, the vortex lattice is incompressible and the vortex density n_v is constant in position space. The remaining four field equations are

$$\begin{aligned} &c_s^2\epsilon^{ij}\partial_j\delta b + 2n_0\Omega\dot{u}^i = 0, \\ &2m\Omega e_i - 2n_0 m\Omega\epsilon_{ij}\dot{u}^j + \partial_j\frac{\partial\mathcal{E}^{(2)}_{\text{el}}}{\partial\partial_j u^i} = 0. \end{aligned} \tag{3.43}$$

From now on, we work in the temporal gauge $a_t = 0$, where $e_i = \dot{a}_i$ and, without loss of generality, look for plane-wave solutions that propagate along the x direction, i.e., where δb, e_i and u^i do not depend on y. As a result, the Gauss law now

implies $u^x = 0$. In Fourier space, the field equations, written in matrix form, are

$$\begin{pmatrix} 0 & c_s^2 k^2 & -2in_0\Omega\omega \\ -i\omega & 0 & i\omega n_0 \\ 0 & -i\omega & -\frac{C_2}{m\Omega}k^2 \end{pmatrix} \begin{pmatrix} a_x \\ a_y \\ u^y \end{pmatrix} = 0. \tag{3.44}$$

The linear system has a nontrivial solution only if the determinant vanishes, which fixes the dispersion relation

$$\omega(k) = \sqrt{\frac{C_2 c_s^2}{2mn_0\Omega^2}}k^2. \tag{3.45}$$

It is known that a vortex lattice in a compressible superfluid ($c_s^{-1} \neq 0$) supports the Tkachenko mode which has the dispersion (3.45) at small momenta [100, 101]. Moreover, since the vortex lattice is incompressible in the LO theory, the dispersion depends only on the shear elastic modulus C_2, but not on the bulk modulus C_1. In one of the next subsections we will find that the inclusion of the NLO electric term gives rise to quartic corrections to the Tkachenko dispersion relation.

Integrating the dual photon

We can extract the Tkatchenko excitation (3.45) at leading-order in an alternative and equivalent way. We can straightforwardly integrate the gauge field in the LO part of the quadratic Lagrangian (3.41) $\mathcal{L}^{(2)}_{\rm LO} = -mc_s^2/(2n_0)\delta b^2 + 2m\Omega e_i u^i + \mathcal{L}_{\rm el}(u^i)$, whereas the elastic part $\mathcal{L}_{\rm el}(u^i)$ only contains the displacement u^i, through the Magnus term and the triangular lattice's energy. We move our description from physical to redundant vector potential a_μ degrees of freedom. In terms of the gauge field fluctuations of the magnetic field $\delta b = \epsilon^{ij}\partial_i a_j$ and electric field $e_i = \dot{a}_i - \partial_i a_t$ we have the Lagrangian

$$\mathcal{L}^{(2)}_{\rm LO}(a_\mu, u^i) = -\frac{mc_s^2}{2n_0}(\epsilon^{ij}\partial_i a_j)^2 + 2m\Omega(\partial_t a_i - \partial_i a_t)u^i + \mathcal{L}_{\rm el}(u^i). \tag{3.46}$$

The theory is quadratic, therefore we progressively integrate over the field configurations a_μ. In our case, only the spatial part of the gauge field enters quadratically[15] in the action, i.e. we deal with some kind of magnetostatic:

$$S[a_i, a_t] = \int dt\, d^2x \left[-\frac{1}{2}a_p K^{pj} a_j + a_i j_1^i\right] + S[a_t, u^i] + S_{\rm el}[u^i] \tag{3.47}$$

[15]Hereby we report the Gaussian integral $\int D\varphi\, e^{i\int d^dx\left[-\frac{1}{2}\varphi K\varphi + J\varphi\right]} = e^{i\int d^dx\left[\frac{1}{2}JK^{-1}J\right]}$.

with $K_{pj} \equiv mc_s^2/n_0\left(\partial_j\partial_p - \partial^2 g_{pj}\right)$ and $j_1^i \equiv -2m\Omega\dot{u}^i$. The kernel of the operator K_{pj} contains the zero element and every smooth vector of the form $\partial_j\Lambda\,(x)$. Therefore, the operator is singular, and we have to fix this issue to find its inverse hence perform the integration. The procedure is due to Fadeev and Popov, and it is a standard trick in electromagnetism and other more complicated gauge theories. It consists of replacing the original action with an effective action that depends on an external parameter ξ

$$S[a_i] \to S_{\text{eff}}[a_i] = S[a_i] - 1/(2\xi)\int dt\; d^2x\; (\partial_p a_p)(\partial_j a_j). \tag{3.48}$$

We can choose the parameter ξ to simplify the calculation as much as possible. Physical predictions should be independent of the choice of ξ. With this mathematical trick, we replace the singular operator with the invertible one $[K_{\text{eff}}]_{pj} \equiv mc_s^2/n_0[-g_{pj}\partial^2+(1-1/\xi)\partial_p\partial_j]$ or, in momentum space, $[K_{\text{eff}}]_{pj} = mc_s^2/n_0[g_{pj}k^2-(1-1/\xi)k_pk_j]$. Its inverse is

$$[K_{\text{eff}}^{-1}]_{pj} = \frac{n_0}{mc_s^2}\left[g_{pj}\frac{1}{k^2} - (1-\xi)\,\frac{k_pk_j}{k^4}\right]. \tag{3.49}$$

At this point, we integrate out the spatial part of the gauge potential. Due to the instantaneous photon, we obtain a non-local action

$$S[a_i, u^i] \to S_{\text{NL}}[u^i] = \int dt\; d^2k\; \frac{2n_0m\Omega^2}{c_s^2}\left[\frac{(\dot{u}^i)^2}{k^2} - \frac{(1-\xi)}{k^4}(k_i\dot{u}^i)^2\right], \tag{3.50}$$

and the full action is $S[u^i] = S_{\text{NL}}[u^i] + 2m\Omega a_t(\partial_i u^i) + S_{\text{el}}\left[u^i\right]$. Integration with respect to the spatial part of the gauge potential a_t fixes the divergenceless of the crystal displacement field $\partial_i u^i = 0$ and cancels the second term in (3.50),

$$S[u^i] = \int dt\; d^2k\; \frac{2n_0m\Omega^2}{c_s^2}\frac{(\dot{u}^i)^2}{k^2} + S_{\text{el}}[u^i]. \tag{3.51}$$

Being a transverse field, we can introduce a scalar field φ such that $u^i = \epsilon^{ij}\partial_j\varphi$. With this procedure the "propagator" of the photon disappears $k^{-2}(\dot{u}^i)^2 \to -\dot{\varphi}^2$. In terms of φ, the elastic part of the action contains spatial derivatives of the fourth-order

$$\mathcal{L}_{\text{el}}(\varphi) = -(n_0m\Omega\epsilon^{ij}\partial_i\varphi\partial_j\dot{\varphi} + C_2[4(\partial_{xy}^2\varphi)^2 + (\partial_x^2\varphi)^2 + (\partial_y^2\varphi)^2 - 2(\partial_x^2\varphi)(\partial_y^2\varphi)]) \tag{3.52}$$

Integrating by parts and, as usual, dropping boundary terms, we obtain the uninvolving quadratic Lagrangian

$$\mathcal{L} = \;\varphi[\partial_t^2 + c_s^2/(2\Omega)\epsilon^{ij}\partial_i\partial_j\partial_t - \frac{C_2c_s^2}{2n_0m\Omega^2}\partial^4]\varphi, \tag{3.53}$$

where we introduced the two-dimensional biharmonic (or bilaplacian) operator $\partial^4 \equiv (\partial_x^4 + 2\partial_{xxyy}^4 + \partial_y^4)$. The second term vanishes for all smooth configurations φ due to the antisymmetric symbol. If we look at the excitation spectrum of the theory by taking plane waves $\partial^4 \to k^4$ the dispersion is

$$\omega(k) = \sqrt{\frac{C_2 c_s^2}{2mn_0\Omega^2}} k^2. \tag{3.54}$$

The above result exactly matches what we obtained in (3.45).

Transport at leading order

We now turn to the computation of the $U(1)$ particle number linear response. To this end one has to determine how the particle number current $j_s^\mu = \epsilon^{\mu\nu\rho}\partial_\nu a_\rho$ responds to variations of the $U(1)$ source $\mathcal{A}_\mu$. In particular, the density susceptibility χ, the longitudinal conductivity σ and the Hall conductivity $\sigma_{\rm H}$ are defined in Fourier space as

$$\begin{aligned}
\chi(\omega,k) &= \frac{\delta n_s}{\delta \mathcal{A}_t}\Big|_{\omega,k}, \\
\sigma(\omega,k) &= \sigma_{xx}(\omega,k) = \frac{i}{\omega}\frac{\delta j_s^x}{\delta \mathcal{A}_x}\Big|_{\omega,k} = \frac{i}{k}\frac{\delta j_s^x}{\delta \mathcal{A}_t}\Big|_{\omega,k}, \\
\sigma_{\rm H}(\omega,k) &= \sigma_{xy}(\omega,k) = -\frac{i}{\omega}\frac{\delta j_s^y}{\delta \mathcal{A}_x}\Big|_{\omega,k} = -\frac{i}{k}\frac{\delta j_s^y}{\delta \mathcal{A}_t}\Big|_{\omega,k}.
\end{aligned} \tag{3.55}$$

In order to extract these functions from the LO effective theory, we first solve the linearised field equations in the presence of the $U(1)$ source, substitute the solutions into the particle number current (3.35), and finally apply the definitions (3.55). As a result, we get

$$\begin{aligned}
\chi(\omega,k) &= \frac{C_2 k^4}{2m^2\Omega^2}\frac{1}{\omega^2 - \frac{C_2 c_s^2}{2mn_0\Omega^2}k^4}, \\
\sigma(\omega,k) &= \frac{iC_2 k^2\omega}{2m^2\Omega^2}\frac{1}{\omega^2 - \frac{C_2 c_s^2}{2mn_0\Omega^2}k^4}, \\
\sigma_{\rm H}(\omega,k) &= \frac{n_0\omega^2}{2m\Omega}\frac{1}{\omega^2 - \frac{C_2 c_s^2}{2mn_0\Omega^2}k^4}.
\end{aligned} \tag{3.56}$$

In the static regime $\omega = 0$, we find $\chi(k) = -n_0/(mc_s^2)$, which satisfies the compressibility sum rule $\chi(k=0) = -\partial n/\partial\mu = -n_0/(mc_s^2)$. We observe that the gapless Tkachenko excitation saturates the transport of particle number at low energies and long wavelengths.

Beyond the leading order

We now go beyond the LO. We will not try to construct the most general NLO Lagrangian, but only include the NLO electric term, which has important physical consequences. First, it will become manifest later that the Galilean symmetry, lost at leading order, is now restored. Second, the Gauss law now reads

$$\partial_i\big(u^i + \frac{1}{2n_0\Omega}e^i\big) = 0, \tag{3.57}$$

and thus the vortex lattice becomes compressible and the displacement field u^i is not transverse any more.

The calculation of the dispersion of excitations is straightforward, but tedious; here we present only the main results, see also Fig. 3.2. In the presence of the electric term one finds two physical modes. The first mode is the Tkachenko mode, which is now elliptically polarized[16]

$$\frac{u^x}{u^y} = i\sqrt{\frac{C_2 c_s^2}{8mn_0\Omega^4}}k^2 + O(k^4), \tag{3.58}$$

and has the dispersion

$$\omega(k) = \sqrt{\frac{C_2 c_s^2}{2mn_0\Omega^2}}\left[k^2 - \frac{2C_2 + mn_0c_s^2}{8mn_0\Omega^2}k^4 + O(k^6)\right]. \tag{3.59}$$

In addition, one finds the gapped Kohn mode with the dispersion

$$\omega(k) = 2|\Omega|\left[1 + \frac{4\,(C_1 + C_2) + mn_0c_s^2}{8mn_0\Omega^2}k^2 + O\left(k^4\right)\right]. \tag{3.60}$$

At zero momentum this mode is circularly polarized. We observe that the Galilean symmetry of the problem is restored by the NLO electric term and ensures that the high-energy Kohn mode is properly captured by the low-energy effective theory.

The computation of the particle number linear response follows the same steps as described in the previous calculation. The analytical expressions for χ, σ and $\sigma_{\rm H}$ are cumbersome. For this reason, here we limit our discussion of the $U(1)$ response functions to a few special regimes.

We start with the density susceptibility χ which vanishes in the homogeneous case $k = 0$, $\omega \neq 0$. This makes sense since particle density should not change under variations of a uniform time-dependent electrostatic potential. In the static

[16] As before, in this subsection we consider a plane-wave ansatz with momentum $\mathbf{k} = (k, 0)$.

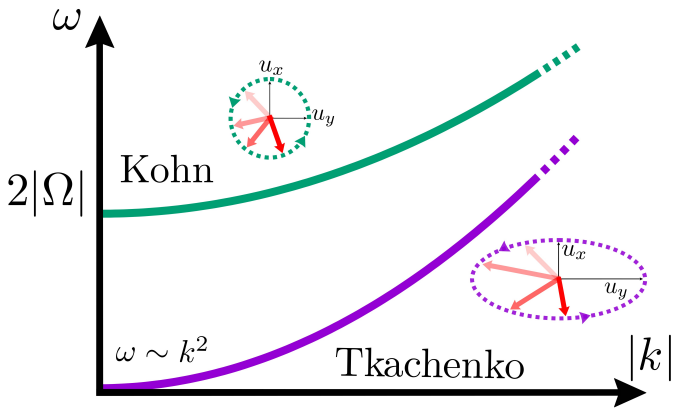

Figure 3.2: Sketch of dispersions and polarizations of Tkachenko and Kohn excitations.

regime, the compressibility sum rule $\chi(k \to 0) = -\partial n/\partial\mu = -n_0/(mc_s^2)$ is satisfied.

Now we turn to the conductivities. In the static regime $\omega = 0$, we find that the vortex lattice behaves as an insulator, i.e., $\sigma(k) = \sigma_{\mathrm{H}}(k) = 0$. Consider now the regime of finite ω, but small k. Expanding conductivities in momentum around $k = 0$, one finds[17]

$$\begin{aligned}\sigma(\omega,k) &= i\frac{n_0\omega}{m(\omega^2-4\Omega^2)} + i\frac{mn_0\omega^2c_s^2 + 2C_2\left(\omega^2+4\Omega^2\right)+4C_1\omega^2}{m^2\omega\left(\omega^2-4\Omega^2\right)^2}k^2 + O\left(k^4\right),\\ \sigma_{\mathrm{H}}(\omega,k) &= -\frac{2n_0\Omega}{m(\omega^2-4\Omega^2)} - \frac{2\Omega\left(mn_0c_s^2+4\left(C_1+C_2\right)\right)}{m^2\left(\omega^2-4\Omega^2\right)^2}k^2 + O\left(k^4\right).\end{aligned} \tag{3.61}$$

The first terms in the Taylor expansion are exact conductivities in the homogeneous $k = 0$ regime and their form is fully fixed by the Kohn theorem. We put together the longitudinal and Hall conductivities into the leading order conductivity tensor

$$\sigma_{ij}^{(0)}(\omega) = \frac{n_0}{m(\omega^2-4\Omega^2)}\left(i\omega\delta_{ij} - 2\Omega\epsilon_{ij}\right). \tag{3.62}$$

Formally, it is possible to extract the leading order result (3.56) from the response functions discussed here. To this end, we introduce a small parameter δ and replace $\omega \to \delta^2\omega$ and $k \to \delta k$ in response functions. The leading order of the

[17] In general, the conductivities depend on the frequency ω and the momentum vector $\mathbf{k}$. In the light of our ansatz, the expressions (3.61) are only valid for momenta $\mathbf{k} = (k, 0)$.

Taylor expansion in δ of the functions χ, σ and $\sigma_{\rm H}$ gives exactly (3.56). Finally, it is important to remark again that we did not attempted to construct the most general theory that includes all NLO terms that are consistent with symmetries. As a result, the subleading corrections to observables, such as the quartic term in the Tkachenko dispersion (3.59) and the quadratic terms in conductivities (3.61), might be modified by the omitted NLO terms.

3.3.4 Dual effective field theory - Lagrange formulation

One might be not fully satisfied with the effective theory (3.33) for the following reason. Although the displacement field u^i carries a spatial index, it does not transform as a vector field under spatial general coordinate transformations (diffeomorphisms) because it is the Goldstone mode of spontaneously broken magnetic translations. Hence, the generalization of the theory (3.33) to a form valid in general curvelinear coordinate is not straightforward. In order to circumvent this problem, we introduce here an alternative formalism used previously to describe solids [108–110]. Instead of displacements, we introduce a set of scalar fields $X^a(t,\mathbf{x})$, with $a = 1,2$, that represent the Lagrange coordinates frozen into the vortex lattice. In other words, any vortex has a constant coordinate X^a along its worldline. Imagine now a two-dimensional curved surface parametrized by a general set of spatial coordinates x^i with a geometry given by a metric tensor g_{ij}. In these coordinates, the effective action of the vortex lattice is given by $S = \int dt d^2x\, \sqrt{g}\mathcal{L}$, with the scalar Lagrangian

$$\mathcal{L} = \frac{m g^{ij} e_i e_j}{2b} - \varepsilon(b) - \pi n_v \varepsilon^{\mu\nu\rho}\epsilon_{ab} a_\mu \partial_\nu X^a \partial_\rho X^b - \mathcal{E}_{\rm el}(U^{ab}) - \varepsilon^{\mu\nu\rho} A_\mu \partial_\nu a_\rho, \quad (3.63)$$

where $g = \det g_{ij}$, $b = \epsilon^{ij}\partial_i a_j/\sqrt{g}$, $\varepsilon^{\mu\nu\rho} = \epsilon^{\mu\nu\rho}/\sqrt{g}$ and $U^{ab} = g^{ij}\partial_i X^a \partial_j X^b$. The vortex number current $j_v^\mu \sim \varepsilon^{\mu\nu\rho}\epsilon_{ab}\partial_\nu X^a \partial_\rho X^b$ couples to the dual gauge field a_μ. In contrast to the theory introduced in Sec. 3.3.2, in this formulation, the $U(1)$ source A_μ has a finite background magnetic field $B = \epsilon^{ij}\partial_i A_j = -2m\Omega$. There is no unique way how the Lagrange coordinates are defined in a solid, which leads to global symmetries that act in internal space. In particular, the action must be invariant under constant internal shifts $X^a \to X^a + l^a$. In addition, the theory is also invariant under discrete internal rotations that map the triangular lattice to itself. This symmetry constraints the form of the elastic term $\mathcal{E}_{\rm el}(U^{ab})$. With n_v transforming as a scalar, the action is invariant under spatial general coordinate transformations. The non-linear theory (3.63) fits naturally into a derivative expansion with the following power-counting scheme ($\epsilon \ll 1$)

$$a_i,\, X^a,\, A_i \sim O(\epsilon^{-1}), \qquad a_t,\, A_t \sim O(\epsilon^0), \qquad \partial_i \sim O(\epsilon^1), \qquad \partial_t \sim O(\epsilon^2). \quad (3.64)$$

The difference in the scaling of space and time originates from the quadratic dispersion of the soft Tkachenko mode. In this power counting, the first term in the Lagrangian (3.63) is of order $O(\epsilon^2)$ and becomes the next-to-leading order correction to the remaining terms in Eq. (3.63) that all scale as $O(\epsilon^0)$ and thus constitute the leading-order part. The Maxwell equations that follow from the Lagrangian (3.63) are

$$\tilde{B} + \pi n_v \varepsilon^{ij} \epsilon_{ab} \partial_i X^a \partial_j X^b = 0, \tag{3.65}$$

$$\tilde{E}_j + 2\pi n_v \epsilon_{ab} \dot{X}^a \partial_j X^b - \varepsilon''(b) \partial_j b = 0, \tag{3.66}$$

where we have introduced $\tilde{B} = B - m\varepsilon^i_{\ j} \partial_i v_s^j$ and $\tilde{E}_j = E_j - m\big(\dot{v}_{s\,j} + g_{mn} v_s^m \partial_j v_s^n\big)$. By taking the variation of the action with respect to X^a we find

$$\pi n_v \varepsilon^{\mu\nu\rho} \epsilon_{ab} \partial_\mu a_\nu \partial_\rho X^b - \frac{1}{\sqrt{g}} \partial_j \big(\sqrt{g} \frac{\partial \mathcal{E}_{\text{el}}}{\partial U^{ab}} g^{ij} \partial_j X^b \big) = 0. \tag{3.67}$$

3.3.5 Theory (3.33) is equivalent to theory (3.63) in Cartesian coordinates

Here we demonstrate that the diffeomorphism-invariant theory defined by the Lagrangian (3.63) reduces in Cartesian coordinates of flat space to (3.33). In this case, $g_{ij} = \delta_{ij}$ and Eq. (3.63) simplifies to

$$\mathcal{L} = \frac{m\delta^{ij} e_i e_j}{2b} - \varepsilon(b) - \pi n_v \epsilon^{\mu\nu\rho} \epsilon_{ab} a_\mu \partial_\nu X^a \partial_\rho X^b - \mathcal{E}_{\text{el}}(U^{ab}) - \epsilon^{\mu\nu\rho} A_\mu \partial_\nu a_\rho. \tag{3.68}$$

In addition, in these coordinates we can choose $X^a = \delta^a_i (x^i - u^i)$ which implies

$$-\pi n_v \epsilon^{\mu\nu\rho} \epsilon_{ab} a_\mu \partial_\nu X^a \partial_\rho X^b \to -m\Omega b \epsilon_{ij} u^i D_t u^j + 2m\Omega e_i u^i - 2m\Omega a_t, \tag{3.69}$$

where we dropped surface terms and used $n_v = m\Omega/\pi$. Now the last term in Eq. (3.69) is compensated by the contribution from the last term in Eq. (3.68) since the source A_μ has a finite background magnetic field $B = -2m\Omega$. This results in a simple shift of the source $A_\mu \to \mathcal{A}_\mu$ which now has zero background magnetic field. Finally, in Cartesian coordinates

$$U^{ab} = \delta^{ij} \partial_i X^a \partial_j X^b = \delta^{ab} - \underbrace{\big(\partial^a u^b + \partial^b u^a - \partial^c u^a \partial^c u^b \big)}_{2u^{ab}} \tag{3.70}$$

and thus U^{ab} is fully determined by the deformation tensor u^{ab}.

3.4 Conclusions and outlook

In this chapter we constructed an effective theory of a quantum vortex lattice in a bosonic Galilean-invariant compressible superfluid. We note that our NLO theory does not have the most general form consistent with symmetries. Despite these shortcomings, we believe that our theory captures properly the excitations and linear response of the quantum vortex lattice. In the future it would be important to perform a systematic construction of the effective theory in its most general form. Regular vortex lattices were also observed in cold atom experiments with rotating fermionic s-wave superfluids [111]. It would be interesting to apply the effective theory we developed to these systems. Moreover, vortex lattices should also be formed in rotating chiral superfluids and it would be interesting to construct effective theories of these states and apply these theories to rotating ^{3}He-A superfluids. The physics of vortices on curved surfaces is fascinating, for review see e.g. [112]. It would be very interesting to apply our effective theory to vortex lattices that live on curved substrates. Finally, one may wonder if the effective theory developed here can be directly applied to a thin superconducting film in an external perpendicular magnetic field. It is known that in this systems in the absence of disorder the triangular vortex lattice is stable under perturbations [113] and is a good candidate for the ground state. In addition, due to inefficient screening the vortices interact logarithmically [114] up to the Pearl length $\Lambda = 2\lambda_L^2/d$, where λ_L is the London penetration length and d is the width of the film. For thin films ($\lambda_L \gg d$) the Pearl length can be very large. Nevertheless, it was shown in [113] that the dispersion relation of lattice vibrations scale at low momenta as $\omega \sim k^{3/2}$ which differs from the quadratic Tkachenko dispersion. Fractional dispersion at low momenta originates from the coupling to the electromagnetic field that propagates in three spatial dimensions. We thus expect that our effective theory of the vortex lattice can be employed also in clean thin superconducting films after dynamical electromagnetism is included.

Chapter 4

Rayleigh edge waves in two-dimensional crystals with Lorentz forces. From skyrmion crystals to gyroscopic media

In this chapter, we extend the investigation of Rayleigh waves, that we encountered in Chapter 1, to the context of two-dimensional elastic solid that are composed of topological textures introduced in the last section of Chapter 2. Similarly to the vortices studied in Chapter 3, also skyrmions obey a transverse dynamics which originates from a Berry term. The term breaks time-reversal and parity symmetries, so it is natural to ask whether this reflects on the excitations the solid exhibits at its boundaries. Therefore, we investigate if a generalisation of Rayleigh waves exists in the two-dimensional skyrmion lattice which is hosted inside a thin-film chiral magnet. We find that the direction of propagation of the Rayleigh modes is determined not only by the chirality of the thin-film, but also by the Poisson ratio of the crystal. We discover three qualitatively different regions distinguished by the chirality of the low-frequency edge waves, and study their properties. Apart from skyrmion crystals, our results are also applicable to edge waves of gyroelastic media and screened Wigner crystals in magnetic fields.

4.1 Introduction

Recent years have seen a new surge of excitement around chiral surface waves in hydrodynamics [115–122]. The role of bulk topology for the existence and robustness of such waves has been vigorously investigated [115, 116, 119, 121, 122]. Chiral surface modes have been also recently used as a tool to measure the bulk

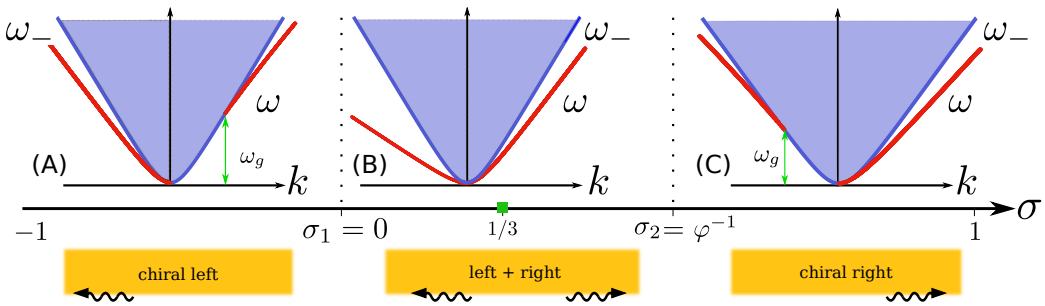

Figure 4.1: Sketched dispersion relations of Rayleigh surface excitations $\omega(k)$ (red) as a function of the Poisson ratio σ. In cases (A) and (C) the low-frequency spectrum is chiral, while in the intermediate regime $0 \leq \sigma \leq \varphi^{-1}$ edge waves of both chiralities are present. Here $\varphi \equiv (1+\sqrt{5})/2$ is the golden ratio. The green square denotes the point $\sigma = 1/3$ where the edge wave spectrum is symmetric. Plotted in blue are cross sections of the gapless bulk excitation.

Hall viscosity of an active fluid [123].

Here we study surface waves in two-dimensional crystals which break parity P (spatial reflection) and time-reversal T symmetry, but preserve the combined PT symmetry. In the quantum realm, well-known examples of such systems are two-dimensional thin-film chiral magnets, which host lattices formed out of skyrmions [51, 124–126], Wigner crystals in a magnetic field [127] and Abrikosov vortex lattices in superconductors and rotating superfluids [128]. In the last few years such crystals were also designed in gyroscopic metamaterials [129, 130] and mass-spring networks subject to Coriolis forces [131].

The general focus of this chapter is the investigation of a long-wavelength effective field theory of a two-dimensional skyrmion lattice, where the Cartesian components of the displacement from equilibrium positions u^x and u^y are coupled by a Berry term [132, 133]. The displacements are assumed to be small, which allows the framework of linear elasticity to be employed. We find that the behaviour of the edge-waves can be tuned by changing the Poisson ratio σ [19]. In fact, we show that there exist three qualitatively distinct phases, captured by the diagram in Fig. 4.1. The phases are distinguished by the propagation direction of their low-frequency surface waves. In the long-wavelength and low-frequency limit we develop an analytic treatment of these edge waves.

4.2 Skyrmion crystal elasticity in thin-film chiral magnets

It is well-known that an elementary skyrmion texture in a ferromagnet experiences an effective magnetic field $\mathcal{B}$ and the associated Lorentz force because it picks up a Berry phase of 2π whenever encircling a spin $1/2$ [134]. Moreover, a skyrmion can be characterised by a finite inertial mass m, which was derived in [135] by integrating out fluctuations of its spatial profile. Hereby we study the surface waves of two-dimensional skyrmion lattices present in thin-film chiral magnets such as $Fe_{0.5}Co_{0.5}Si$ [125] and FeGe [126]. Starting from the continuum theory of [132, 133], the skyrmion dynamics is described by a field theory of coarse-grained elastic variables $u^i(\mathbf{x})$ with $i = x, y$, denoting the displacements of skyrmions from their equilibrium positions, see [51] for a pedagogical exposition. The action of the skyrmion displacement field is given by

$$S[u^i] = \int dt\, d^2x \left[\frac{\rho}{2}\dot{u}^2 - \frac{\rho\Omega}{2}\epsilon_{ij}u^i\dot{u}^j - \mathcal{E}_{\rm el}(u_{ij}) \right], \tag{4.1}$$

where the overdot denotes the time derivative, ρ is the mass density of the skyrmions, $\Omega = \mathcal{B}/m$ is the cyclotron frequency associated with the effective magnetic field $\mathcal{B}$, $u_{ij} \equiv \partial_{(i}u_{j)}$ is the symmetric linearised strain tensor, and $\mathcal{E}_{\rm el}(u_{ij})$ the elastic energy density, dictated by the geometry of the crystal. The convention for the completely antisymmetric Levi-Civita symbol is $\epsilon_{xy} = -\epsilon_{yx} = 1$ and summation over repeated indices is understood. At low frequencies, the Berry term in Eq. (4.1), which gives rise to an effective Lorentz force, dominates the first term that encodes the Newtonian dynamics. As a result, u^x and u^y form a canonically conjugate pair of variables in the limit $m \to 0$. The Berry term breaks the time-reversal T ($t \to -t$) and parity P ($x \to -x$, $u^x \to -u^x$) symmetries, but preserves their combination.

We assume that skyrmions form a triangular lattice, whose symmetry class, C_6, limits $\mathcal{E}_{\rm el}(u_{ij})$ in two dimensions to the isotropic form [18, 19]

$$\mathcal{E}_{\rm el}\left(u_{ij}\right) = 2C_1u_{kk}^2 + 2C_2\tilde{u}_{ij}^2, \tag{4.2}$$

where $\tilde{u}_{ij} \equiv u_{ij} - (u_{kk}\delta_{ij})/2$ is the traceless symmetric part of the strain tensor. The *compressional* elastic modulus $2C_1$ quantifies the change of energy due to deformations that preserve the shape of the system but change its volume, while the *shear* modulus C_2 fixes the energy cost of volume-preserving deformations. In the context of effective field theories, C_1 and C_2 are just parameters of the derivative expansion and can take arbitrary non-negative values.

While the action in (4.1) is the effective theory governing skyrmion lattice dynamics, at long wavelengths it also describes elastic gyroscopic systems in the

limit of small nutation angle [136]. Moreover, it can also be used to describe certain screened Wigner crystals in magnetic fields [137].

The action (4.1) is quadratic and the resulting equations of motion are linear

$$\ddot{u}^i + \Omega\epsilon_{ij}\dot{u}^j = 2v_1\partial_i\left(\partial_p u^p\right) + v_2\partial^2 u^i, \tag{4.3}$$

where we introduced $v_1 \equiv 2C_1/\rho$, $v_2 \equiv 2C_2/\rho$. Assuming an infinite system that respects magnetic translational invariance in both directions, the equations of motion (4.3) are algebraic in frequency/wavevector space. Contrary to the situation where the Berry term is absent, the modes do not decouple into the longitudinal and transverse components. The set of equations (4.3) can be solved with elementary methods, and the two solutions for the dispersion relations are given by

$$\omega_{\mp}^2 = \frac{\Omega^2}{2} + (v_1+v_2)k^2 \mp k^2\sqrt{v_1^2 + (v_1+v_2)\frac{\Omega^2}{k^2} + \frac{\Omega^4}{4k^4}}. \tag{4.4}$$

Due to their cumbersome form, the polarizations $\epsilon_{\pm} \equiv u_{\pm}^x/u_{\pm}^y$ are not presented in the general case here. In this problem we can identify two distinct physical regimes: (i) for small wavevectors/large magnetic fields the negative branch of Eq. (4.4) gives rise to a gapless *magnetophonon* mode with the quadratic dispersion

$$\omega_-(k) = \frac{\sqrt{v_2\left(2v_1+v_2\right)}}{\Omega}k^2\left[1 + O\left(\frac{k^2}{\Omega^2}\right)\right], \tag{4.5}$$

while the positive branch represents a gapped *magnetoplasmon* mode, dispersing as

$$\omega_+(k) = \Omega\left[1 + \left(\frac{v_1+v_2}{\Omega^2}\right)k^2 + O\left(\frac{k^4}{\Omega^4}\right)\right]. \tag{4.6}$$

The latter mode is guaranteed to have the gap $\omega = \Omega$ at $k = 0$ by the Kohn theorem [138]; the system is analogous to a collection of single-species charged particles in a uniform magnetic field that interact through a potential which depends only on their relative distances. In the zero wavevector limit, the polarization of the Kohn mode is circular and its chirality is fixed by the sign of the effective magnetic field $\mathcal{B}$. (ii) In the limit of large wavevectors, the Newtonian term dominates over the Berry term in Eq. (4.3) and we asymptotically recover two linearly dispersing sound modes of a time-reversal invariant two-dimensional solid[1] similar to the ones from Chapter 1. In particular, at large momenta, the magnetophonon (4.5) merges into the transverse ($k_i u_-^i = 0$) mode dispersing as

[1] In the absence of the Berry term the system supports a transverse and a longitudinal sound modes with respective group velocities $c_t^2 \equiv 2C_2/\rho$ and $c_l^2 \equiv (4C_1+2C_2)/\rho$.

$\omega_- = c_t k[1 + O(\Omega^2/k^2)]$, while the magnetoplasmon (4.6) becomes the longitudinally polarized ($\epsilon_{ij} k_i u_+^j = 0$) mode with $\omega_+ = c_l k[1 + O(\Omega^2/k^2)]$.
The Lagrangian naturally fits into a derivative expansion within the power-counting scheme $u^i \sim O(1)$, $\partial_i \sim O(\varepsilon)$, $\partial_t \sim O(\varepsilon^2)$ where we introduced a small parameter $\varepsilon \ll 1$. The difference in the power-counting of temporal and spatial derivatives originates from the soft quadratic dispersion of the magnetophonon. All terms in the Lagrangian (4.1), except for the Newtonian term $\rho \dot{u}^2/2$, are of order $O(\varepsilon^2)$, defining the leading-order (LO) Lagrangian. On the other hand, the Newtonian term scales as ε^4 and is less relevant at low frequencies, and thus is of the next-to-leading order (NLO). The inclusion of this term allows us to establish the crossover of edge waves that exist in the chiral system to the ordinary Rayleigh waves in the absence of a Berry term. We notice here that other NLO terms such as second-order elasticity $\tilde{\lambda}_{ijklmn} \partial_i \partial_j u_k \partial_k \partial_m u_n$ or the dissipationless phonon Hall viscosity $\eta_{ijkl} \partial_i u_j \partial_k \dot{u}^l$ [139] are not included.
We recall that in elastic media internal stresses and forces are encoded in the stress tensor $T_{ij} = \delta \mathcal{E}_{\rm el}/\delta u_{ij}$ (1.28). For a two-dimensional triangular crystal with the elastic energy density (4.2) the stress tensor is

$$T_{ij} = 4C_1 u_{kk} \delta_{ij} + 4C_2 \tilde{u}_{ij}. \tag{4.7}$$

4.3 Rayleigh edge modes

Next, we turn to the study of exponentially localised Rayleigh waves that propagate on the edge of the skyrmion lattice. The breaking of time-reversal and parity symmetries in (4.1) due to the Berry term suggests that such modes might be chiral, i.e., propagating only in one direction, see e.g. [137] and [140].
For the sake of simplicity, we consider the skyrmion crystal to fill the lower half-space with $y < 0$. Without loss of generality we also choose $\Omega > 0$. The translational invariance in time and along the horizontal direction motivates the ansatz $\mathbf{u}(x, y, t) = \mathbf{u}\, e^{i(kx - \omega t)} e^{\kappa y}$ for a solution of (4.3). The wavevector along the boundary k and the frequency ω are assumed to be real; confinement near the edge of the system requires the real part of κ to be positive.
First, in order to make the following calculation more transparent, we shall focus on the low-frequency limit and drop the NLO Newtonian term $\sim \dot{u}^2$ in the model (4.1). The edge ansatz inserted into Eq. (4.3) results in a characteristic equation for κ with two solutions

$$\kappa_{1,2}(k, \omega) = \sqrt{k^2 \pm \frac{\Omega}{\sqrt{v_2(2v_1 + v_2)}} \omega} + \mathcal{O}(k^2). \tag{4.8}$$

The corresponding eigenvectors $\mathbf{u}_{1,2}\,(k, \omega)$ are functions of the wavevector k and frequency ω. Interestingly, here, in contrast to the ordinary Rayleigh construction,

both solutions $\kappa_{1,2}$ originate from the single magnetophonon branch.

The general solution with given k and ω is obtained by forming a linear superposition of $\mathbf{u}_{1,2}(k,\omega)$ with two complex constants a, b

$$\mathbf{u}(x,y,t) = e^{i(kx-\omega t)}(a\,\mathbf{u}_1 e^{\kappa_1 y} + b\,\mathbf{u}_2 e^{\kappa_2 y}). \tag{4.9}$$

Due to the PT symmetry of the model, the dispersion satisfies $\omega(k) = -\omega(-k)$, hence it is sufficient to study only the interval $\omega \geq 0$. Here we will assume that the crystal is free at the boundary $y = 0$. In this case there are no macroscopic forces acting on it from the outside. Thus, there is no flux of linear momentum across the boundary surface, resulting in the so-called stress-free boundary conditions

$$T_{xy}(x, y = 0) = T_{yy}(x, y = 0) \stackrel{!}{=} 0. \tag{4.10}$$

Substituting the ansatz (4.9) into the boundary conditions (4.10) results in the linear system of equations for a and b

$$\begin{pmatrix} ik\sigma\epsilon_1 + \kappa_1 & ik\sigma\epsilon_2 + \kappa_2 \\ ik + \kappa_1\epsilon_1 & ik + \kappa_2\epsilon_2 \end{pmatrix} \begin{pmatrix} a \\ b \end{pmatrix} = 0, \tag{4.11}$$

where we have introduced the two-dimensional Poisson ratio

$$\sigma \equiv (2C_1 - C_2)/(2C_1 + C_2) \tag{4.12}$$

and the shorthand $\epsilon_{1,2} \equiv u^x_{1,2}/u^y_{1,2}$.
The dispersion relation $\omega(k)$ for the edge waves is obtained from the characteristic equation for the matrix in Eq. (4.11). In the following we investigate the interval $-1 \leq \sigma \leq 1$, where the elastic system is stable.
Substitution of the two edge modes into (4.11) yields a dispersion relation $\omega(k)$ of the form

$$\omega(k) = \alpha \frac{\sqrt{v_2(2v_1 + v_2)}}{\Omega} k^2, \tag{4.13}$$

with α being a non-negative and real solution of an unwieldy algebraic equation, which we investigate in detail in Section 4.4. This equation does not depend on the magnitude of k, but only on its sign. As a consequence, the equations for positive and negative k are in general different, resulting in different solutions $\alpha(\text{sign}(k), \sigma)$, which we will denote by $\alpha_\pm(\sigma)$. We show the numerical solution of $\alpha_\pm(\sigma)$ in Fig. 4.2. As the value of σ is varied, one finds three qualitatively different regimes. For $\sigma < 0$ only the α_- branch exists: edge waves can only propagate towards left, while propagation to the right is forbidden. We analytically find that for $\sigma > \varphi^{-1} = (\sqrt{5} - 1)/2$, i.e. the inverse golden ratio, the edge

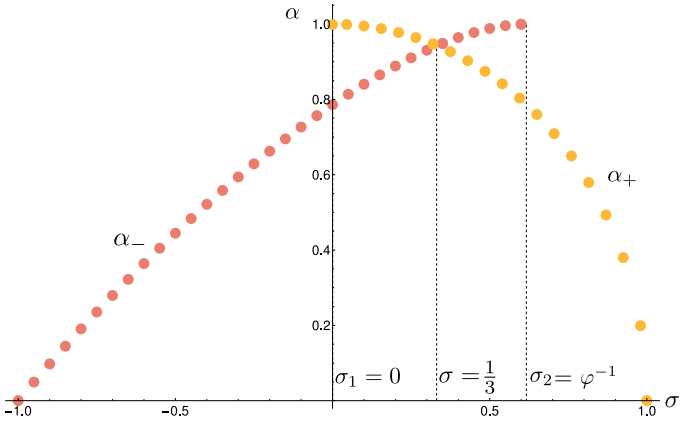

Figure 4.2: For small momenta the dispersion relation has the quadratic form $\omega = \alpha\sqrt{v_2(2v_1+v_2)}/\Omega\, k^2$. When only one of the branches $\alpha_\pm$ exists, the edge wave propagates unidirectionally. This happens for $\sigma < 0$ and $\sigma > \varphi^{-1}$, see Section 4.4.

waves are once again chiral, but with propagation in the opposite direction. In the interval $0 \leq \sigma \leq \varphi^{-1}$ both branches of $\alpha_\pm$ exist and consequently edge waves can propagate in both directions. The dispersion of the surface waves usually is asymmetric, since in general $\alpha_+ \neq \alpha_-$. However, it is clear from Fig. 4.2, that at the point $\sigma = 1/3$ [2] the spectrum is symmetric, see more in the next Section for the analytical justification, where we also determine the value $\alpha_\pm = 2\sqrt{2}/3$.

In the presence of the sub-leading Newtonian term we solved the edge problem numerically. The resulting spectrum is sketched in Fig. 4.1. The inclusion of the Newtonian term results in propagation in a forbidden direction for momentum and frequency larger than a critical value k_{crit} and $\omega_g \equiv \omega(k_{\text{crit}})$. We checked that ordinary Rayleigh waves are recovered for $\omega \gg \omega_g$.

In order to illustrate our findings, we have carried out finite-difference simulations of the dynamics encoded by (4.3) subject to the boundary conditions (4.10) on a 500×500 spatial grid. Fig. 4.3 shows simulation snapshots for different values of the Poisson ratio. The initial condition for the displacement field is identical in all three simulations: the elastic medium has zero displacement everywhere, except for a small central region near the lower horizontal boundary, where it is deformed. Starting with this condition, we let the system evolve over time (in [141] we provide a simulation video). We observe that while the excitation decays partially into the bulk of the medium, some part remains localised near the edge and travels along the boundary. For $\sigma = -0.8$ and $\sigma = +0.8$, one

[2] A microscopic model that realises the value $\sigma = 1/3$ is the triangular lattice of equal masses connected through nearest neighbours identical springs.

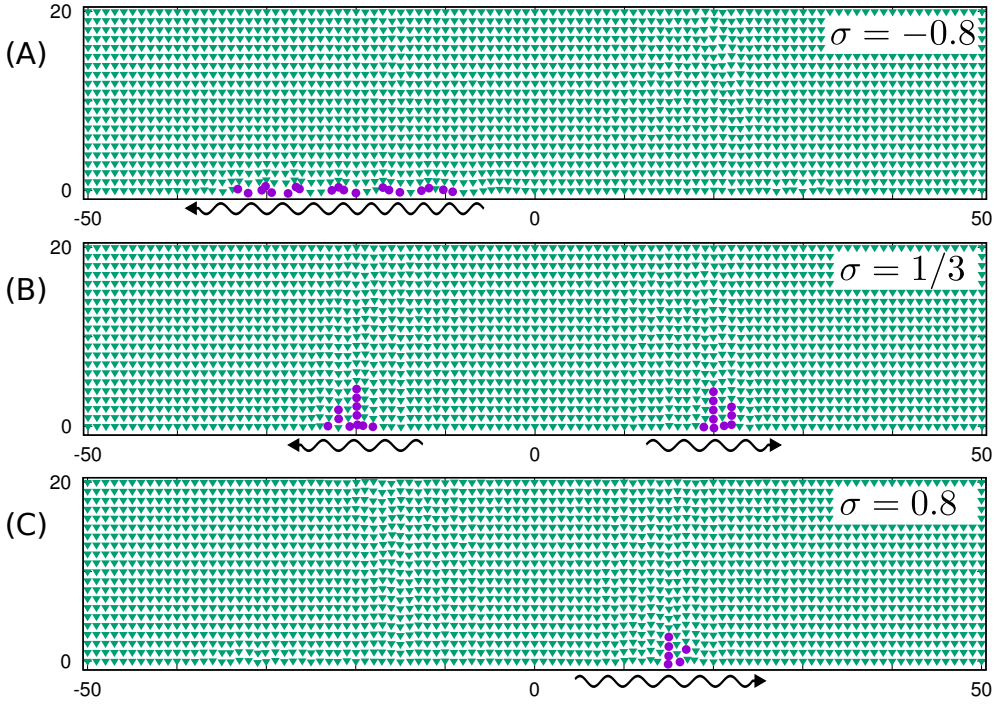

Figure 4.3: Edge excitations as seen in finite-difference simulations [141]. In all three plots, the system was displaced in a small region near the boundary at $x = 0$ and evolved over time. The three values of σ are representative of the three regimes shown in Fig. 4.1. To guide the eye, we coloured in magenta the grid points that have large amplitude defined by a threshold value.

clearly sees how the edge excitations travel unidirectionally and in opposite directions for the two Poisson ratios. For $\sigma = 1/3$, we observe two edge excitations that travel symmetrically in both directions.

To investigate the transition between the three regimes, we studied the magnitude of the frequency gap ω_g as a function of the Poisson ratio σ. The result is displayed in Fig. 4.4. The figure demonstrates that the non-chiral regime ($\omega_g = 0$) exists inside a finite interval $\sigma_1 < \sigma < \sigma_2$. This implies that the gap vanishes in a non-analytic way, reminiscent of the behaviour of an order parameter near a continuous phase-transition. Indeed, we find that the gap ω_g vanishes linearly near the critical ratios $\sigma_1 = 0$ and $\sigma_2 = \varphi^{-1}$, see the insets of Fig. 4.4.

A particularly simple case of surface modes is found in the limit where the compressional modulus C_1 vanishes, i.e. for $\sigma = -1$. In the time-reversal invariant setting, this *maximally auxetic* problem emerges in the twisted Kagome lattice [142]. For our system, we find that at $\sigma = -1$ edge modes exist and the frequency spectrum is a flat band. This implies that once a deformation is introduced at the

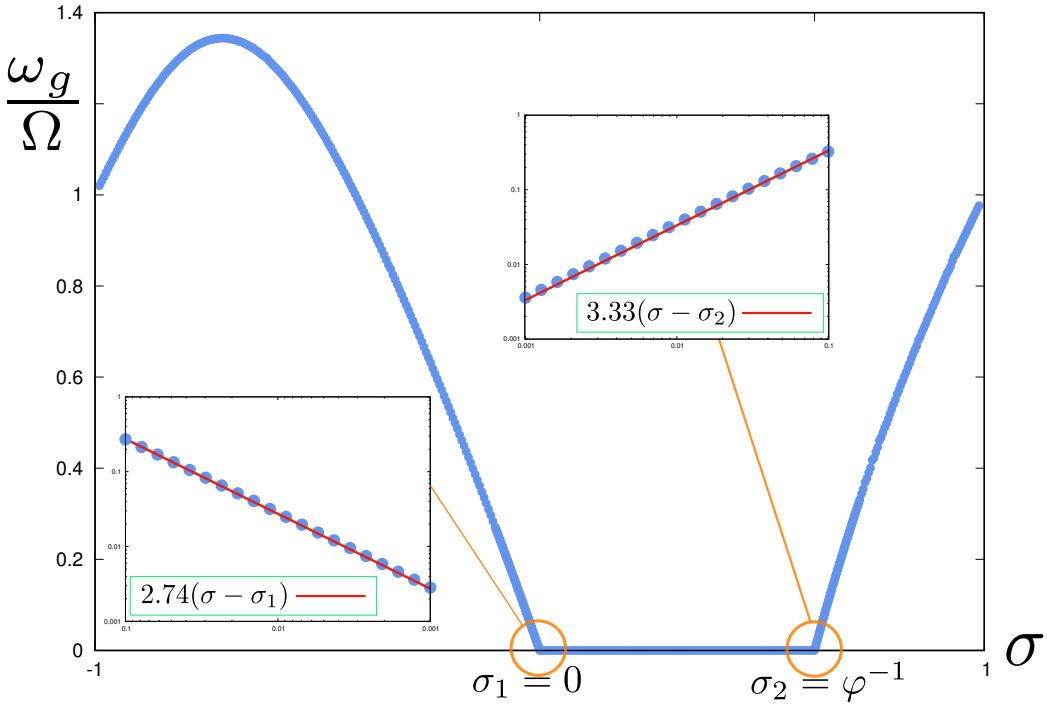

Figure 4.4: Frequency gap ω_g of the edge waves as a function of the Poisson ratio σ. The gap is zero in the interval $[\sigma_1, \sigma_2]$. The insets show that the gap vanishes linearly near the critical points σ_1 and σ_2.

edge of the system, it does not propagate but remains there forever frozen. Such excitations have been studied in the literature [142–144] and are known as floppy modes. It is interesting to note that these solutions have a hidden holomorphicity property related to the fact that, when $\sigma = -1$, the boundary conditions (4.10) become the Cauchy-Riemann equations for the field $u_x + iu_y$.

4.4 Analytic values of σ_1 and σ_2, edge-wave dispersions at $\sigma = 1/3$, $\sigma = \sigma_{1,2}$ and floppy modes

Insertion of the edge-wave ansatz into the stress-free boundary condition (4.11) results in an equation for $\alpha_\pm$:

$$\frac{2(\sigma-1)\left(\alpha_+^2\left(\sigma\left(-\sqrt{\frac{1}{1-\sigma}}\sqrt{2-2\alpha_+^2}+2\sqrt{1-\alpha_+}-2\sqrt{\alpha_++1}\right)+\sqrt{\frac{1}{1-\sigma}}\sqrt{2-2\alpha_+^2}-2\sqrt{2}\sqrt{\frac{1}{1-\sigma}}\sigma^2\right)+(\sigma+1)^2\left(\sqrt{1-\alpha_+}-\sqrt{\alpha_++1}\right)+(\sigma+1)^2\alpha_+\left(\sqrt{1-\alpha_+}+\sqrt{\alpha_++1}\right)\right)}{(\sigma-1)^2\alpha_+^2-(\sigma+1)^2} = 0 \tag{4.14}$$

$$\frac{2(\sigma-1)\left(\alpha_-^2\left(\sigma\left(\sqrt{\frac{1}{1-\sigma}}\sqrt{2-2\alpha_-^2}+2\sqrt{1-\alpha_-}-2\sqrt{\alpha_-+1}\right)-\sqrt{\frac{1}{1-\sigma}}\sqrt{2-2\alpha_-^2}+2\sqrt{2}\sqrt{\frac{1}{1-\sigma}}\sigma^2\right)+(\sigma+1)^2\left(\sqrt{1-\alpha_-}-\sqrt{\alpha_-+1}\right)+(\sigma+1)^2\alpha_-\left(\sqrt{1-\alpha_-}+\sqrt{\alpha_-+1}\right)\right)}{(\sigma-1)^2\alpha_-^2-(\sigma+1)^2} = 0 \tag{4.15}$$

We are considering non-negative values of ω, thus $\alpha_\pm \geq 0$. The form of the spectrum (4.13) yields for κ given by (4.8) the values $\kappa_{1,2} = \sqrt{1 \pm \alpha}|k|$. In order to have both $\kappa_{1,2}$ real, the condition $\alpha \leq 1$ must be satisfied. The analytic values of σ_1 and σ_2 can be found by imposing these limits. We first note that for $\alpha_+ \to 1$ one finds $\sigma \to 0$ using Eq. (4.14), and thus $\sigma_1 = 0$. The value σ_2 is obtained by letting $\alpha_- \to 1$ in Eq. (4.15). In this limit that equation reduces to $\sigma_2\sqrt{1-\sigma_2} - 1 + \sigma_2 = 0$ with solution $\sigma_2 = \frac{\sqrt{5}-1}{2} \equiv \varphi^{-1}$, which is the inverse of the golden ratio φ.

4.4.1 Symmetric point $\sigma = 1/3$

When $\sigma = 1/3$, both equations (4.14) and (4.15) reduce to the same form, thus $\alpha_+ = \alpha_-$. The equation that is satisfied by $\alpha_\pm$ is

$$\left(-3\sqrt{3-3\alpha^2} + 3\sqrt{1-\alpha} - 3\sqrt{\alpha+1} + \sqrt{3}\right)\alpha^2 + 8\left(\sqrt{1-\alpha} + \sqrt{\alpha+1}\right)\alpha + \\ + 8\left(\sqrt{1-\alpha} - \sqrt{\alpha+1}\right) = 0.$$

It is straightforward to verify that the only admissible solution is $\alpha_\pm = 2\sqrt{2}/3$. Thus the long-wavelength edge-wave dispersion at $\sigma = 1/3$ takes on the particularly simple form $\omega = 2\sqrt{\frac{2}{3}\frac{v_2}{\Omega}}k^2$.

Asymptotic behaviour of $\alpha_\pm$ at $\sigma = \pm 1$

When $\sigma \to 1^-$ the value of the corresponding α_+ tends to 0. By setting

$$\sigma = 1 - \epsilon \tag{4.16}$$
$$\alpha = \delta \tag{4.17}$$

in equation (4.14) and expanding in small δ, ϵ, we arrive at the equation $2\delta\epsilon - \sqrt{2}\delta^2\sqrt{\epsilon} = 0$ which has the solution $\delta = \sqrt{2}\sqrt{\epsilon}$. This yields the asymptotic $\alpha_+ \sim \sqrt{2}\sqrt{1-\sigma}$ as $\sigma \to 1^-$ and as a consequence $\omega \sim (2v_2/\Omega)k^2$ as $\sigma \to 1^-$. When $\sigma \to -1^+$, the value of α_- tends to 0. Here we set

$$\sigma = -1 + \epsilon \tag{4.18}$$
$$\alpha = \delta \tag{4.19}$$

and upon expanding (4.15) we find $\delta = 3\epsilon/2$ and thus

$$\alpha_- \sim \frac{3}{2}(1+\sigma) \text{ as } \sigma \to -1^+ \tag{4.20}$$

and therefore

$$\omega \sim \frac{3v_2}{2\Omega}(1+\sigma)k^2 \text{ as } \sigma \to -1^+. \tag{4.21}$$

Since $\sigma \to -1^+$ is equivalent to $v_1 \to 0$, we can also write this asymptotic relation as

$$\omega \sim \frac{6v_1}{\Omega}k^2 \text{ as } v_1 \to 0. \tag{4.22}$$

In both limits, $\sigma \to -1^+$ and $\sigma \to 1^-$, the spectra become flat. Such flat spectra are associated with excitations called floppy modes.

4.4.2 Floppy modes at $\sigma = -1$

As discussed above, for $\sigma = -1$ the system supports floppy modes. Setting $\sigma = -1$ and inserting the edge-wave ansatz (4.9) into the equations of motion (4.3) produces two modes with $\kappa_\mp = \sqrt{k^2 - (\omega^2 \pm \omega\Omega)/v_2}$ and circular polarizations $\epsilon_\mp = \pm i$. The boundary conditions (4.10) enforce either $\omega = 0$ or $\omega = \Omega$ and $\kappa_\mp = |k|$. The latter is automatically satisfied for the $\omega = 0$ bulk mode. But, for $\omega = \Omega$, the κ_+-mode violates this condition. For $\omega = 0$ we find the floppy mode

$$\mathbf{u} = \left(-i \text{ sign}(k), 1\right)^{\mathrm{T}} e^{ikx + |k|y}, \tag{4.23}$$

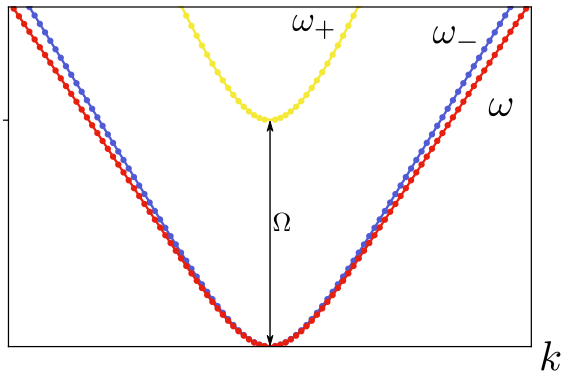

Figure 4.5: Numerical solution of the edge wave dispersion (red) for equal elastic moduli $C_1 = C_2$. For comparison, also the dispersions relations of the bulk modes ω_- (blue) and ω_+ (yellow) are plotted.

while the time-dependent solution with $\omega = \Omega$ only exists for $k > 0$ and has the form

$$\mathbf{u} = (-i, 1)^{\mathrm{T}} e^{i(kx-\Omega t)+ky}. \tag{4.24}$$

We assumed above that $\Omega > 0$. If, instead, $\Omega < 0$, then the time-dependent solution has the frequency $\omega = -\Omega$. This change of sign modifies the sign of the allowed k values in Eq. (4.24) and thereby reverses the wave's propagation direction.

Symmetric edge spectrum

In Subsection 4.4.1, we have shown that a symmetric spectrum of edge excitations emerges for the value of Poisson ratio $\sigma = 1/3$, i.e. for equal elastic moduli, $C_1 = C_2 \equiv C$. Hereby we show that this property holds even at NLO, see Figure 4.5. The proof is based on the characteristic equation $d(k, \omega) = 0$ of the matrix appearing in the boundary conditions (4.11).

The expressions are cumbersome and it turns out to be more convenient to study the parity property of the auxiliary function

$$\tilde{d}\,(k, \omega) \equiv d\,(k, \omega) \,/\, \left[\epsilon_+\,(k, \omega) - \epsilon_-\,(k, \omega)\right] \tag{4.25}$$

instead of the characteristic polynomial $d\,(k, \omega)$. In terms of the inverse decay lengths $\kappa_{\mp}\,(k, \omega)$ and the polarizations $\epsilon_{\mp}\,(k, \omega)$ the auxiliary function takes the

following form

$$\tilde{d}\left(k,\omega\right)=\left(k^{2}+3\kappa_{-}\kappa_{+}\right)+\left(\kappa_{+}-\kappa_{-}\right)\left[\underbrace{\frac{\epsilon_{-}\epsilon_{+}-3}{\epsilon_{+}-\epsilon_{-}}\left(ik\right)}_{\equiv g(k,\omega)}\right]. \tag{4.26}$$

We will argue that the auxiliary function $\tilde{d}$ is an even function of the wavevector k. First, after introducing $2C/\rho\equiv v$, we notice that

$$\kappa_{\mp}\left(k,\omega\right)=\sqrt{k^{2}-\left(2\omega^{2}\pm\omega\sqrt{3\Omega^{2}+\omega^{2}}\right)/3v} \tag{4.27}$$

are even functions of k. As a result, all the functions outside the square brackets in (4.26) are even. Polarization functions have no parity symmetry

$$\epsilon_{\mp}\left(k,\omega\right)=-i\frac{3\Omega^{2}\omega+2k\sqrt{3v\left(-2\omega^{2}\mp\sqrt{3\Omega^{2}\omega^{2}+\omega^{4}}+3vk^{4}\right)}}{\omega^{2}-\sqrt{3\Omega^{2}\omega^{2}+\omega^{4}}-6vk^{2}},$$

however, together with (ik), they lead to a function inside the square brackets

$$\begin{aligned}g\left(k,\omega\right)=\ & \frac{-k^{2}}{\sqrt{\omega^{2}\Omega^{2}+\omega^{4}/3}}\left[\sqrt{-v\left(2\omega^{2}+\sqrt{3\omega^{2}\Omega^{2}+\omega^{4}}-3vk^{2}\right)}\right.\\ & \left.+\sqrt{-v\left(2\omega^{2}-\sqrt{3\omega^{2}\Omega^{2}+\omega^{4}}-3vk^{2}\right)}\right]\end{aligned}$$

which is manifestly even under the change of sign of the wavevector. This proves that $\tilde{d}\left(k,\omega\right)=\tilde{d}\left(-k,\omega\right)$ therefore the edge-wave spectrum at $\sigma=1/3$ is indeed symmetric, $\omega(k)=\omega(-k)$.

Complex formulation of elasticity and holomorphicity at $\sigma=-1$

When the Poisson ratio takes on the value $\sigma=-1$, the edge-wave solutions have a hidden property. To see this we reformulate the elasticity equations in complex form by combining the real components u_x and u_y into one complex field $\psi\equiv u_x+iu_y$. The equations of motion (4.3) are

$$\begin{aligned}&\ddot{u}_x+\Omega\dot{u}_y-2v_1\partial_x(\partial_x u_x+\partial_y u_y)-v_2(\partial_x^2+\partial_y^2)u_x=0\\ &\ddot{u}_y-\Omega\dot{u}_x-2v_1\partial_y(\partial_x u_x+\partial_y u_y)-v_2(\partial_x^2+\partial_y^2)u_y=0.\end{aligned}$$

By multiplying the second equation by i and adding it to the first, we obtain

$$\ddot{\psi} - i\Omega\dot{\psi} - 4v_1(\partial_{\bar{z}}^2\bar{\psi} + \partial_z\partial_{\bar{z}}\psi) - 4v_2\partial_z\partial_{\bar{z}}\psi = 0, \tag{4.28}$$

where we introduced the complex derivatives $\partial_z \equiv \left(\partial_x - i\partial_y\right)/2$ and $\partial_{\bar{z}} \equiv \left(\partial_x + i\partial_y\right)/2$. The boundary conditions (4.10) in real space read

$$\partial_x u_y + \partial_y u_x = 0 \tag{4.29}$$

$$\sigma\partial_x u_x + \partial_y u_y = 0 \tag{4.30}$$

Multiplying the second equation by i and adding it to the first, we obtain the boundary conditions in complex form

$$(3-\sigma)\partial_{\bar{z}}\psi = (1+\sigma)(\partial_{\bar{z}}\bar{\psi} + \partial_z\bar{\psi} + \partial_z\psi). \tag{4.31}$$

At $\sigma = -1$ the boundary conditions (4.29) and (4.30) are the Cauchy-Riemann equations for the real and imaginary parts of ψ at $y = 0$. In addition, the real parts of the modes (4.23) and (4.24) give rise to ψ's that are holomorphic functions of the complex variable $z \equiv x + iy$ in the bulk. In particular, the time-independent mode yields $\psi = i\exp(-i|k|z)$, while the time-dependent mode is $\psi = i\exp(-ikz + i\Omega t)$. Using a conformal transformation we can map these edge-modes, which are localised near the boundary of the complex half-plane, onto edge-waves that propagate along the boundary of an arbitrarily shaped region. In other words, the transformed solutions will satisfy the boundary conditions on the new edge and solve the bulk (Laplace) equations of motion [145].

4.5 Conclusions and outlook

We analysed Rayleigh edge waves that travel on the edge of two-dimensional crystals in the presence of Lorentz forces and mapped out how their propagation direction depends on the Poisson ratio, see Fig. 4.1. The existence of these waves is not protected by topology, but rather originates from spontaneously broken translational symmetry. In addition to skyrmion crystals, we expect our findings to be directly applicable to boundary excitations of screened Wigner crystals in an external magnetic field [137]. Moreover, our results shed new light on elastic gyroscopic systems [146], where edge modes are currently under active investigation [147, 148]. Our work indicates that in all these systems the chirality of Rayleigh edge waves can be controlled by changing the elastic properties of the medium.

Extensions of this study to Abrikosov vortex crystals in superconductors and superfluids [128] are non-trivial exciting frontiers. It would be also intriguing to generalize this work and investigate edge excitations in two-dimensional crystals, where time-reversal breaking originates from a different mechanism, such as for example the odd elasticity discovered in [149, 150].

Conclusions

In this thesis, we studied effective theories for crystals made of topological solitons. The approach we used allows describing these crystalline states in terms of coarse-grained collective variables, irrespectively from the microscopic details that lead to the crystal formation. As a matter of fact, from the elasticity viewpoint, the vortex lattice that appears in superfluids, and the skyrmion lattice in chiral magnets share several common characteristics. Furthermore, the dynamics of both systems obeys similar transverse forces which originate from Lorentz-like terms.

We devoted Chapter 1 to review the theory of elasticity, introducing its main concepts and tools we used throughout our work. In simple terms, we can think about linear elasticity as a continuum distribution of a collection of Hookean springs, in which strain plays the role of the spring's deformation and stress the role of the force.

In Chapter 2 we introduced topological solitons and the concept of topological conservation laws in field theories. We gave specific examples of topologically non-trivial configurations. As a warm-up example, we discussed topological properties of kinks in one spatial dimension. Then we examined quantised vortices and two-dimensional skyrmions.

Our result in Chapter 3 for the quantum vortex lattice in a bosonic Galilean-invariant compressible superfluid showed how to construct an effective theory systematically in the derivative expansion. We argued that our description is more natural than a previous approach [104]. Our theory encodes the correct excitation spectrum, and we extracted the linear response and transport, which can be determined in experiments. While our theory directly applies to bosonic superfluids, fermionic s-wave superfluids form regular vortex lattices observed in experiments with cold atoms [111]. Thus, it would be interesting to use the effective theory we developed for these systems. Rotating chiral p+ip superfluids should as well form vortex lattices, and it would be fascinating to construct effective theories of these states. Vortices exhibit peculiar features when put on curved surfaces [112]. For this reason, it would be exciting to apply our effective theory to vortex lattices that live on curved substrates and in microgravity situations [151]. Moreover, we

expect we can describe vortex lattice low-energy dynamics in thin films of clean superconductors if we include the effects of three-dimensional dynamical electromagnetism in our theory.

In Chapter 4 we focused on the edge physics of skyrmion crystals that emerge in certain chiral magnets. Our goal was to determine whether the boundary of the crystal supports exponentially-confined, propagating waves analogous to those found by Rayleigh in [39]. Indeed, we showed they exist, and they possess a chiral nature. The Poisson ratio of the crystal determines the edge-waves propagation directions. Our results were obtained both from a numerical approach and an analytic one. Additionally, we used finite-difference simulations to confirm our findings.

The natural question is to ask if the vortex lattice in compressible superfluids supports a chiral edge wave, and if we can give complete mappings of its propagation direction in terms of crystal parameters. We have conducted preliminary investigations and did not find any evidence of them, even though we do not exclude they might appear from our theory at higher-order in the derivative expansion.

Bibliography

[1] P. W. Anderson. More is different. *Science*, 177(4047):393–396, 1972.

[2] John McGreevy. Where do quantum field theories come from?

[3] Hitoshi Murayama. Theory colloquium: When a symmetry breaks, July 2019. Twentyfourth Arnold Sommerfeld Lecture Series.

[4] Steven Weinberg. Phenomenological lagrangians. *Physica A: Statistical Mechanics and its Applications*, 96(1):327–340, 1979.

[5] R.P. Feynman. Chapter ii application of quantum mechanics to liquid helium. volume 1 of *Progress in Low Temperature Physics*, pages 17–53. Elsevier, 1955.

[6] E. J. Yarmchuk, M. J. V. Gordon, and R. E. Packard. Observation of stationary vortex arrays in rotating superfluid helium. *Phys. Rev. Lett.*, 43:214–217, Jul 1979.

[7] JR Abo-Shaeer, C Raman, JM Vogels, and Wolfgang Ketterle. Observation of vortex lattices in bose-einstein condensates. *Science*, 292(5516):476–479, 2001.

[8] Michael E Peskin. Mandelstam-'t hooft duality in abelian lattice models. *Ann. Phys.*, 113(1):122–152, 1978.

[9] Chandan Dasgupta and BI Halperin. Phase transition in a lattice model of superconductivity. *Phys. Rev. Lett.*, 47(21):1556, 1981.

[10] Sergej Moroz, Carlos Hoyos, Claudio Benzoni, and Dam Thanh Son. Effective field theory of a vortex lattice in a bosonic superfluid. *SciPost Phys.*, 5:39, 2018.

[11] S Mühlbauer, B Binz, F Jonietz, C Pfleiderer, A Rosch, A Neubauer, R Georgii, and P Böni. Skyrmion lattice in a chiral magnet. *Science*, 323(5916):915–9, February 2009.

[12] T. H. R. Skyrme. The Origins of Skyrmions. *Int. J. Mod. Phys. A*, 3:2745–2751, 1988.

[13] Claudio Benzoni, Bhilahari Jeevanesan, and Sergej Moroz. Rayleigh edge waves in two-dimensional crystals with lorentz forces: From skyrmion crystals to gyroscopic media. *Phys. Rev. B*, 104:024435, Jul 2021.

[14] Lev Davidovich Landau and Evgenii Mikhailovich Lifshitz. *Course of theoretical physics*. Elsevier, 2013.

[15] Herbert Goldstein, Charles Poole, and John Safko. *Classical mechanics*. American Association of Physics Teachers, 2002.

[16] H. Helmholtz. Über integrale der hydrodynamischen gleichungen, welche den wirbelbewegungen entsprechen. 1858(55):25–55, 1858.

[17] Arnold Sommerfeld. *Mechanics of deformable bodies: Lectures on theoretical physics, Vol. 2*, volume 2. Elsevier, 2016.

[18] L. D Landau and E. M Lifshitz. *Course of Theoretical Physics: Theory of Elasticity*. Butterworth-Heinemann, 1986.

[19] Paul M Chaikin and Tom C Lubensky. *Principles of Condensed Matter Physics*. Cambridge University Press, 1995.

[20] Johannes Altenbach, Holm Altenbach, and Victor A Eremeyev. On generalized cosserat-type theories of plates and shells: a short review and bibliography. *Archive of Applied Mechanics*, 80(1):73–92, 2010.

[21] Mysore NL Narasimhan. *Principles of continuum mechanics*. Wiley-Interscience, 1993.

[22] Benny Lautrup. *Physics of continuous matter: exotic and everyday phenomena in the macroscopic world*. CRC press, 2011.

[23] Kip S Thorne and Roger D Blandford. *Modern Classical Physics: Optics, Fluids, Plasmas, Elasticity, Relativity, and Statistical Physics*. Princeton University Press, 2017.

[24] William S Slaughter. *The linearized theory of elasticity*. Springer Science & Business Media, 2012.

[25] Robert E Newnham. *Properties of materials: anisotropy, symmetry, structure*. Oxford University Press on Demand, 2005.

[26] Thomas H. Courtney. *Mechanical Behavior of Materials*. Waveland Pr Inc, 2 edition, 2005.

[27] Charles Kittel. *Introduction to Solid State Physics; 8th ed.* Wiley, Hoboken, NJ, 2005.

[28] Viatcheslav Mukhanov. *Physical Foundations of Cosmology*. Cambridge Univ. Press, Cambridge, 2005.

[29] Johannes Kepler. *Epitome Astronomiae Copernicanae Usitata forma Quaestionum & Responsionum conscripta, inque VII.* Schönwetterus, 1635.

[30] A. Zee. *Fly by Night Physics: How Physicists Use the Backs of Envelopes*. Princeton University Press, 2020.

[31] J. T. Lewis, A. Lehoczky, and C. V. Briscoe. Elastic constants of the alkali halides at 4.2°k. *Phys. Rev.*, 161:877–887, Sep 1967.

[32] Marc André Meyers and Krishan Kumar Chawla. *Mechanical behavior of materials*. Cambridge university press, 2008.

[33] G Neville Greaves, A L Greer, Roderic S. Lakes, and Tanguy Rouxel. Poisson's ratio and modern materials. *Nature materials*, 10 11:823–37, 2011.

[34] Leighton Feynman and Sands. The feynman lectures on physics, volume ii, 2013. Accessed at https://www.feynmanlectures.caltech.edu/II_38.html.

[35] Roderic Lakes. Foam structures with a negative poisson's ratio. *Science*, 235(4792):1038–1040, 1987.

[36] Graeme W. Milton. Composite materials with poisson's ratios close to — 1. *Journal of the Mechanics and Physics of Solids*, 40(5):1105–1137, 1992.

[37] Roderic Lakes. Advances in negative poisson's ratio materials. *Advanced Materials*, 5(4):293–296, 1993.

[38] Cross Tory, Hoffer Kevin, Jones David, Kirschner Patrick, Langvin Elizabeth, and Meschter James. *Auxetic structures and footwear with soles having auxetic structures*. U.S. Patent 9402439B2, 2013.

[39] Lord Rayleigh. On waves propagated along the plane surface of an elastic solid. *Proceedings of the London Mathematical Society*, s1-17(1):4–11, 1885.

[40] Seth Stein and Michael Wysession. *An introduction to seismology, earthquakes, and earth structure*. John Wiley & Sons, 2009.

[41] THR Skyrme. A non-linear theory of strong interactions. *Proceedings of the Royal Society of London. Series A. Mathematical and Physical Sciences*, 247(1249):260–278, 1958.

[42] T. H. R. Skyrme. A unified model of k- and pi -mesons. *Proceedings of the Royal Society of London. Series A, Mathematical and Physical Sciences*, 252(1269):236–245, 1959.

[43] T. H. R. Skyrme and Basil Ferdinand Jamieson Schonland. A non-linear field theory. *Proceedings of the Royal Society of London. Series A. Mathematical and Physical Sciences*, 260(1300):127–138, 1961.

[44] T. H. R. Skyrme. Particle states of a quantized meson field. *Proceedings of the Royal Society of London. Series A, Mathematical and Physical Sciences*, 262(1309):237–245, 1961.

[45] J. K. Perring and T. H. R. Skyrme. A Model unified field equation. *Nucl. Phys.*, 31:550–555, 1962.

[46] Tony Hilton Royle Skyrme. A unified field theory of mesons and baryons. *Nuclear Physics*, 31:556–569, 1962.

[47] Ian J. R. Aitchison. Tony skyrme and the origins of skyrmions, 2020.

[48] William Thomson. 4. on vortex atoms. *Proceedings of the Royal Society of Edinburgh*, 6:94–105, 1869.

[49] Horace Lamb. *Hydrodynamics*. Dover, 1945.

[50] A Zee. *Quantum Field Theory in a Nutshell; 1st ed.* In a nutshell. Princeton Univ. Press, Princeton, NJ, 2003.

[51] Jung Hoon Han. *Skyrmions in Condensed Matter*, volume 278. Springer, 2017.

[52] Anthony Zee. *Quantum field theory in a nutshell*. Princeton university press, 2010.

[53] L. Landau, E. Lifshitz, and A. King. Electrodynamics of continuous media. *American Journal of Physics*, 29:647–648, 1960.

[54] Mark J. Ablowitz and Harvey Segur. *Solitons and the Inverse Scattering Transform*. Society for Industrial and Applied Mathematics, 1981.

[55] Vladmir G. Makhankov, Y. Rybakov, and V. I. Sanyuk. The skyrme model. 1993.

[56] Sidney Coleman. *Aspects of Symmetry: Selected Erice Lectures*. Cambridge University Press, 1985.

[57] R Rajaraman. *Solitons and instantons: an introduction to solitons and instantons in quantum field theory*. North-Holland, 1982.

[58] École d'été de physique théorique, A. Comtet, T. Jolicœur, S. Ouvry, and F. David. Aspects topologiques de la physique en basse dimension : Les houches, session lxix, 7-31 july 1998 = topological aspects of low dimensional systems. 1999.

[59] R. H. Hobart. On the Instability of a Class of Unitary Field Models. *Proceedings of the Physical Society*, 82(2):201–203, August 1963.

[60] G. H. Derrick. Comments on nonlinear wave equations as models for elementary particles. *Journal of Mathematical Physics*, 5(9):1252–1254, 1964.

[61] Piers Coleman. *Introduction to Many-Body Physics*. Cambridge University Press, 2015.

[62] Lev P Pitaevskii. Vortex lines in an imperfect bose gas. *Sov. Phys. JETP*, 13(2):451–454, 1961.

[63] Mark Srednicki. *Quantum field theory*. Cambridge University Press, 2007.

[64] Michael E Peskin and Daniel V Schroeder. *An introduction to quantum field theory*. Westview, Boulder, CO, 1995. Includes exercises.

[65] Mehran Kardar. *Statistical Physics of Fields*. Cambridge University Press, 2007.

[66] Adriaan MJ Schakel. *Boulevard of broken symmetries: effective field theories of condensed matter*. World Scientific Publishing Company, 2008.

[67] Grigory E Volovik. *The universe in a helium droplet*, volume 117. Oxford University Press on Demand, 2003.

[68] A. A. Belavin and A. M. Polyakov. Metastable states of two-dimensional isotropic ferromagnets. *Soviet Journal of Experimental and Theoretical Physics Letters*, 22:245, November 1975.

[69] Markus Garst. *Topological Skyrmion Dynamics in Chiral Magnets*, pages 29–53. Springer International Publishing, Cham, 2016.

[70] Steven Weinberg. *The quantum theory of fields*, volume 2. Cambridge university press, 1995.

[71] T. Brauner. Noether currents of locally equivalent symmetries. *arXiv: High Energy Physics - Theory*, 2019.

[72] Peter Woit. The west coast metric is the wrong one. https://www.math.columbia.edu/ woit/wordpress/?p=7773.

[73] Laurie M Brown. *Feynman's Thesis — A New Approach to Quantum Theory*. World Scientific, 2005.

[74] Xiao-Gang Wen. *Quantum field theory of many-body systems: from the origin of sound to an origin of light and electrons*. Oxford University Press on Demand, 2004.

[75] E. P. Gross. Structure of a quantized vortex in boson systems. *Il Nuovo Cimento*, 20(3):454–477, May 1961.

[76] Alexander Altland and Ben Simons. *Condensed Matter Field Theory*. Cambridge University Press, 2006.

[77] Mike H Anderson, Jason R Ensher, Michael R Matthews, Carl E Wieman, and Eric A Cornell. Observation of bose-einstein condensation in a dilute atomic vapor. *science*, 269(5221):198–201, 1995.

[78] K. B. Davis, M. O. Mewes, M. R. Andrews, N. J. van Druten, D. S. Durfee, D. M. Kurn, and W. Ketterle. Bose-einstein condensation in a gas of sodium atoms. *Phys. Rev. Lett.*, 75:3969–3973, Nov 1995.

[79] L.P. Pitaevskiĭ and S. Stringari. *Bose-Einstein Condensation and Superfluidity*. International series of monographs on physics. Oxford University Press, 2016.

[80] Peter W. Higgs. Nobel lecture: Evading the goldstone theorem. *Rev. Mod. Phys.*, 86:851–853, Jul 2014.

[81] DT T Son and M Wingate. General coordinate invariance and conformal invariance in nonrelativistic physics: Unitary Fermi gas. *Ann. Phys. (N. Y).*, 321:197–224, 2006.

[82] Martin Greiter, Frank Wilczek, and Edward Witten. Hydrodynamic Relations in Superconductivity. *Mod. Phys. Lett. B*, 3:903, 1989.

[83] X.G. Wen. *Quantum Field Theory of Many-Body Systems*. Oxford Graduate Texts. OUP Oxford, 2004.

[84] Anthony Zee. *Quantum field theory in a nutshell*. Princeton university press, 2010.

[85] Dung-Hai Lee and Matthew P. A. Fisher. Anyon Superconductivity and Charge-Vortex Duality. *International Journal of Modern Physics B*, 5(16-17):2675–2699, January 1991.

[86] Piers Coleman. *Introduction to Many-Body Physics*. Cambridge University Press, 2015.

[87] F D M Haldane and Yong-Shi Wu. Quantum dynamics and statistics of vortices in two-dimensional superfluids. *Phys. Rev. Lett.*, 55(26):2887–2890, December 1985.

[88] Ping Ao and David J. Thouless. Berry's phase and the magnus force for a vortex line in a superconductor. *Phys. Rev. Lett.*, 70:2158–2161, Apr 1993.

[89] N R Cooper. Rapidly Rotating Atomic Gases. *Adv. Phys.*, 57:539, 2008.

[90] E B Sonin. Vortex oscillations and hydrodynamics of rotating superfluids. *Rev. Mod. Phys.*, 59(1):87, 1987.

[91] Immanuel Bloch, Jean Dalibard, and Wilhelm Zwerger. Many-body physics with ultracold gases. *Rev. Mod. Phys.*, 80(3):885–964, July 2008.

[92] Alexander L. Fetter. Rotating trapped bose-einstein condensates. *Rev. Mod. Phys.*, 81:647–691, May 2009.

[93] EB Sonin. Tkachenko waves. *JETP Lett.*, 98(11):758–768, 2014.

[94] VK Tkachenko. On vortex lattices. *Sov. Phys. JETP*, 22:1282, 1965.

[95] VK Tkachenko. Stability of vortex lattices. *Sov. Phys. JETP*, 23(6):1049–1056, 1966.

[96] VK Tkachenko. Elasticity of vortex lattices. *Sov. Phys. JETP*, 29:945, 1969.

[97] GE Volovik and VS Dotsenko. Hydrodynamics of defects in condensed media, using as examples vortices in rotating he ii and disclinations in a planar magnet. *Soviet Phys. JETP*, 78(1):132–148, 1980.

[98] Gordon Baym and Elaine Chandler. The hydrodynamics of rotating superfluids. i. zero-temperature, nondissipative theory. *J. Low Temp. Phys.*, 50(1):57–87, 1983.

[99] Elaine Chandler and Gordon Baym. The hydrodynamics of rotating superfluids. ii. finite temperature, dissipative theory. *J. Low Temp. Phys.*, 62(1):119–142, Jan 1986.

[100] EB Sonin. Vortex-lattice vibrations in a rotating helium ii. *JETP Lett.*, 43:1027, 1976.

[101] Gordon Baym. Tkachenko Modes of Vortex Lattices in Rapidly Rotating Bose-Einstein Condensates. *Phys. Rev. Lett.*, 91(11):110402, September 2003.

[102] I Coddington, Peter Engels, Volker Schweikhard, and Eric A Cornell. Observation of tkachenko oscillations in rapidly rotating bose-einstein condensates. *Phys. Rev. Lett.*, 91(10):100402, 2003.

[103] VN Popov. Quantum vortices and phase transitions in bose systems. *Sov. Phys. JETP*, 37(341):2–33, 1973.

[104] Haruki Watanabe and Hitoshi Murayama. Redundancies in Nambu-Goldstone Bosons. *Phys. Rev. Lett.*, 110(18):181601, May 2013.

[105] Lev D Landau and EM Lifshitz. *Theory of Elasticity*, volume 7. Elsevier, New York, 1986.

[106] Sergej Moroz and Carlos Hoyos. Effective theory of two-dimensional chiral superfluids: gauge duality and Newton-Cartan formulation. *Phys. Rev. B*, 91:064508, 2015.

[107] AJ Beekman, D Sadri, and J Zaanen. Condensing nielsen–olesen strings and the vortex–boson duality in 3+ 1 and higher dimensions. *New Journal of Physics*, 13(3):033004, 2011.

[108] Davison E Soper. *Classical field theory*. Courier Dover Publications, 2008.

[109] H Leutwyler. Phonons as goldstone bosons. *Helv.Phys.Acta*, 70(275), 1997.

[110] D. T. Son and M. Wingate. General coordinate invariance and conformal invariance in nonrelativistic physics: Unitary Fermi gas. *Annals Phys.*, 321:197–224, 2006.

[111] M. W. Zwierlein, J. R. Abo-Shaeer, A. Schirotzek, C. H. Schunck, and W. Ketterle. Vortices and superfluidity in a strongly interacting fermi gas. *Nature*, 435(7045):1047–1051, 06 2005.

[112] Ari M. Turner, Vincenzo Vitelli, and David R. Nelson. Vortices on curved surfaces. *Rev. Mod. Phys.*, 82:1301–1348, Apr 2010.

[113] Alexander L. Fetter and P. C. Hohenberg. The mixed state of thin superconducting films in perpendicular fields. *Phys. Rev.*, 159:330–343, Jul 1967.

[114] J Pearl. Current distribution in superconducting films carrying quantized fluxoids. *App. Phys. Lett.*, 5(4):65–66, 1964.

[115] Pierre Delplace, J. B. Marston, and Antoine Venaille. Topological origin of equatorial waves. *Science*, 358(6366):1075–1077, 2017.

[116] Suraj Shankar, Mark J. Bowick, and M. Cristina Marchetti. Topological sound and flocking on curved surfaces. *Phys. Rev. X*, 7:031039, Sep 2017.

[117] Alexander G. Abanov, Tankut Can, and Sriram Ganeshan. Odd surface waves in two-dimensional incompressible fluids. *SciPost Phys.*, 5:10, 2018.

[118] A. Bogatskiy and P. Wiegmann. Edge wave and boundary layer of vortex matter. *Phys. Rev. Lett.*, 122:214505, May 2019.

[119] Anton Souslov, Kinjal Dasbiswas, Michel Fruchart, Suriyanarayanan Vaikuntanathan, and Vincenzo Vitelli. Topological waves in fluids with odd viscosity. *Phys. Rev. Lett.*, 122:128001, Mar 2019.

[120] Alexander G. Abanov, Tankut Can, Sriram Ganeshan, and Gustavo M. Monteiro. Hydrodynamics of two-dimensional compressible fluid with broken parity: Variational principle and free surface dynamics in the absence of dissipation. *Phys. Rev. Fluids*, 5:104802, Oct 2020.

[121] C. Tauber, P. Delplace, and A. Venaille. Anomalous bulk-edge correspondence in continuous media. *Phys. Rev. Research*, 2:013147, Feb 2020.

[122] Gian Michele Graf, Hansueli Jud, and Clément Tauber. Topology in shallow-water waves: a violation of bulk-edge correspondence. *arXiv:2001.00439*, 2020.

[123] Vishal Soni, Ephraim S Bililign, Sofia Magkiriadou, Stefano Sacanna, Denis Bartolo, Michael J Shelley, and William TM Irvine. The odd free surface flows of a colloidal chiral fluid. *Nature Physics*, 15(11):1188–1194, 2019.

[124] Sebastian Mühlbauer, Benedikt Binz, F Jonietz, Christian Pfleiderer, Achim Rosch, Anja Neubauer, Robert Georgii, and Peter Böni. Skyrmion lattice in a chiral magnet. *Science*, 323(5916):915–919, 2009.

[125] XZ Yu, Yoshinori Onose, Naoya Kanazawa, JH Park, JH Han, Yoshio Matsui, Naoto Nagaosa, and Yoshinori Tokura. Real-space observation of a two-dimensional skyrmion crystal. *Nature*, 465(7300):901–904, 2010.

[126] XZ Yu, Naoya Kanazawa, Yoshinori Onose, K Kimoto, WZ Zhang, Shintaro Ishiwata, Yoshio Matsui, and Yoshinori Tokura. Near room-temperature formation of a skyrmion crystal in thin-films of the helimagnet fege. *Nature materials*, 10(2):106–109, 2011.

[127] H. Fukuyama. Two-dimensional wigner crystal under magnetic field. *Solid State Communications*, 17(10):1323–1326, Nov 1975.

[128] Edouard B. Sonin. *Dynamics of Quantised Vortices in Superfluids*. Cambridge University Press, 2016.

[129] Lisa M. Nash, Dustin Kleckner, Alismari Read, Vincenzo Vitelli, Ari M. Turner, and William T. M. Irvine. Topological mechanics of gyroscopic metamaterials. *PNAS*, 112(47):14495–14500, 2015.

[130] Pai Wang, Ling Lu, and Katia Bertoldi. Topological phononic crystals with one-way elastic edge waves. *Phys. Rev. Lett.*, 115:104302, Sep 2015.

[131] Henrik Ronellenfitsch and Jörn Dunkel. Chiral topological phases in designed mechanical networks. *Frontiers in Physics*, 7:178, 2019.

[132] Olga Petrova and Oleg Tchernyshyov. Spin waves in a skyrmion crystal. *Physical Review B*, 84(21):214433, 2011.

[133] Jiadong Zang, Maxim Mostovoy, Jung Hoon Han, and Naoto Nagaosa. Dynamics of skyrmion crystals in metallic thin films. *Phys. Rev. Lett.*, 107:136804, Sep 2011.

[134] Michael Stone. Magnus force on skyrmions in ferromagnets and quantum hall systems. *Phys. Rev. B*, 53:16573–16578, Jun 1996.

[135] Imam Makhfudz, Benjamin Krüger, and Oleg Tchernyshyov. Inertia and chiral edge modes of a skyrmion magnetic bubble. *Physical review letters*, 109(21):217201, 2012.

[136] M Garau, MJ Nieves, G Carta, and M Brun. Transient response of a gyro-elastic structured medium: Unidirectional waveforms and cloaking. *International Journal of Engineering Science*, 143:115–141, 2019.

[137] I. D'Amico and G. Vignale. Continuum elasticity theory of edge waves in a two-dimensional electron liquid with finite-range interactions. *Phys. Rev. B*, 60(3):2084–2092, 1 1999.

[138] Walter Kohn. Cyclotron resonance and de haas-van alphen oscillations of an interacting electron gas. *Phys. Rev.*, 123:1242–1244, Aug 1961.

[139] Maissam Barkeshli, Suk Bum Chung, and Xiao-Liang Qi. Dissipationless phonon hall viscosity. *Phys. Rev. B*, 85(24):245107, 2012.

[140] Yu P. Monarkha, F. M. Peeters, and S. S. Sokolov. Edge excitations of a two-dimensional electron solid in a magnetic field. *Journal of Physics Condensed Matter*, 9(7):1537–1545, Feb 1997.

[141] A video which shows a finite-difference simulation of the system's edge waves can be found at https://youtu.be/yf7MzCQC5y4.

[142] Kai Sun, Anton Souslov, Xiaoming Mao, and TC Lubensky. Surface phonons, elastic response, and conformal invariance in twisted kagome lattices. *PNAS*, 109(31):12369–12374, 2012.

[143] MF Thorpe. Bulk and surface floppy modes. *Journal of Non-Crystalline Solids*, 182(1-2):135–142, 1995.

[144] CL Kane and TC Lubensky. Topological boundary modes in isostatic lattices. *Nature Physics*, 10(1):39–45, 2014.

[145] Tristan Needham. *Visual Complex Analysis*. Oxford University Press, 1998.

[146] M. Brun, I. S. Jones, and A. B. Movchan. Vortex-type elastic structured media and dynamic shielding. *Proceedings of the Royal Society A: Mathematical, Physical and Engineering Sciences*, 468(2146):3027–3046, 2012.

[147] MJ Nieves, G Carta, V Pagneux, and M Brun. Rayleigh waves in microstructured elastic systems: Non-reciprocity and energy symmetry breaking. *International Journal of Engineering Science*, 156:103365, 2020.

[148] Yuchen Zhao, Xiaoming Zhou, and Guoliang Huang. Non-reciprocal rayleigh waves in elastic gyroscopic medium. *Journal of the Mechanics and Physics of Solids*, 143:104065, 2020.

[149] Colin Scheibner, Anton Souslov, Debarghya Banerjee, Piotr Surowka, William TM Irvine, and Vincenzo Vitelli. Odd elasticity. *Nature Physics*, 16(4):475–480, 2020.

[150] Debarghya Banerjee, Vincenzo Vitelli, Frank Jülicher, and Piotr Surówka. Active viscoelasticity of odd materials. *Physical Review Letters*, 126(13):138001, 2021.

[151] Ethan R Elliott, Markus C Krutzik, Jason R Williams, Robert J Thompson, and David C Aveline. Nasa's cold atom lab (cal): system development and ground test status. *npj Microgravity*, 4(1):1–7, 2018.

Acknowledgements

With the following, I would like to thank part of the people who entered my life during these PhD years and whose profound impact probably will never fade away. First of all, I would like to thank my supervisor Sergej Moroz, who gave me the opportunity and trust of being his first PhD student. Your ability to 'see beyond the mountains' of formalisms, unwieldy equations and bizarre concepts to understand the key mechanisms of physics and explain them in simple terms always amazed me. Also, your patience and kindness lived up far beyond my wildest imagination. Then, I would like to thank my office mate Umberto, with whom I enjoyed sharing most of this journey, part of the questions, all of the coffee. Billa as well was a key element of these years. Your unwavering love for knowledge is remarkable, and I hope you will be able to reach the goals you deserve. I think you are the only active physicist I met who still dives into books the size of a bedside table for the pure joy of learning! Thanks Giovanni for the refreshing walks and discussions. Social life in a foreign country was a hard shot, even more during pandemic years. I was fortunate enough to have met *Les Misérables*. They already know that I will be forever in debt with them. Un ulteriore ringraziamento agli amici di sempre e a quelli già ringraziati nelle precedenti tesi. Per ultima, voglio ringraziare la mia famiglia, che é stata sempre presente nonostante la distanza, gli eventi e le vicissitudini, ed il cui affetto non é mai mancato.
Sono stato un ragazzo fortunato.